UNIVERSIDADE DE ÉVORA

TOPOLOGICAL AND DYNAMICAL COMPLEXITY IN EPIDEMIOLOGICAL AND ECOLOGICAL DYNAMICAL SYSTEMS

Carla Cristina Morbey Rodrigues
(MSc. in Applied Mathematics)

PhD Thesis in Mathematics

Supervisor: Professor Doutor Jorge das Neves Duarte
Co-supervisors: Professor Doutor Carlos Correia Ramos and Professor Doutor Josep Sardanyés Cayuela

June 2016

TOPOLOGICAL AND DYNAMICAL COMPLEXITY IN EPIDEMIOLOGICAL AND ECOLOGICAL DYNAMICAL SYSTEMS

ABSTRACT

In this work, we address a contribution for the rigorous analysis of the dynamical complexity arising in epidemiological and ecological models under different types of interactions.

Firstly, we study the dynamics of a tumor growth model, governing tumor cells interacting with healthy tissue cells and effector cells of the immune system. By using the theory of symbolic dynamics, we characterize the topological entropy from one-dimensional iterated maps identified in the dynamics. This analysis is complemented with the computation of the Lyapunov exponents, the fractal dimension and the predictability of the chaotic dynamics.

Secondly, we provide the analytical solutions of the mentioned tumor growth model. We apply a method for solving strongly nonlinear systems - the Homotopy Analysis Method (HAM) - which allows us to obtain a one-parameter family of explicit series solutions.

Due to the importance of chaos generating mechanisms, we analyze a mathematical ecological model mainly focusing on the impact of species rates of evolution in the dynamics. We analytically proof the boundedness of the trajectories of the attractor. The complexity of the coupling between the dynamical variables is quantified using observability indices. The topological entropy of existing one-dimensional iterated maps is characterized using symbolic dynamics. To extend the previous analysis, we study the predictability and the likeliness of finding chaos in a given region of the parameter space.

We conclude our research work with the analysis of a HIV-1 cancer epidemiological model. We construct the explicit series solution of the model. An optimal homotopy analysis approach is used to improve the computational efficiency of HAM by means of appropriate values for the convergence control parameter.

We end up this dissertation presenting some final considerations.

KEY-WORDS: life science models, dynamical systems theory, differential equations, homotopy analysis method, analytical solutions.

COMPLEXIDADE DINÂMICA E TOPOLÓGICA EM SISTEMAS DINÂMICOS EPIDEMIOLÓGICOS E ECOLÓGICOS

RESUMO

Este trabalho constitui um contributo para a análise rigorosa da complexidade dinâmica de modelos epidemiológicos e ecológicos submetidos a diferentes tipos de interações.

Primeiramente, estudamos a dinâmica de um modelo de crescimento tumoral, representando a interacção de células tumorais com tecidos saudáveis e células efectoras do sistema imunitário. Usando a teoria da dinâmica simbólica, caracterizamos a entropia topológica de aplicações unidimensionais identificadas na dinâmica. Esta análise é complementada com o cálculo dos expoentes de Lyapunov, dimensão fractal e o cálculo da previsibilidade dos atractores caóticos.

Seguidamente, apresentamos soluções analíticas do modelo de crescimento tumoral mencionado. Aplicamos um método para resolver sistemas fortemente não lineares - o Método de Análise Homotópica (HAM) - o qual nos permite obter uma família a um parâmetro de soluções explícitas em forma de série.

Devido à importância dos mecanismos geradores de caos, analisamos um modelo matemático em ecologia, centrando-nos no impacto das taxas de evolução das espécies na dinâmica. Provamos analiticamente a compacticidade das trajectórias do atractor. A complexidade do acoplamento entre as variáveis dinâmicas é quantificada utilizando índices de observabilidade. A entropia topológica de aplicações unidimensionais é caracterizada usando a dinâmica simbólica. Para estender a análise anterior, estudamos a previsibilidade e a probabilidade de encontrar comportamento caótico numa determinada região do espaço de parâmetros.

Concluímos o nosso trabalho de investigação com a análise de um modelo epidemiológico tumoral HIV-1. Construímos uma solução explícita do modelo. Usamos uma análise homotópica optimal para melhorar a eficiência computacional do HAM através de valores apropriados para o parâmetro de controlo da convergência.

Terminamos esta dissertação com a apresentação de algumas considerações finais.

PALAVRAS-CHAVE: modelos das ciências da vida, teoria dos sistemas dinâmicos, equações diferenciais, método de análise homotópica, soluções analíticas.

Ao meu Pai

"– Non, dit le petit prince. Je cherche des amis. Qu'est-ce que signifie "apprivoiser"?
– C'est une chose trop oubliée, dit le renard. Ça signifie "créer des liens..."
– Créer des liens ?
– Bien sûr, dit le renard.
Tu n'es encore pour moi qu'un petit garçon tout semblable à cent mille petits garçons.
Et je n'ai pas besoin de toi. Et tu n'as pas besoin de moi non plus.
Je ne suis pour toi qu'un renard semblable à cent mille renards.
Mais, si tu m'apprivoises, nous aurons besoin l'un de l'autre.
Tu seras pour moi unique au monde. Je serai pour toi unique au monde...
⋮
Le renard se tut et regarda longtemps le petit prince:
– S'il te plaît... apprivoise-moi! dit-il.
– Je veux bien, répondit le petit prince, mais je n'ai pas beaucoup de temps.
J'ai des amis à découvrir et beaucoup de choses à connaître.
– On ne connaît que les choses que l'on apprivoise, dit le renard
Les hommes n'ont plus le temps de rien connaître.
Ils achètent des choses toutes faites chez les marchands.
Mais comme il n'existe point de marchands d'amis, les hommes n'ont plus d'amis.
Si tu veux un ami, apprivoise-moi!
– Que faut-il faire ? dit le petit prince.
– Il faut être très patient, répondit le renard."

Antoine de Saint-Exupéry - Le Petit Prince

AGRADECIMENTOS

Esta tese de doutoramento foi uma longa viagem, com alguns obstáculos pelo caminho e não teria sido possível terminá-la sem o apoio e a ajuda inestimável de algumas pessoas.

Em primeiro lugar, quero agradecer ao meu orientador e amigo, Professor Doutor Jorge das Neves Duarte, pela disponibilidade, paciência, dedicação, partilha de conhecimentos e acima de tudo, compreensão pelo meu ritmo de trabalho.

À Cristina, pela sua presença, amizade e sugestões.

Aos co-orientadores, Professor Doutor Carlos Correia Ramos e Professor Doutor Josep Sardanyés Cayuela, pelo conhecimento transmitido, indispensável para a realização deste trabalho.

Aos meus filhotes, Cristina, Carolina e Miguel, ao Miguel e à minha mãe, os mais prejudicados ao longo de todo este percurso. Espero poder compensá-los por toda a atenção que lhes foi retirada.

Contents

[1]This study has been published in [52].
[2]This study has been published in [66].
[3]This study has been published in [86].

[4]This study has been submitted for publication in [132].

Chapter 1

Introduction and Preliminaries

The application of mathematical concepts and methods is considered fundamental in the progress of various areas of knowledge, such as engineering, chemistry, physics, economics, biology, ecology, among others. The issues raised by these areas turn out to be truly exciting, playing a decisive role in the development of theories and new branches of mathematics itself.

A special field of mathematics, regarding its concept richness and applicability, is the theory of dynamical systems (discrete and continuous), in particular the so-called nonlinear science. The theory of dynamical systems involves in a harmonious and indispensable way three major areas of mathematics: analysis, algebra and geometry. The nonlinear dynamics is related with the study of systems where a small change in a parameter can lead to sudden and drastic changes in the quantitative and qualitative behavior. The analysis of nonlinear interactions reveals how qualitatively new structures arise and how they relate to the theory already established. The use of computer techniques is usually identified as the primary catalyst for the development of nonlinear science, revealing a structured character behind the complexity. Surprisingly, the models constructed in various areas of knowledge, considering the fundamental principles of complexity, reveal to share a

number of important properties. The remarkable applicability of nonlinear science in areas as diverse as seemingly unrelated, gives it the special status of a possible factor of methodological unification in various areas of knowledge. In an interdisciplinary context, and by exploring common structures in different systems, scientists study and model the complexity of nature and society. The new techniques and concepts provide effective methods for modeling and simulation of sudden and irreversible changes in the natural and social systems.

The concepts and methodologies of dynamical systems theory have their origins in Newtonian mechanics. There, as in other fields of natural sciences and engineering disciplines, the evolution rule of dynamical systems is given implicitly by a relation that gives the state of the system only in a short time into the future. The French mathematician Henri Poincaré (1854-1912) is considered one of the founders of dynamical systems. Poincaré published two classical monographs, "New Methods of Celestial Mechanics" (1892–1899) and "Lectures on Celestial Mechanics" (1905–1910). In these works, he successfully applied the results of their research to the problem of the motion of three bodies and studied in detail the behavior of solutions (frequency, stability, asymptotic, etc). These papers included the Poincaré recurrence theorem, which states that certain systems will, after a sufficiently long but finite time, return to a state very close to the initial state. In 1898 Jacques Hadamard published an influential study of the chaotic motion of a free particle gliding frictionlessly on a surface of constant negative curvature, called "Hadamard's billiards". Hadamard was able to show that all trajectories are unstable, that all particle trajectories diverge exponentially from one another with a positive Lyapunov exponent. In the years that followed, the study of dynamical systems has been greatly enriched by

the contributions of others mathematicians, namely, Aleksandr Lyapunov (1857-1918), a Russian mathematician who developed important approximation methods. This methods, which Lyapunov developed arround 1899, made it possible to define the stability of sets of ordinary differential equations. He created the modern theory of stability dynamical systems. George David Birkhoff (1884–1944), an American mathematician, is a reference in ergodic theory. In 1913, Birkhoff proved Poincaré's "Last Geometric Theorem" a special case of the three-body problem, a result that made him world famous. In 1927, he published his "Dynamical Systems". In 1936, Kolmogorov (1903-1987), a Russian mathematician contributed to the field of ecology and generalized the Lotka–Volterra model of predator-prey systems. Stephen Smale (1930-) made significant advances as well. After having made great strides in topology, he then turned to the study of dynamical systems, where he made significant advances as well. His first contribution was the so-called *Smale horseshoe* that gave rise significant research in dynamical systems. Oleksandr Mykolaiovych Sharkovsky (1936-), an Ukrainian mathematician developed in 1964 the Sharkovsky's Theorem on the periods of discrete dynamical systems. One of the implications of the theorem is that if a discrete dynamical system on the real line has a periodic point of period 3, then it must have periodic points of every other period.

By 1975, some scientists around the world were aware of the existence of a new type of movement in dynamic systems - called *chaos*. James Yorke and T.Y. Li coined the mathematical term *chaos* in a paper they published in 1975 entitled "Period three implies chaos". This term has been introduced to denote an aperiodic dynamic behavior that occurs in a deterministic system which exhibits sensitivity to initial conditions. What is truly amazing is that this type of behavior can occur in systems apparently very simple.

In applications, chaos theory uses concepts as *catastrophes*, *bifurcations*, *strange attractors*, *periodicities* and *applications on the interval*. All these threads cannot be effectively studied by traditional analytical methods, which are mainly related to linearity and stability. Before the advent of fast computing machines, solving a dynamical system required sophisticated mathematical techniques and could only be accomplished for a small class of dynamical systems. The main catalyst for the development of chaos theory was the electronic computer. Much of the mathematics of chaos theory involves repeated iterations of simple mathematical formulas, which would be impractical of doing by hand. Electronic computers made these repeated calculations practical, while figures and images made it possible to visualize these systems. Chaos theory got its start in the field of ergodic theory. Later studies, also on the topic of nonlinear differential equations, were carried out by George David Birkhoff, Andrey Nikolaevich Kolmogorov, Mary Lucy Cartwright, John Edensor Littlewood and Stephen Smale. Except for Smale, these studies were all directly inspired by physics: the three-body problem in the case of Birkhoff, turbulence and astronomical problems in the case of Kolmogorov, and radio engineering in the case of Cartwright and Littlewood.

The theory of nonlinear dynamical systems (chaos theory) ened up to be an interdisciplinary area of research and has affected almost every field of science in the last 30 years. Given the complexity of biological systems, the concepts and methods of chaos theory are widely applied, and particularly appreciated, in the context of physiology. This is suggested by experimental studies and has also been encouraged by very successful modeling. A plausible and compelling reason to apply chaos theory to these areas of science is due to the fact that the chaotic behavior is not at all a rare or pathological occurrence. In

addition, the results may be relevant both from a mathematical point of view and from the point of view of the life sciences.

The research work that has been carried out, in a truly interdisciplinary environment, is closely related with the analysis and characterization of biological dynamical models in realistic parameter spaces using effective and efficient methods to obtain analytical solutions, which represents a significant effort that opens the opportunity to deeply explore the dynamics – this represents a milestone, only possible now with the very recent introduction of new analytical methods for highly nonlinear problems.

In addition, numerical techniques are used to compute different measures of complexity, such as observability indices (which indicate the most significant dynamical variable that must be studied), Lyapunov exponents, entropy, predictability (which is particularly important in the epidemiological context), among others. These tools are applied with the purpose of contributing to a rigorous analysis of models and they can help to predict the dynamical behavior of biological systems and to improve/create more realistic mathematical modeling. In the context of epidemiology, the extensions of some mathematical models should lead to better understanding of infections and treatment processes, allowing computer simulation of mechanisms which are difficult to monitor in vivo.

All the research work is inherently highly collaborative, where the close interaction between scientists of different disciplines is crucial for realism and significance of the obtained theoretical results. The work is an incursion of mathematics - using analytical, numerical and computational methods - into biology, carried out by a research team with mathematicians and biologists.

It is important to note that the underlying research involves a comprehensive computer

programming work and the numerical simulations were carried out entirely by the participants in this dissertation. The software used corresponds to Mathematica 9.0 program of Wolfram Research.

In the following paragraph we present definitions and results that will be instrumental in characterizing the dynamics of the models within the theory of discrete and continuous dynamical systems.

1.1 Elements of the theory of discrete dynamical systems: symbolic dynamics and topological entropy

Time is a continuous variable, nevertheless, we sometimes find it helpful to treat time as if it were discrete. This is particularly true for systems that are affected by conditions that vary periodically with the time. Many important properties of linear systems with periodic conditions could be obtained by considering only a sequence of states at times differing by multiples of the period. This is equivalent of treating the time as a discrete variable. The same applies to nonlinear systems with periodic conditions. For example: biological, social and economic systems are affected by the seasons and these vary approximately periodically with a period of one year; for some insects a more appropriate period is the day; many mechanical, electrical and electronic systems are subject to determinate periodic conditions. Sometimes the use of a discrete time variable is not a mere matter of convenience, it becomes compulsory since the data, upon which the laws of motion are based, may only be available once in a period, because it is too difficult to obtain them at all times (as it is common for some economical and medical data). The approximation of treating differential equations, with time as the independent variable as difference equations also requires the time to be treated as discrete.

Any physical systems, whose state evolves with time is a dynamical system. Dynamical systems originally arose in the study of systems of differential equations used to model physical phenomena. The motions of the planets, or of mechanical systems, or of molecules in a gas, can be modeled by such systems.

A dynamical system is a tuple (T, M, f) where T is a monoid, M is a set and f is a function

$$f : X \subset T \times M \to M.$$

The function $f(x, t)$ is called the evolution function of the dynamical system: it associates to every point in the set M a unique image, depending on the variable t, called the evolution parameter. In other words f specifies how the state evolves with time. M is called phase space or state space, while the variable x represents an initial state of the system.

Two main types of dynamical systems are encountered in applications: those for which the time variable is discrete ($t \in \mathbb{Z}$ or $\mathbb{N}$) and those for which it is continuous ($t \in \mathbb{R}$). A discrete dynamical system, is a tuple (T, M, f) where T is the set of integers, M is a manifold locally diffeomorphic to a Banach space, and f is a function. Discrete dynamical systems can be represented as the iteration of a function, i.e.

$$x_{t+1} = f(x_t) \;\; t \in \mathbb{Z} \text{ or } \mathbb{N}. \tag{1.1}$$

A real dynamical system, real-time dynamical system, continuous time dynamical system, or flow is a tuple (T, M, f) with T an open interval in the real numbers $\mathbb{R}$, M a manifold locally diffeomorphic to a Banach space, and f a continuous function. When t is continuous, the dynamics are usually described by a differential equation

$$\frac{dx}{dt} = X(x). \tag{1.2}$$

In this work we have restricted T to the non-negative integers.

As pointed out previously, the evolution rule of dynamical systems is an implicit relation that gives the state of the system for only a short time into the future. The relation is either a differential equation, difference equation or other time scale. The determination of the state for all future times requires iterating the relation many times. The iteration procedure is referred to as solving the system or integrating the system. If the system can be solved, given an initial point it is possible to determine all its future positions, a collection of points known as a trajectory or orbit. One of the fundamental questions of dynamics concerns the behavior of the sequence $x, f(x), f^2(x), \ldots, f^n(x), \ldots$ of a given map or a class of maps. For discrete-time dynamical systems, the orbits are sequences while for real dynamical systems, the orbits are curves. In the language of difference equations we are interested in investigating the behavior of solutions of Eq. (1.1).

Let $X \subseteq \mathbb{R}^n$ be a compact metric space and $f : X \to X$ a continuous map. For each $x_0 \in X$, the iteration of (1.1) generates a sequence, which defines the orbit or trajectory of x_0 under f.

Definition 1 *Starting from an initial point $x_0 \in X$, the set of all iterates of the point x_0 is called the (positive)* ***orbit*** *of x_0*

$$O(x_0) = \left\{x_0, f(x_0), f^2(x_0), \ldots, f^n(x_0), \ldots\right\} = \{f^n(x_0)\}_{n=0}^{\infty} \tag{1.3}$$

where for $n \in \mathbb{N}$, f^n is the composition of f with itself n times

$$f^n(x_0) = \underbrace{(f \circ f \circ \cdots \circ f)}_{n \text{ times}}(x_0)$$

Many parts of the qualitative theory of differential equations and dynamical systems deal with asymptotic properties of solutions and with what happens with the system after

a long period of time. The simplest kind of behavior is exhibited by equilibrium points, or fixed points, and by periodic orbits. Of particular importance is finding orbits that consist of one point. Such points are called fixed points, or equilibrium points.

Definition 2 *A point $x_0 \in X$ is said to be a* ***fixed point*** *of the map f if $f(x_0) = x_0$.*

Closely related to fixed points are the eventually fixed points. These are the points that reach a fixed point after finitely many iterations.

Definition 3 *A point $x_0 \in X$ is an* ***eventually fixed point*** *if there exists N such that $f^{n+1}(x_0) = f^n(x_0)$ whenever $n \geq N$.*

One of the main objectives in the theory of dynamical systems is the study of the behavior of orbits near fixed points, i.e, the behavior of solutions of a differential equation near equilibrium points.

Definition 4 *Let $f : X \to X$ be a map and x_0 be a fixed point of f, where X is an interval in the set of real numbers $\mathbb{R}$. Then:*

1. x_0 is said to be ***stable*** *if $\forall_{\epsilon>0}\ \exists_{\delta>0} : |x - x_0| < \epsilon \Rightarrow |f^n(x) - x_0| < \delta$ for all $n \in \mathbb{N}$, and all $x \in X$. Otherwise, the fixed point x_0 will be called* ***unstable****.*

2. x_0 is said to be ***attracting*** *if $\exists_{\eta>0} : |x - x_0| < \eta \Rightarrow \lim_{n\to+\infty} f^n(x) = x_0$.*

3. x_0 is said to be ***asymptotically stable*** *if it is both stable and attracting.*

Fixed points may be divided into two types: hyperbolic and nonhyperbolic. A fixed point x_0 of a map f is said to be **hyperbolic** if $|f'(x_0)| \neq 1$. Otherwise, it is **nonhyperbolic**.

Theorem 1 *Let x_0 be a hyperbolic fixed point of a map f, where f is continuously differentiable at x_0.*

1. *If $|f'(x_0)| < 1$, then x_0 is* ***asymptotically stable.***

2. *If $|f'(x_0)| > 1$, then x_0 is* ***unstable.***

The stability criteria for nonhyperbolic fixed points is more complex to analise. We have to consider the two cases, $f'(x_0) = 1$ and $f'(x_0) = -1$, separately.

Theorem 2 *Let x_0 be a fixed point of a map f such that $f'(x_0) = 1$. If $f'''(x_0) \neq 0$ and continuous, then the following statements hold:*

1. *If $f''(x_0) \neq 0$, then x_0 is* ***unstable.***

2. *If $f''(x_0) = 0$ and $f'''(x_0) > 0$, then x_0 is* ***unstable.***

3. *If $f''(x_0) = 0$ and $f'''(x_0) < 0$, then x_0 is* ***asymptotically stable.***

To establish the stability criteria for the case when $f'(x_0) = -1$, we need to introduce the notion of the **Schwarzian derivative**

Definition 5 *The* ***Schwarzian derivative*** *of f at x is defined by*

$$Sf(x) = \frac{f'''(x)}{f'(x)} - \frac{3}{2}\left(\frac{f''(x)}{f'(x)}\right)^2.$$

Theorem 3 *Let x_0 be a fixed point of a map f such that $f'(x_0) = -1$. If $f'''(x_0)$ is continuous, then the following statements hold:*

1. *If $Sf(x_0) < 0$, then x_0 is* ***asymptotically stable.***

2. *If* $Sf(x_0) > 0$, *then* x_0 *is* ***unstable.***

The notion of periodicity is an important concept in the field of dynamical systems. Its importance stems from the fact that many physical phenomena have certain patterns that repeat themselves. These patterns produce cycles or periodic cycles, where a cycle is the orbit of a periodic point.

Definition 6 *The point* $x_0 \in X$ *is a* ***periodic point*** *of* f *with period* k *if* $f^k(x_0) = x_0$, *for some integer* $k \geq 1$. *The periodic point* x_0 *has* ***prime period*** k_0 *if*

$$f^{k_0}(x_0) = x_0 \text{ and } f^n(x_0) \neq x_0 \text{ whenever } 0 < n < k_0. \tag{1.4}$$

The least value of k *satisfying (1.4) is called the period of the point* x_0 *and the orbit of* x_0, *i.e.*

$$\left\{x_0, f(x_0), f^2(x_0), \ldots, f^{k-1}(x_0)\right\}, \tag{1.5}$$

is said to be a ***periodic orbit*** *of period* k *or a* $k-$*cycle of* f.

Definition 7 *Let* f *be a function. The point* x_0 *is* ***eventually periodic*** *with period* k *if there exists* N *such that* $f^{n+k}(x_0) = f^n(x_0)$ *whenever* $n \geq N$.

Theorem 4 *Let* $O(x_0) = \left\{x_0, f(x_0), f^2(x_0), \ldots, f^{k-1}(x_0)\right\}$ *be the orbit of the* k*-periodic point* x_0, *where* f *is a continuously differentiable function at* x_0. *Then the following statements hold true:*

1. x_0 *is* ***asymptotically stable*** *if* $\left|f'(x_0) f'(f(x_0)) \ldots f'\left(f^{k-1}(x_0)\right)\right| < 1$.
2. x_0 *is* ***unstable*** *if* $\left|f'(x_0) f'(f(x_0)) \ldots f'\left(f^{k-1}(x_0)\right)\right| > 1$.

Remark 1 $f'(x_0) f'(f(x_0)) \ldots f'\left(f^{k-1}(x_0)\right) = \frac{d}{dx} f^k(x_0)$.

It is reasonable to ask how many other periodic points a continuous map f has, supposing that f has a orbit with period three, and what prime periods are represented. These questions are answered, at least in part, by the Li-Yorke theorem and by the Sharkovsky theorem. In 1975 James Yorke and Tien-Yien Li published the article "Period Three Implies Chaos" where they proved that not only does the existence of a period-3 cycle imply the existence of cycles of all periods, but in addition it implies the existence of an uncountable infinitude of points that never map to any cycle (chaotic points), a property known as *period three implies chaos.*

Theorem 5 ***(Li-Yorke)*** *Let $X \subseteq \mathbb{R}$ be an interval. If a continuous function $f : X \to X$ has a point of period 3, then it has a point of period k for every $k \geq 1$.*

Li and Yorke's paper was responsible for introducing the word "chaos" into the mathematical vocabulary. Soon afterward, it was found that Li-Yorke's theorem is only a special case of the Sharkovsky theorem [1]. In 1964, the Ukranian mathematician Oleksandr Sharkovsky introduced a new ordering $\prec$ on the positive integers in which 3 appears first.

Definition 8 ***(Sharkovsky order)*** *Sharkovsky's ordering of the natural numbers is*

$$3 \prec 5 \prec 7 \prec \ldots \prec 3 \times 2 \prec 5 \times 2 \prec 7 \times 2 \prec \ldots \prec 3 \times 2^2 \prec 5 \times 2^2 \prec 7 \times 2^2 \prec \ldots$$

$$\ldots \prec 3 \times 2^n \prec 5 \times 2^n \prec 7 \times 2^n \prec \ldots \prec 2^3 \prec 2^2 \prec 2 \prec 1$$

The relation $p \prec q$ indicates p precedes q in the order. When writing the order, all odd numbers except one are listed in ascending order, then two times every odd numbers, then 2^2 times each odd number, and so on. When all of these values are taken, the ordering

is completed by listing the powers of 2 *in descending order. Every natural number can be found exactly once in Sharkovsky's ordering.*

Note that this ordering is not a well-ordering, we write $p \prec q$ or $q \succ p$ whenever p is to the left of q. The Sharkovsky ordering has the following doubling property:

$$p \prec q \text{ if and only if } 2p \prec 2q.$$

This is because the odd numbers greater than 1 appear at the left-hand side of the list, the number 1 appears at the right-hand side, and the rest of $\mathbb{N}$ is included by successively doubling these remaining pieces, and inserting these doubled strings inward. Sharkovsky showed that this ordering describes which numbers can be periods for a continuous map of an interval. Sharkovsky's theorem says the following:

Theorem 6 ***(Sharkovsky Theorem)*** *Let $X \subseteq \mathbb{R}$ be an interval. If a continuous function $f : X \to X$ has a periodic point of period p, then it has a point of period q for every q with $p \prec q$.*

Notice that the first term in the Sharkovsky ordering is 3. Thus, if we apply Sharkovsky's theorem with $n = 3$ we get the Li-Yorke theorem. But clearly, Sharkovsky's theorem is much deeper. Sharkovsky's theorem states that if f has a periodic point of least period m and m precedes n in the above ordering, then f has also a periodic point of least period n. As a consequence, we see that if f has only finitely many periodic points, then they must all have periods which are powers of two. Furthermore, if there is a periodic point of period three, then there are periodic points of all other periods. Sharkovsky's theorem does not state that there are stable cycles of those periods, just that there are cycles of

those periods. For systems such as the logistic map, the bifurcation diagram shows a range of parameter values for which apparently the only cycle has period 3. In fact, there must be cycles of all periods there, but they are not stable and therefore not visible on the computer generated picture.

In maps, there can be (and generally are) sets of points which are left unchanged by the dynamics. More precisely, for any point in the set, there is always some point in the set which maps into its place, so the set doesn't change. The set is its own image. These sets are called invariant. A point is attracted to an invariant set if, when we follow its trajectory for long enough, it always gets closer to the set. If all points sufficiently close to the invariant set are attracted to it, then the set is an attractor. An attractor's basin of attraction consists in all the points which are attracted to it. The reasons for thinking about attractors, basins of attraction, are that, first, they control the long-run behavior of the system, and, second, they let us think about dynamics, about change over time. An asymptotically stable fixed point or a cycle is called an *attractor*. The orbits off all nearby points tend to the attractor. The maximal set that is attracted to an attractor M is called the basin of attraction of M.

Definition 9 *Let x_0 be an asymptotically stable fixed point of a map f. Then the* ***basin of attraction*** *$W^s(x_0)$ of x_0 is defined as the maximal interval J containing x_0 such that if $x_0 \in J$, then $f^n(x_0) \to x_0$ as $n \to +\infty$.*

How many periodic attractors can a differentiable map have? In 1978, David Singer more or less answered the above question. The main tool used in Singer's theorem is the Schwarzian derivative. He observed that this property is preserved under iteration and that it has important consequences in unimodal and multimodal dynamics.

Definition 10 *Let I be the compact interval $[a,b]$ and $f: I \to I$ a* ***piecewise strictly monotone*** *continuous map. This means that f has a finite number of turning points*

$$a < c_1 < c_2 < \ldots < c_m < b,$$

points where f has a local extremum, and f is strictly monotone on each of the $m+1$ intervals

$$I_1 = [a, c_1[\,, I_2 =]c_1, c_2[\,, \ldots, I_{m+1} =]c_m, b]\,.$$

*Such a map is called $m-$**modal** if $f(\partial I) \subseteq I$. If $m = 1$ then f is called **unimodal**. Each such maximal interval on which f is monotone is called a **lap** of f, and the total number of distinct laps is called the **lap number** of f and it is usually denoted by $\ell = \ell(f)$.*

If f is a $m-$modal map, let us denote by $Crit_f$ the set of turning points or critical points

$$Crit_f = \{c_1, c_2, \ldots, c_m\}$$

Schwarzian derivative plays an important role in characterizing some metric properties of maps. Maps with a negative Schwarzian derivative on the whole interval may have at most $m+2$ attracting periodic orbits, where m is the number of extremes in f. Most maps of physical interest have negative Schwarzian derivative on the whole interval of definition.

Definition 11 *Let $f: I \to I$ be a C^3 (third derivatives exist and are continuous) $m-$modal map. The* ***Schwarzian derivative*** *of f at x is defined as*

$$Sf(x) = \frac{f'''(x)}{f'(x)} - \frac{3}{2}\left(\frac{f''(x)}{f'(x)}\right)^2$$

for all $x \in I \setminus \{c_1, c_2, \ldots, c_m\}$.

We may compute the Schwarzian derivative of a composition

$$S(f \circ g)(x) = Sf(g(x)) \cdot \left[g'(x)\right]^2 + Sg(x).$$

There are very important consequences of negative Schwarzian derivative for the dynamics of the map [2]:

1. If $Sf < 0$ and $Sg < 0$ then $S(f \circ g) < 0$. So, negative Schwarzian derivative is preserved under iteration, i.e., if $Sf < 0$ then $Sf^n < 0$ for all $n \in \mathbb{N}$.

2. If $Sf < 0$ then for every periodic attracting orbit there is a critical point of f or an endpoint of I, which is attracted by this orbit

Theorem 7 ***(Singer's Theorem)*** *Let f be a continuous piecewise monotone map, defined on the closed interval I, such that $Sf(x) < 0$ for all $x \in I$. If f has m critical points in I, then for every $k \in \mathbb{Z}^+$, the map f has at most $(m+2)$ attracting $k-$cycles. The immediate basin of any attracting periodic orbit contains either a critical point of f or a boundary point of the interval I.*

1.1.1 Symbolic dynamics

Symbolic dynamics is a rapidly growing part of dynamical systems. Originally arose as an attempt to study such systems by means of discretizing space as well as time. The basic idea is to divide up the set of possible states into a finite number of pieces, and keep track of which piece the state of the system lies in at every tick of the clock. Each piece is associated with a "symbol", and in this way the evolution of the system is described by an infinite sequence of symbols. This leads to a "symbolic" dynamical system that mirrors and helps us to understand the dynamical behavior of the original system.

The beginnings of symbolic dynamics are often traced back to Jacques Hadamard when he applied this idea in 1898 to more complicated systems called geodesic flows on surfaces of negative curvature. The main point of his work is that there is a simple description of the possible sequences that can arise this way. He showed that there is a finite set of forbidden pairs of symbols, and that the possible sequences are exactly those that do not contain any forbidden pair. This is an example of one of the fundamental objects to study in symbolic dynamics called a shift of finite type. Later discoveries of Morse, Hedlund [3] and others in the 1920's, 1930's, and 1940's showed that in many circumstances such a finite description of the dynamical systems is possible. These ideas led in the 1960's and 1970's to the development of powerful mathematical tools to investigate a class of extremely interesting mappings called hyperbolic diffeomorphisms.

The symbolic coding of the intervals of a piecewise monotonic map and the study of these symbolic sequences allows us to analyze qualitative aspects of the dynamical system in two perspectives: the kneading theory and the theory of Markov partitions. In this work we mainly follow the results concerning Markov partitions ([4], [5] and [6]).

The kneading theory

Kneading theory, introduced by John Milnor and William Thurston [4] provides an effective calculus for describing the qualitative behavior of the iterates of a piecewise monotone mapping f of a closed interval I of the real line into itself. Applications of the theory include piecewise linear models, counting of fixed points, computing the total variation, and constructing an invariant measure with maximal entropy. Some important topological invariants, such as topological entropy, can be computed in terms of the kneading determinant.

Consider that the map $f : I \to I$, where $I = [a, b]$ is a compact interval of the real line, is a $m-$ modal map and denote by c_j, $j = 1, 2, \ldots, m$ the m critical points of f. This map has $m + 1$ monotone branches, defined on $m + 1$ subintervals $I_i = [c_{i-1}, c_i]$, $1 \leq i \leq m+1$, (consider $c_0 = a$ and $c_{m+1} = b$). We compute the images by $f, f^2, \ldots, f^n, \ldots$ of a critical point c_j, $1 \leq j \leq m$, and we obtain its orbit (1.3). So, any numerical trajectory $x_1 x_2 \ldots x_i \ldots$ in this map corresponds to a symbolic sequence $\sum = S_1 S_2 \ldots S_k \ldots$ where the symbols S_k belongs to the m-modal alphabet, with $2m + 1$ symbols, depending on where the point x_i falls in.

If $f^n(c_j)$ belongs to an open interval $I_i =]c_{i-1}, c_i[$, then we associate to it a symbol L_i with $1 \leq i \leq m + 1$. If $f^n(c_j) = c_k$, $1 \leq k \leq m$, then we associate to it a symbol C_k. So, to each critical points c_j, we associate a symbolic sequence, called the address of $f^n(c_j)$, denoted by $S_0 S_1 S_2 \ldots S_n \ldots$, where the symbols S_k belongs to the m-modal alphabet, with $2m + 1$ symbols.

The set

$$\mathcal{A} = \{L_1, C_1, L_2, C_2, \ldots, L_m, C_m, L_{m+1}\}$$

will be the alphabet of the m-modal map f and the collection of all infinite symbol sequences of $\mathcal{A}$ will be defined by the set

$$\mathcal{A}^{\mathbb{N}} = \left\{x = (x_i)_{i \in \mathbb{N}} : x_i \in \mathcal{A} \text{ for all } i \in \mathbb{N}\right\}.$$

Without lack of generality we assume that the first critical point of the multimodal map f is maxima.

Definition 12 *Let $f : I \to I$ be a $m-$modal map. We define the **address** of $x \in I$, written $ad(x)$, to be one of the symbols L_i, $1 \leq i \leq m + 1$, or C_j, $1 \leq j \leq m$, according*

to:

$$ad\left(x\right)=\begin{cases} L_i, & \text{if } x\in int(I_i) \\ C_j, & \text{if } x=c_j \end{cases}.$$

For a given map, each point x in the interval may serve as a seed that starts an iteration to yield a symbolic sequence, this sequence is called the itinerary of x.

Definition 13 *Let $f:I\to I$ be a $m-$modal map. The **itinerary** of a point $x\in I$ is the sequence of addresses*

$$It_f\left(x\right)=ad\left(x\right),\ ad\left(f\left(x\right)\right),\ ad\left(f^2\left(x\right)\right),\ldots,ad\left(f^n\left(x\right)\right),\ldots, \tag{1.6}$$

*or equivalently, the (possibly infinite) word in the symbols L_i and C_j formed by concatenating the elements of the sequence (1.6). This infinite sequence is the symbolic itinerary of x. We will say that the itinerary $It\left(x\right)$ is **eventually periodic** if there exists an integer $p\geq 1$ so that the address $ad\left(f^n\left(x\right)\right)$ is equal to $ad\left(f^{n+p}\left(x\right)\right)$ for all large n. The smallest of such p will be called the **eventual period**.*

The itineraries of the critical points play a special role in the admissibility conditions of the symbolic sequence. They are also called kneading sequences.

Definition 14 *Let $f:I\to I$ be a $m-$modal map. The itineraries of the critical points of f, $f\left(c_j\right)$, $j=1,2,\ldots,m$ are called the kneading sequences of f*

$$\mathcal{K}_j\left(f\right)=It_f\left(f\left(c_j\right)\right),\ \ j=1,\ldots m$$

and the ordered set of the kneading sequences $\mathcal{K}\left(f\right)=\left(\mathcal{K}_1\left(f\right),\mathcal{K}_2\left(f\right),\ldots,\mathcal{K}_m\left(f\right)\right)$ we call the kneading invariant of the map f.

Notice that $It(x)$ and $It(f(x))$ are related in a very simple way. If $It(x) = S_1S_2S_3....$ so $It(f(x)) = S_2S_3....$, because $f^n(f(x)) = f^{n+1}(x)$. This motivates the definition of the shift map σ on sequences.

Definition 15 *The shift map* $\sigma : \mathcal{A}^{\mathbb{N}} \to \mathcal{A}^{\mathbb{N}}$ *is defined by*

$$\sigma(S_0S_1S_2S_3....) = S_1S_2S_3....$$

If we have a finite sequence $S = S_0S_1S_2 \cdots S_n$ *the shift operator acts*

$$\sigma(S_0S_1S_2 \cdots S_n) = S_1S_2 \cdots S_nS_0$$

In other words, the shift map forgets the first symbol of the sequence. The shift operator acts on admissible sequences of length greater than one.

Many numerical orbits may corrrespond to one and the same symbolic sequence. On the other hand, different symbolic sequences must correspond to different initial points in the phase space. However, an arbitrarily given symbolic sequence, may not be generated in a $m-$modal map. A symbolic sequence is called an admissible sequence at a given parameter, if one can choose an initial point to produce a numerical orbit of the map which leads to the given symbolic sequence, using a given partition of the interval. The admissibility condition is based on the ordering rule of symbolic sequences.

First, we need the notion of parity. To each symbol $L_i \in \mathcal{A}$, with $i \in \{1, 2, \ldots, m+1\}$, let us define a sign $\varepsilon : \mathcal{A} \to \{-1, 0, 1\}$ where

$$\varepsilon(L_i) = \begin{cases} 1, & f \text{ is increasing on the lap } I_i \\ -1, & f \text{ is decreasing on the lap } I_i \end{cases}$$

and $\varepsilon(C_j) = 0$ for all $j = 1, 2, \ldots m$, and adopt the multiplication rule for the signals. For any finite symbolic sequence, $S = S_0 S_1 S_2 \ldots S_n$, we define the parity of S, denoted by $\mathcal{P}(S)$, as

$$\mathcal{P}(S) = \varepsilon(S_0) \cdot \ldots \cdot \varepsilon(S_n)$$

so that, if S represents the beginning of the itinerary of x, then:

1. S is even, i.e, $\mathcal{P}(S) = +$, if f^n is sense-preserving near x,

2. S is odd, i.e, $\mathcal{P}(S) = -$, if f^n is sense-reversing near x.

Second, the ordering of symbolic sequences is based on the natural order of real numbers on the interval. Defining the order on the symbols, one can extend it to an order on the sequences. Let $\mathcal{A}$ denote the set of possible addresses under f. We endow $\mathcal{A}$ with the order in the real axis

$$L_1 \prec C_1 \prec L_2 \prec C_2 \prec \ldots \prec L_m \prec C_m \prec L_{m+1} \tag{1.7}$$

so that

$$ad(x) \prec ad(y) \Rightarrow x < y.$$

Third, an even common leading string preserves the order of subsequences following it, while an odd common leading string reverses the order. Let $\mathcal{A}^{\mathbb{N}}$ be the set of all sequences written with the alphabet $\mathcal{A}$.

Definition 16 *We define an ordering $\prec$ on the set $\mathcal{A}^{\mathbb{N}}$ such that: given two symbolic sequences $P \neq Q$ with a common leading string Σ, where Σ is a finite word in $\mathcal{A}^{\mathbb{N}}$, and the next symbol $P_0 \neq Q_0$, the order of P_0 and Q_0 in the sense of the natural order (1.7)*

is the order of P and Q if Σ is even; the order of P_0 and Q_0 is opposite to that of P and Q if Σ is odd. This is $P \prec Q$ if $P_0 \prec Q_0$ and $\mathcal{P}(\Sigma) = +1$ or $Q_0 \prec P_0$ if $\mathcal{P}(\Sigma) = -1$.

This order is originated by the fact that when $x < y$ then $It_f(x) \preceq It_f(y)$ and $It_f(x) \prec It_f(y)$ then $x < y$.

Denoting the kneading sequences of the critical points c_j by $\mathcal{K}_{c_j}$, the admissibility conditions for a symbolic sequence Σ read

$$\mathcal{K}_{c_{j-1}} \leq \mathcal{L}_j(\Sigma) \leq \mathcal{K}_{c_j} \text{ where } c_j \text{ is a maximal point}$$

or

$$\mathcal{K}_{c_j} \leq \mathcal{L}_j(\Sigma) \leq \mathcal{K}_{c_{j-1}} \text{ where } c_j \text{ is a minimal point}$$

Given an arbitrary sequence Σ, we denote $\mathcal{L}_j(\Sigma)$ the set of all subsequences that follow a letter L_j in the given sequence, the sets $\mathcal{L}_j(\Sigma)$ contains all the shifts of Σ.

Example 1 *Let f be a unimodal map on the interval $I = [a, b]$. The map f has a single critical point c in I, and is monotone increasing on the left of c and decreasing on the right.To set up the symbolic sequence of this system we must first separate the phase space into disjoint regions. By creating this partition we can go from a continuous description of a physical process to a discrete description composed of a finite symbols. We define $I_L = [a, c[$, $I_c = \{c\}$ and $I_R =]c, b]$. Computing the images $f, f^2, \ldots, f^n, \ldots$ of the critical point c we obtain its numerical orbit $O(c)$*

$$O(c) = \left\{x_i : x_i = f^i(c),\ i \in \mathbb{N}^0\right\}$$

We partition the phase space, i.e, the interval I, into a left part L and a right part R. We care only about on which side of c a point $f^i(c)$ falls. If $f^i(c) < c$ we record a

letter L*, while if* $f^i(c) > c$ *a letter* R*. If* $f^i(c) = c$ *we record the letter* C*. In this way, from the numerical orbit* $O(c)$ *we get a symbolic sequence* $S = CS_1S_2 \ldots S_k \ldots$ *where* $S_k \in \{L, C, R\}$*,*

$$S_k = ad\left(f^i(c)\right) = \begin{cases} L & , f^i(c) < c \\ C & , f^i(c) = c \\ R & , f^i(c) > c \end{cases}$$

We define the kneading sequence $\mathcal{K}(f)$ *of the unimodal map* f *to be the itinerary of* $f(c)$*, i.e,* $\mathcal{K}(f) = It_f(f(c))$*. If* $O(c)$ *is a* $k-$*cycle the kneading invariant is* $\mathcal{K}(f) = S_1S_2 \ldots S_kC$*.*

For the unimodal map, considering $\mathcal{A} = \{L, C, R\}$ *we have a natural order* $L < C < R$ *which reflects the order of real numbers on the interval* I*. The parity is inherited in the symbols of applied dynamics, as we always partition the interval in accordance with the monotonicity of the mapping function, so* $\varepsilon(L) = +1$*,* $\varepsilon(R) = -1$ *and* $\varepsilon(C) = 0$*. Given two symbolic sequences* $P = \Sigma\mu \ldots$ *and* $Q = \Sigma\nu \ldots$ *with a common leading string* Σ *and the next symbol* $\mu \neq \nu$*. We say* $P \prec Q$ *if* $\mu \prec \nu$ *and* $\mathcal{P}(\Sigma) = +1$ *or* $P \prec Q$ *and* $\mu \succ \nu$ *if* $\mathcal{P}(\Sigma) = -1$*.*

The admissibility condition is based on the ordering of symbolic sequences and follows from the fact that the kneading sequence $\mathcal{K}(f)$ *is the largest sequence starting from a point in the dynamical invariant range. Given an arbitrary sequence* Σ*, we denote* $\mathcal{L}(\Sigma)$ *the set of all subsequences that follow a letter* L *in the given sequence, and by* $\mathcal{R}(\Sigma)$ *the set of all subsequences that follow a letter* R *in the given sequence. The sets* $\mathcal{L}(\Sigma)$ *and* $\mathcal{R}(\Sigma)$ *contains all the shifts of* Σ*. A symbolic sequence* Σ *is admissible if and only if:*

$$\mathcal{L}(\Sigma) \leq \mathcal{K} \text{ and } \mathcal{R}(\Sigma) \leq \mathcal{K}$$

Let $\mathcal{A}_L = \{L_1, L_2, \ldots, L_m, L_{m+1}\}$ and $\mathcal{A}_C = \{C_1, C_2, \ldots, C_m\}$ be two alphabets

and $\mathcal{A} = \mathcal{A}_L \cup \mathcal{A}_C$. Let $\mathcal{V}$ be a vector space of dimension $m+1$ defined over the integers having the formal symbols in $\mathcal{A}_L$ as a basis, then to each sequence of symbols $S = S_0 S_1 S_2 \ldots S_k \ldots = It_f(x)$, $x \in I$, we can associate a sequence $\theta(x) = \theta_0(x)\,\theta_1(x)\,\theta_2(x)\ldots\theta_k(x)\ldots$ of vectors from $\mathcal{V}$ by setting

$$\theta_k(x) = \prod_{i=0}^{k-1} \varepsilon(S_i)\, S_k$$

where $k > 0$ and

$$\theta_0 = S_0,\ \varepsilon(L_{2j+1}) = +1,\ \varepsilon(L_{2j}) = -1 \text{ and } \varepsilon(C_i) = 0.$$

Choosing a linear order in the vector space $\mathcal{V}$ in such a way that the base vectors satisfy

$$L_1 < L_2 < \ldots < L_m < L_{m+1}$$

we are able to lexicographically order the sequences θ, that is

$$\theta \prec \theta^* \text{ iff } \theta_0 = \theta_0^*, \ldots, \theta_{i-1} = \theta_{i-1}^* \text{ and } \theta_i \prec \theta_i^* \text{ for some integer } i \geq 0.$$

Introducing t as an undetermined variable and taking θ_k as the coefficients of a formal power series in θ, we obtain

$$\theta = \theta_0 + \theta_1 t + \theta_2 t^2 + \ldots = \sum_{k=0}^{+\infty} \theta_k t^k.$$

Milnor and Thurston introduced basic invariants called kneading increments, kneading matrices and kneading determinants.

The kneading increments are formal power series that measure the discontinuity evaluated at the critical points c_j. For the case of a m-modal map we have $m-$ kneading increments, one for each critical point c_j, defined by

$$\upsilon_j = \theta_{c_j^+}(t) - \theta_{c_j^-}(t), \quad j \in 1, 2, \ldots, m \tag{1.8}$$

where $\theta(x)$ is the invariant coordinate of each symbolic sequence associated to the itinerary of each point c_j, and

$$\theta_{c_j^{\pm}}(t) = \lim_{x \to c_j^{\pm}} \theta_x(t).$$

After separating the terms associated with the symbols $L_1, L_2, \ldots, L_m, L_{m+1}$ of the alphabet $\mathcal{A}_L$, the kneading increments υ_j are written in the form

$$\upsilon_j = N_{j1}L_1 + N_{j2}L_2 + \ldots + N_{jm+1}L_{m+1}\ , j = 1, 2, \ldots, m$$

Using this we define the kneading matrix $N_f(t)$ by

$$N_f(t) = [N_{ji}] = \begin{bmatrix} N_{11}(t) & \cdots & N_{1m+1}(t) \\ \vdots & \ddots & \vdots \\ N_{m1}(t) & \cdots & N_{mm+1}(t) \end{bmatrix}$$

This is an $m \times (m+1)$ matrix, with entries in the ring $\mathbb{Z}[[t]]$ of integer formal power series. From this matrix, we compute the kneading determinant which is defined from the kneading matrix by

$$D(t) = (-1)^{j+1} \frac{D_j(t)}{1 - \varepsilon(L_j)\, t},\ j = 1, 2, \ldots, m$$

where $D_j(t)$ is the determinant of the $m \times m$ matrix which is obtained by deleting the $j - th$ column of the kneading matrix $N_f(t)$.

Example 2 *The symbolic orbit of the turning point c, determine the period-5 kneading sequence* $(CRLLL)^{\infty}$. *So we have*

$$c^+ \to (RRLLL)^{\infty} \ \textit{and}\ c^- \to (LRLLL)^{\infty}$$

The invariant coordinates of the sequence $(CRLLL)^{\infty}$ *associated with the critical point* c *are:*

$$\begin{aligned}\theta_{c^+} &= \frac{t^2+t^3+t^4}{1-t^5}L+\frac{1-t}{1-t^5}R\\ \theta_{c^-} &= \frac{1-t^2-t^3-t^4}{1+t^5}L+\frac{t}{1+t^5}R\end{aligned}$$

The kneading increment of the critical point, $\upsilon_c=\theta_{c^+}-\theta_{c^-}$ *is*

$$\upsilon_c=\frac{-1+2t^2+2t^3+2t^4+t^5}{1-t^{10}}L+\frac{1-2t+t^5}{1-t^{10}}R$$

So, the kneading matrix $N_f(t)=\left[\begin{array}{cc} N_{11}(t) & N_{12}(t)\end{array}\right]$, *is*

$$N_f(t)=\left[\begin{array}{cc} \frac{-1+2t^2+2t^3+2t^4+t^5}{1-t^{10}} & \frac{1-2t+t^5}{1-t^{10}}\end{array}\right]$$

and the kneading determinant is

$$D(t)=\frac{1-2t+t^5}{(1-t^{10})(1-t)}.$$

The smallest positive real root of $D(t)$ *determines the topological entropy, i.e,* $h_{top}=-\log t_{\min}$ *. As the smallest positive root is* $t=0.518\,79$ *the topological entropy is* $h_{top}=0.656\,26$ *(see subsection 1.1.2).*

Markov partitions theory

When $O(c)$ is a k-periodic orbit, we obtain a sequence of symbols that can be characterized by a block of length k, the kneading sequence $S^{(k)}=S_1S_2...S_{k-1}C$. The orbit $O(c)$, which is made of k ordered points x_i, determines a partition $\mathcal{P}^{(k-1)}$ of the dynamical invariant range $I=\left[f^2(c),f(c)\right]=[x_2,x_1]$ into $k-1$ subintervals labeled by I_1, I_2,..., I_{k-1}. The subintervals I_i do not overlap with each other. At most they may only have common end points. This partition is associated to a $(k-1)\times(k-1)$ transition matrix $M=[m_{ij}]$,

where the rows and columns are labeled by the subscript of subintervals and the matrix elements are defined as

$$m_{ij} = \begin{cases} 1 & , \ f(I_i) \cap I_j \neq 0 \\ 0 & , \ f(I_i) \cap I_j = 0 \end{cases}$$

Let $\lambda_1, \lambda_2, \ldots, \lambda_{k-1}$ be the eigenvalues of the transition matrix M, then its spectral radius $\rho(M)$ is defined as

$$\rho(M) = \max\{|\lambda_1|, |\lambda_2|, \ldots, |\lambda_{k-1}|\}.$$

1.1.2 Topological Entropy

Dynamical systems generated by iterated maps are used to describe the chaotic behavior of physical and other natural phenomena. The topological entropy of a map is one of the quantitative measures of the complexity of these dynamical systems. It was first introduced in 1965 by Adler, Konheim and McAndrew. Essentially, it is associated with counting the number of monotone branches in $f^n(x)$, or the number of maxima and minima of $f^n(x)$, or the number of orbital points of periodic orbits with period not exceeding n. These three numbers do not differ much from each other.

The topological entropy describes in a suggestive way the exponential complexity of the orbit structure with a single nonnegative real number [7]. For a system given by an iterated function, the topological entropy represents the exponential growth rate of the number of distinguishable orbits of the iterates.

Definition 17 *The **growth rate** of the lap number of f^n (f^n denotes the n^{th} iterate of f) is*

$$s(f) = \lim_{n\to\infty} \sqrt[n]{\ell(f^n)}$$

Definition 18 *The topological entropy of a map f, denoted by $h_{top}(f)$, is given by*

$$h_{top}(f) = \log s(f).$$

For a piecewise linear Markov map, f, the topological entropy is given by

$$h_{top}(f) = \log \lambda_{\max}(M(f)),$$

where $\lambda_{\max}(M(f))$ is the spectral radius of the transition matrix $M(f)$ ([4], [5] and [8]).

Example 3 *Consider the period 5 kneading sequence $(RLLRC)^{\infty}$. Its successive orbital points are obtained by shifting the periodic sequence by one letter at a time, i.e*

$$\begin{aligned} x_0 &= CRLLRCRLLR\ldots \\ x_1 &= RLLRCRLLRC\ldots \\ x_2 &= LLRCRLLRCR\ldots \\ x_3 &= LRCRLLRCRL\ldots \\ x_4 &= RCRLLRCRLL\ldots \\ x_5 &= x_0 \end{aligned}$$

These points are ordered in the following way:

$$x_2 < x_3 < x_0 < x_4 < x_1$$

The dynamical invariant $U = [x_2, x_1]$ is now divided into four subintervals $I_1 = [x_2, x_3]$, $I_2 = [x_3, x_0]$, $I_3 = [x_0, x_4]$ and $I_4 = [x_4, x_1]$. It follows from monotonicity and continuity consideration that these subintervals map into each other:

$$f(I_1) = I_2 \cup I_3,\ f(I_2) = I_4,\ f(I_3) = I_3 \cup I_4 \text{ and } f(I_4) = I_1 \cup I_2$$

This result may be represented by a transfer matrix

$$M = \begin{bmatrix} 0 & 1 & 1 & 0 \\ 0 & 0 & 0 & 1 \\ 0 & 0 & 1 & 1 \\ 1 & 1 & 0 & 0 \end{bmatrix}$$

The characteristic polynomial associated with the transition matrix is

$$P_M(t) = 1 - t - t^2 - t^3 + t^4$$

and consequently the spectral radius of $M, \rho(M) = 1.7221$ *and consequently the topological entropy of the map is given by* $h_{top} = \log 1.722\,1 = 0.54354$.

1.2 Lyapunov exponents, Kaplan-Yorke dimension and predictability

Lyapunov exponents, dimensions and entropies are different ways of characterizing properties for chaotic attractors. How closely dynamics and geometry are related is expressed by theoretical results which relate Lyapunov exponents (dynamics) and dimensions (geometry). In this section, we measure the Lyapunov exponents, the Kaplan-Yorke dimension and the predictability.

1.2.1 Lyapunov exponents

A convenient indicator of the exponential divergence of initially close points, characteristic of the chaotic attractors, are the Lyapunov exponents. In a complete data analysis we would like to determine all the Lyapunov exponents ([9], [10], [11]). A discussion about the Lyapunov exponents as a quantitative measure of the rate of separation of infinitesimally closed trajectories, as well as a computation method, can be found in [12]. In the next lines, we will briefly explain the procedure used to compute the Lyapunov exponents.

This mathematical derivation of the Lyapunov characteristic exponents is followed by its interpretation with respect to the determination of the Kaplan-Yorke dimension and the predictability. The characteristic Lyapunov exponents measure the typical rate of exponential divergence of nearby trajectories in the phase space, i. e., they give us information on the rate of growth of a very small error on the initial state of the system.

Let us consider a set of nonlinear evolution equations of the form

$$\dot{\mathbf{x}} = \mathbf{F}(\mathbf{x}, t) \tag{1.9}$$

where $\mathbf{x} = (x_1, x_2, ..., x_n) \in \mathbb{R}^n$ $(n \geq 3)$ and $\mathbf{F} = (F_1, F_2, ..., F_n)$ is a differentiable function. Assuming that the motion takes place in a bounded region of the phase space, we study the infinitesimal distance between two trajectories, $\delta\mathbf{x}(t) = \mathbf{x}(t) - \mathbf{x}^*(t)$, which is regarded as a vector, $\boldsymbol{\eta}(t) = (\eta_1(t), \eta_2(t), ..., \eta_n(t))^T$, satisfying the linear equation $\dot{\boldsymbol{\eta}} = \mathbf{J}\ \boldsymbol{\eta}$. Solving this linear law over the time range $t_0 \leq t \leq t_f$, we obtain a solution of vectors $\boldsymbol{\nu}_i(t) \in \mathbb{R}^n$ $(i = 1, 2, ..., n)$. Now, let us consider orthogonal vectors to $\boldsymbol{\nu}_i(t)$, with norm represented by $N_i(j)$, for every time step $\tau = t_{j+1} - t_j$, $j = 0, 1, ..., m$ and $m = \frac{t_f - t_0}{\tau}$. The Lyapunov exponents for the nonlinear system of differential equations are given by

$$\lambda_i = \lim_{m \longrightarrow +\infty} \frac{\sum_{j=1}^{m} \ln N_i(j)}{m\tau} \qquad (i = 1, 2, ..., n)\,. \tag{1.10}$$

The Lyapunov exponents and the topological entropy are both suitable tools for the description of chaotic behavior. In the literature, the positive topological entropy and the positivity of the leading Lyapunov exponent are introduced as two important definitions of chaos. These two definitions are not equivalent but they share the same nature, i. e., the sensitive dependence on initial conditions. This sensitivity is very suitable for qualitative analysis, however it is not particularly fit for quantitative computation [13].

The numerical results presented in the literature indicate that any map that is strictly hyperbolic, i. e., a map for which the absolute value of the first derivative is everywhere greater than 1, displays rapid convergence of the topological and metrical entropies to the maximum Lyapunov exponent. These type of maps have no infinite singularities in their asymptotic invariant probability distributions. In contrast to these systems, if the underlying dynamics has singularities in its asymptotic distribution, then one might expect an overestimation (or slow convergence) of the topological entropy to the maximum Lyapunov exponent. This is precisely the typical discrepancy that occurs in logistic-type maps, like the ones we have studied ([13], [14], [15]).

1.2.2 Kaplan-Yorke dimension

The Kaplan-Yorke dimension (commonly called Lyapunov dimension) is elegantly related to the Lyapunov exponents. By ordering the Lyapunov exponents from the largest (most positive) to the smallest (most negative), it is a simple matter to count the maximum number of exponents whose cumulative sum is positive. Let $\lambda_1 \geqslant \lambda_2 \geqslant ... \geqslant \lambda_n$ be the Lyapunov exponents of an attractor of a continuos-time dynamical system. Let k be the largest integer such that $\lambda_1 + \lambda_2 + ... + \lambda_k \geqslant 0$. The Kaplan-Yorke dimension is given by

$$D_L = k + \frac{\lambda_1 + \lambda_2 + ... + \lambda_k}{|\lambda_{k+1}|}.$$

If no such k exists, as is the case for a stable hyperbolic equilibrium point, D_L is defined to be 0. If the attractor is chaotic, the Kaplan-Yorke dimension is almost always a non-integer (please see [12], for more details about the computation method of the Lyapunov dimension). This illustrates the relationship between dynamics (Lyapunov exponents) and attractor geometry. The Lyapunov dimension D_L represents the upper bound for the

information dimension of the system [16]. This consideration motivates the study of another important dynamical measure related with the Lyapunov exponents - dynamics predictability.

1.2.3 Predictability

The ability to predict the future state of a dynamical system, given the present one, turns out to be particularly relevant with major implications in applied biology.

The development of studies with the purpose of quantitatively characterizing and formalizing the sensitivity to initial conditions have had special importance on the theory of dynamical systems. Two tightly linked indicators for measuring the rate of the error growth and information produced by a dynamical system are: the Lyapunov exponents and the Kolmogorov-Sinai (or metric) entropy [15]. In this context, the special connection between these two indicators allows us to characterize fine-grained properties of the system. The maximal Lyapunov exponent, λ_1, gives us a first quantitative information on how fast we lose the ability of predicting the system evolution. The sum of the all positive Lyapunov characteristic exponents gives us an estimate of a more physical quantity called Kolmogorov-Sinai (or metric) entropy ([15], [17], [18], [19], [20]),

$$h_{KS} = \sum_{\lambda_i > 0} \lambda_i.$$

This intrinsic invariant quantity of the system has a singular relevance for the characterization of the predictability. Dynamically, the inverse of the Kolmogorov-Sinai entropy,

$$P = \frac{1}{h_{KS}}, \tag{1.11}$$

characterizes the predictability of the system. The predictability denotes a mean time

scale up to which predictions may be possible [16]. Naturally, higher values of h_{KS} imply lower values of the predictability $1/h_{KS}$, that is, the more chaotic, the less predictable.

1.3 The homotopy analysis method

Given the remarkable importance of models in applied mathematics, particularly in biology and life sciences, a great deal of numerical algorithms for approximating solutions have been used in diverse computational studies. Without doubt the numerical algorithms have been extremely important in the study of complex dynamical systems. However, they allow us to analyze the dynamics at discrete points only, thereby making it impossible to obtain continuous solutions.

In general, exact, closed-form solutions of nonlinear equations are extremely difficult to obtain. Perturbation techniques have been successfully used to solve many nonlinear equations. Indeed, the use of perturbation methods represents a considerable contribution to the understanding and development of nonlinear science. Usually based on small/large physical parameters (called perturbation quantities), perturbation methods transform a nonlinear equation into sub-problems that are mostly linear. However, a great deal of nonlinear equations do not contain such kind of perturbation quantities at all. Unfortunately, the analytic approximations gained with perturbation techniques often become invalid when the perturbation quantities enlarge. In addition, given the strong dependence of perturbation methods upon physical small parameters, we have nearly no freedom to choose equation-type and solution expression of high-order approximation equations, which are often very difficult to solve. Due to these restrictions, perturbation methods are mostly valid in the context of weakly nonlinear problems.

One the other hand, some non-perturbation methods, such as Lyapunov's Artificial Small Parameter Method [21], the δ-expansion method [22, 23] and the Adomian's decomposition method [24, 25, 26, 27], were proposed in the literature. Essentially, both of these two methods transform a nonlinear problem into linear sub-problems without small physical parameters. Nevertheless, they have two main restrictions, namely: there is no freedom and flexibility to choose the nonlinear operators involved in the methodology and there is no way to guarantee the convergence of the approximation series solutions. Therefore, like perturbation methods, the traditional non-perturbation methods are often valid for weakly nonlinear problems.

As a consequence, it turns out to be extremely valuable to develop a new kind of analytic approximation methodology which should have three fundamental characteristics: (i) It is independent of any small/large physical parameters; (ii) It gives us freedom and flexibility to choose equation-type and solution expression of high-order approximation series; (iii) It provides us a convenient way to guarantee the convergence of approximation series.

One such general analytic technique, which has the three advantages mentioned above, used to get convergent series solutions of strongly nonlinear problems is the so-called Homotopy Analysis Method (HAM), developed by Shijun Liao (see, for instance, [28], [29] and [30]), with contributions of other researchers in theory and applications.

In this context, nearly all limitations and restrictions of the traditional methods (such as the Lyapunov's Artificial Small Parameter Method [21], the Adomian Decomposition Method ([24], [25] and [31]), among others) can be overcome by means of HAM. In addition, it has been generally proved in the literature ([29], [32] and [33]) that the Lyapunov's

Artificial Small Parameter Method [21], the Adomian Decomposition Method ([24], [25] and [31]) and the so-called Homotopy Perturbation Method are special cases of the HAM, for some convenient choice of an auxiliary operator and a particular value of a convergence control parameter h. In particular the Homotopy Perturbation Method, that appeared in the literature after the early work of Liao, was only a special case of the HAM for $h = -1$.

Based on *homotopy*, a fundamental concept in topology and differential geometry [34], the HAM allows us to construct a continuous mapping of an initial guess approximation to the exact solutions of the considered equations, using a chosen linear operator. Indeed, the method enjoys considerable freedom in choosing auxiliary linear operators. The HAM represents a truly significant milestone that converts a complicated nonlinear problem into an infinite number of simpler linear sub-problems [30]. Since Liao's work [29], the HAM has been successfully employed in fluid dynamics [35], in the Fitzhugh-Nagumo model [36], as well as to obtain soliton solutions also for the Fitzhugh-Nagumo system [37]. This analytical technique has been also used in complex systems in ecology [38, 39], in epidemiology [40], as well as in models of interactions between tumors and oncolytic viruses [41].

Frequently, in order to have an effective analytical approach of strongly nonlinear equations for higher values of time t, the simple idea is to apply the HAM in a sequence of subintervals of time with a certain step, giving rise to the so-called Step Homotopy Analysis Method (SHAM). In fact, the homotopy analysis methodology is more general in theory and widely valid in practice for the study of nonlinear problems than other analytic approximation procedures. Indeed, this methodology has been successfully applied to solve a wide variety of nonlinear problems (please see for instance, [42], [43], [44] references

therein), particularly, there has been a growing interest in applying HAM to biological models (please see some illustrative examples in [40]).

In this thesis, based on the notations and definitions of the HAM, we investigate the applicability and effectiveness of the SHAM for finding accurate analytical solutions. This newly developed analytical technique was lately applied to the fractional Lorenz system [45].

1.3.1 Explicit series solution

For the sake of clarity, we outline in this section a brief description of the HAM (please see [29], [40], [42] and references therein). The analytical approach will be used in a sequence of intervals, giving rise to the step homotopy analysis method. In the context of HAM, each equation of a system of ordinary differential equations

$$\dot{x}_i = f_i\left(t, x_1, ..., x_n\right), \; x_i(t_0) = x_{i,0}, \; i = 1, 2, ..., n, \tag{1.12}$$

can be written in the form

$$\mathcal{N}_i\left[x_1(t), x_2(t)..., x_n(t)\right] = 0, \; i = 1, 2, ..., n,$$

where $\mathcal{N}_1, \mathcal{N}_2, ..., \mathcal{N}_n$ are nonlinear operators, $x_1(t), x_2(t)..., x_n(t)$ are unknown functions and t denotes the independent variable. The analytical procedure starts with a construction of the so-called *zeroth-order deformation equation*

$$(1-q)\, L\left[\phi_i\left(t;q\right) - x_{i,0}(t)\right] = qh\mathcal{N}_i\left[\phi_1\left(t;q\right), ..., \phi_n\left(t;q\right)\right], \tag{1.13}$$

where $q \in [0,1]$ is called *the homotopy embedding parameter*, h is *the convergence control parameter,* L is an auxiliary linear operator, $x_{i,0}(t)$ are initial guesses for the solutions and

$\phi_i(t;q)$ are unknown functions. It is clear that when $q=0$ and $q=1$, it holds

$$\phi_i(t;0) = x_{i,0}(t) \text{ and } \phi_i(t;1) = x_i(t).$$

Following (1.13), when q increases from 0 to 1, the function $\phi_i(t;q)$ varies from the initial guess $x_{i,0}(t)$ to the solution $x_i(t)$. Expanding $\phi_i(t;q)$ in MacLaurin series with respect to q at $q=0$, we get

$$\phi_i(t;q) = x_{i,0}(t) + \sum_{m=1}^{+\infty} x_{i,m}(t) q^m, \tag{1.14}$$

where the series coefficients x_i are defined by

$$x_{i,m}(t) = \frac{1}{m!} \frac{\partial^m \phi_i(t;q)}{\partial q^m}\bigg|_{q=0}. \tag{1.15}$$

Considering the convergence of the homotopy series (1.14) and using the relation $x_i(t) = \phi_i(t;1)$ we obtain the so-called homotopy series solutions

$$x_i(t) = x_{i,0}(t) + \sum_{m=1}^{+\infty} x_{i,m}(t), \quad i = 1,2,...,n,$$

which are precisely the solutions of the original nonlinear equations. Differentiating the $zero^{th}$-order deformation Eqs. (1.13) m times with respect to the homotopy parameter q, we obtain the m^{th}-order deformation equations

$$L\left[x_{i,m}(t) - \chi_m x_{i,m-1}(t)\right] = h\mathcal{R}_{i,m}\left[x_{1,m-1}(t),...,x_{n,m-1}(t)\right], \quad i = 1,2,...,n, \tag{1.16}$$

where

$$\mathcal{R}_{i,m}\left[x_{1,m-1}(t),...,x_{n,m-1}(t)\right] = \frac{1}{(m-1)!} \frac{\partial^{m-1} \mathcal{N}_i\left[\phi_1(t;q),...,\phi_n(t;q)\right]}{\partial q^{m-1}}\bigg|_{q=0}$$

and

$$\chi_m = \begin{cases} 0, & m \leq 1 \\ 1, & m > 1 \end{cases}.$$

A one-parameter family of explicit series solutions is obtained by solving the linear equations (1.16). In the presence of some strongly nonlinear problems, it is usually appropriate to apply the HAM in a sequence of subintervals giving rise to the so-called Step Homotopy Analysis Method (SHAM).

1.3.2 Interval of convergence and optimum value from an appropriate ratio

Following [46], let us consider $k+1$ homotopy terms $x_0(t)$, $x_1(t)$, $x_2(t)$, ..., $x_k(t)$ of an homotopy series

$$x(t) = x_0(t) + \sum_{m=1}^{+\infty} x_m(t). \tag{1.17}$$

For a preassigned value of parameter h, the convergence of the homotopy series is not affected by a finite number of terms. Therefore, it is sufficient to keep track of magnitudes of the ratio defined by

$$\left| \frac{x_k(t)}{x_{k-1}(t)} \right| \tag{1.18}$$

and whether it remains less than unity for increasing values of k. Taking (1.18), and requiring this ratio to be as close to zero as possible, we can determine an optimal value for the convergence control parameter h. For such a value, the rate of convergence of the homotopy series (1.17) will be the fastest (and as a consequence, the remainder of the series will rapidly decay). For a prescribed h, if the ratio is less than unity, then the convergence of HAM is guaranteed. In other words, this is a sufficient condition for the convergence of the homotopy analysis method. This implies that in the cases where the limit for the ratio in (1.18) cannot be reached or tends to unity, the method may still

converge or fail to do so. It is appropriate to search for an optimum value of h, i.e., a value of h that gives rise to a ratio (1.18) as small as possible. Taking a time interval Ω, the ratio

$$\beta = \frac{\int_{\Omega} [x_k(t)]^2 \, dt}{\int_{\Omega} [x_{k-1}(t)]^2 \, dt}$$

represents a more convenient way of evaluating the convergence control parameter h. In fact, given an order of approximation, the curves of ratio β versus h indicate not only the effective region for the convergence control parameter h, but also the optimal value of h that corresponds to the minimum of β. Now, plotting β versus h, as well as by solving

$$\frac{\int_{\Omega} [x_k(t)]^2 \, dt}{\int_{\Omega} [x_{k-1}(t)]^2 \, dt} < 1 \quad \text{and} \quad \frac{d\beta}{dh} = 0,$$

the interval of convergence and the optimum value for parameter h can be simultaneously achieved.

1.4 Positively invariant sets

A significant preliminary question to answer before doing any further analysis of the long-term behavior of chaotic attractors is to find conditions for which trajectories will not "escape to infinity", so that they will remain confined to a compact set [47]. Taking a system of three ordinary differential equations of the form

$$\begin{cases} \frac{dx_1}{dt} = f_{x_1}(x_1, x_2, x_3) \\ \frac{dx_2}{dt} = f_{x_2}(x_1, x_2, x_3) \\ \frac{dx_3}{dt} = f_{x_3}(x_1, x_2, x_3) \end{cases},$$

let us consider a new function $\Psi = x_1 + x_2 + x_3$, i.e., the sum of the dynamical variables involved in the 3D system. The temporal derivative of Ψ is

$$\frac{d\Psi}{dt} = \frac{dx_1}{dt} + \frac{dx_2}{dt} + \frac{dx_3}{dt}.$$

Adding $\varepsilon\Psi$ to $\frac{d\Psi}{dt}$, gives $\frac{d\Psi}{dt} + \varepsilon\Psi = \chi(\vec{x})$, for $\varepsilon > 0$. An upper bound of $\chi(\vec{x})$ is given by $\chi(\vec{x}) \leq L$. It follows that $d\Psi/dt \leq -\varepsilon\Psi + L$. Using the differential form of the Gronwall's inequality [48], we find

$$\Psi(t) \leq \Psi(0)e^{-\varepsilon t} + \frac{L}{\varepsilon}\left(1 - e^{-\varepsilon t}\right) \leq \max\left(\frac{L}{\varepsilon}, \Psi(0)\right).$$

Therefore, we can conclude that the trajectories starting from any arbitrary initial condition will remain confined to a compact set.

1.5 Observability analysis

When a dynamical system is investigated, there are usually some variables that provide a better representation of the underlying dynamics. More precisely, in a number of practical situations, the choice of the *observable* does influence our ability to extract dynamical information of a given attractor. This fact results, in a considerable degree, from the complexity of the coupling between the dynamical variables. With the computation of *observability indices*, this coupling complexity can be estimated and the variables can be ranked [49, 50, 51]. In the context of nonlinear dynamics, the choice of the observable has a direct relation with problems such as control, model building and synchronization (see [50] and references therein). It is important to notice that, despite the potential practical importance of this concept, observability has not been commonly addressed by the research community in theoretical biology. The following method thus provides an

illustration of how our understanding of nonlinear problems can be enhanced by the theory of observability. In the next lines we perform an observability analysis which involves a mathematical structure provided by the theory of observability - the definition of the *observability matrix* [49, 50, 51]. Let us consider a dynamical system

$$\frac{d\mathbf{x}}{dt}(t) = \mathbf{f}(\mathbf{x}(t)),$$

where t is the time, $\mathbf{x} \in \mathbb{R}^m$ is the state vector and $\mathbf{f}$ is the nonlinear vector field. This system is called the *original system*. The observable variable is obtained using a measurement function $h : \mathbb{R}^m \to \mathbb{R}$, such that $s(t) = h(\mathbf{x}(t))$. In this work our system has three ordinary differential equations ($m = 3$) of the form

$$\begin{cases} \frac{dx_1}{dt} = f_{x_1}(x_1, x_2, x_3) \\ \frac{dx_2}{dt} = f_{x_2}(x_1, x_2, x_3) \\ \frac{dx_3}{dt} = f_{x_3}(x_1, x_2, x_3) \end{cases},$$

which can be reconstructed in a three-dimensional space. More precisely, using a variable s, the reconstructed portrait is spanned by the derivative coordinates according to

$$\begin{cases} X_1 = s \\ X_2 = \frac{ds}{dt} \\ X_3 = \frac{d^2s}{dt^2} \end{cases}.$$

The successive temporal derivatives of s constitute a *derivative vector*. The dynamics of this space defined by the three derivative coordinates is expected to be equivalent, in a certain sense, to the dynamics of the system defined by the original coordinates. In order to analyze the quality of the reconstructed space, we study the properties of a coordinate

transformation Φ_s between the original dynamical variables and the derivative coordinates,

$$(x_1, x_2, x_3) \overset{\Phi_s}{\rightarrow} (X_1, X_2, X_3)\,,$$

where the subscript s indicates the dynamical variable from which the reconstruction is undertaken. For the observable variable s, the transformation Φ_s reads

$$\Phi_s = \begin{cases} X_1 = s \\ X_2 = \frac{ds}{dt} = f_s \\ X_3 = \frac{d^2s}{dt^2} = \frac{\partial f_s}{\partial x_1} f_{x_1} + \frac{\partial f_s}{\partial x_2} f_{x_2} + \frac{\partial f_s}{\partial x_3} f_{x_3} \end{cases},$$

where f_s can either represent f_{x_1}, f_{x_2}, or f_{x_3}, which are the three components of the vector field $\mathbf{f}$. The coordinate transformation contains information on the nature of the coupling between the dynamical variables "seen from one observable point of view". In our study, we are going to consider three coordinate transformations Φ_{x_1}, Φ_{x_2} and Φ_{x_3}. In the context of the observability theory, it is critical to investigate in what conditions a dynamical state can be constructed from a single variable and how the nature of the couplings may effect the observability of a given system.

Theoretically, in order to reconstruct a dynamical state from s, the striking case occurs when the transformation Φ_s defines a diffeomorphism, i. e., Φ_s is a continuous invertible function whose inverse is differentiable. In other words, the coordinate transformation Φ_s defines a diffeomorphism from the original phase in the reconstructed one if the determinant of its jacobian matrix, $J(\Phi_s)$, never vanishes for each point of the phase space.

Therefore, the study of the jacobian matrix $J(\Phi_s)$ is critical and gives us relevant information for the characterization of the coordinate transformation Φ_s. In particular, the map Φ_s is locally invertible at a given point $\mathbf{x_0}$ if the Jacobian matrix has full rank,

i.e., if $rank\left(\frac{\partial \Phi_s}{\partial \mathbf{x}}\big|_{\mathbf{x}=\mathbf{x_0}}\right) = m$. As a consequence, the original dynamical system is locally observable if the previous sufficient condition for local invertibility holds. A central result of the observability theory establishes that the Jacobian matrix $J(\Phi_s)$ can be interpreted as the *observability matrix*, O_s, defined for nonlinear systems [50]. This definition for O_s provides a clear link between the observability of a dynamical system, from an observable s, and the existence of singularities in Φ_s, which seemed to be lacking in the literature. In the context of nonlinear systems, there are regions in phase space that are naturally less observable than others. Following [50], the degree of observability attained from a given variable is quantified with the respective observability index using a value average along an orbit

$$\delta_s = \frac{1}{t_f}\sum_{t=0}^{t_f}\frac{\left|\lambda_{\min}[O_s^T O_s, \mathbf{x}(t)]\right|}{|\lambda_{\max}[O_s^T O_s, \mathbf{x}(t)]|}, \tag{1.19}$$

where t_f is the final time considered (without loss of generality the initial time was set to be $t = 0$) and T represents the transposition of matrices. The term $\lambda_{\min}[O_s^T O_s, \mathbf{x}(t)]$ indicates the minimum eigenvalue of matrix $O_s^T O_s$ estimated at a point $\mathbf{x}(t)$ (likewise for $\lambda_{\max}[O_s^T O_s, \mathbf{x}(t)]$). Hence, $0 \leq \delta_s \leq 1$, and the lower bound of $\delta_s(\mathbf{x})$ is reached when the system is unobservable at point $\mathbf{x}(t)$. It is important to emphasize that the observability indices are local quantities interpreted as relative values and the established average is particularly useful in order to portray an overall picture of the coupling complexity between the dynamical variables. Each time series arises from a given set of parameters of a particular system. In this sense, being a function of a dynamical state $\mathbf{x}(t)$, the observability indices are considered local quantities in terms of the parameter values. Given the orbit $\mathbf{x}(t)$, the observability value results from a time average over that orbit. In this

sense, the observability indices are considered averaged values along an orbit.

Our present application of the outlined formalism, where the observability matrix is interpreted as the Jacobian matrix of the coordinate transformation in study, $O_s = J(\Phi_s)$, leads to the computation of the observability indices of x_1, x_2 and x_3. From the previous values, the variables can be ranked in descending degree of observability.

Chapter 2

Topological complexity and predictability in the dynamics of a tumor growth model with Shilnikov's chaos[1]

Cancer is a generic term which designates a large class of diseases with a common pattern: the normal mechanism of cells proliferation and programmed death breaks down, giving place to a rapid creation of abnormal cells, which can grow beyond their usual boundaries and invade other organs. Due to the considerable medical, scientific and technological improvements over the last years, several cancers can be detected early and effective treatments exist. However, despite these remarkable advances, our understanding of cancer is far from complete and an established cure for this disease remains elusive, extremely difficult to discover [53].

The analysis of cancer growth systems is, without doubt, critical to any attempt to study important phenomena involved in tumor growth and to predict its future behavior. Tumor growth systems represent a web of complex interactions among different body

[1]This study has been published in [52].

cells, depending upon many key factors such as tumor severity, patient age, sex and immune system state, or treatment strategy, among other factors. The analysis and the understanding of this physiological complexity, historically studied through experimental and clinical observations, can be complemented with the study of mathematical models that incorporate critical interactions between tumor cells, healthy tissue cells and activated immune cells. It has been shown in the literature that these interactions are the main components of these models which may yield a variety of dynamical outcomes ([53], [54], [55], [56], [57] and [58]).

The interest of applying chaos theory to biological systems, more specifically to chaotic tumor dynamics, relies in that chaos can give place to recognizable, repeatable structures at different scales, such as fractals, and both topological and dynamical properties can be studied to determine important and practical measures like predictability. In this context, chaotic behavior was recently reported in the Itik-Banks cancer model [59]. Itik and Banks showed, by applying Shilnikov's theorem, that system Eqs. (2.1)-(2.3) has Shilnikov-like connections [59]. Roughly, such a theorem states that a dynamical system contains (an infinite number of) Smale horseshoes, if it has a Shilnikov connection (i.e., homoclinic or near homoclinic connection) consisting of a hyperbolic fixed point with a two-dimensional stable (spiral) and a one-dimensional unstable manifold. Together with the application of Shilnikov's theorem, the authors computed the Lyapunov exponents (hereafter LE) for a single parameter combination, obtaining one positive LE, thus numerically characterizing chaos. They finally computed the Lyapunov dimension also for the same single parameter combination, obtaining a fractal dimension near to the dimension of the Rössler attractor [60]. The analyses of Itik and Banks identified a new chaotic attractor and left open

a collection of questions pertaining to chaotic tumor behavior in terms of symbolic dynamics, chaos generating mechanisms and measurements of complexity corresponding to physiological relevant parameter regions.

In the present chapter we analyze both topological and dynamical properties of the strange attractor found in the Itik-Banks model. This chapter is organized as follows. In Section 2.1 we explain the mathematical model analyzed. Section 2.2, which includes the analyses of the chaotic attractor, is divided into two subsections. In the first subsection we study the iterated maps in terms of symbolic dynamics theory, computing the topological entropy focusing on two key parameters determining inactivation of effector and tumor cells. Here we also compute codimension-two bifurcation diagrams showing the ordering periods for the same parameters. The second subsection includes the computation of the spectrum of Lyapunov exponents, the fractal dimension, and the predictability of the dynamics. In short, we numerically prove the existence of chaotic scenarios described by Itik and Banks which are characterized by positive topological entropy and positive maximal Lyapunov exponent of the three-dimensional cancer model. We find that the dynamics is eminently sensitive to the effector cells inactivation rate by the tumor cells, given by parameter a_{31}. We also found that the dynamics in the chaotic attractor is highly unpredictable at low inactivation rates of effector cells by tumor cells. In the Conclusions Section we interpret the identified properties of the chaotic attractor in terms of cancer cells viability.

2.1 Mathematical model of tumor growth

We analyze the Itik-Banks cancer model [59], which considers three interacting cell populations: tumor cells, healthy host cells and effector immune cells. Effector cells are the relative short-lived activated cells of the immune system that defend the body in an immune response. This model describes important aspects of the growth cancer dynamics in a well-mixed system (e.g., liquid cancers such as leukemia, lymphoma or myeloma). In order to simplify the mathematical analysis, the initial model was non-dimensionalized by Itik and Banks [59]. The scaled resulting system of differential equations is given by

$$\frac{dx_1}{dt} = x_1\left(1 - x_1\right) - a_{12}x_1x_2 - a_{13}x_1x_3, \tag{2.1}$$

$$\frac{dx_2}{dt} = r_2x_2\left(1 - x_2\right) - a_{21}x_1x_2, \tag{2.2}$$

$$\frac{dx_3}{dt} = \frac{r_3x_1x_3}{x_1 + k_3} - a_{31}x_1x_3 - d_3x_3. \tag{2.3}$$

The variables x_1, x_2 and x_3 denote, respectively, the fraction of tumor cells, healthy host cells and effector immune cells against their specific maxima carrying capacities k_1, k_2 and k_3 (see *Section 2* in [59]). In the context of biology, the dimensionless parameters have the meaning and values (or range) presented in the Table 2.1.

We use the same parameter values of [59], focusing our work on the study of parameters a_{13} and a_{31}. These parameters are chosen to analyze the effect of the inactivation interactions between tumor and effector immune cells in the outcome of the overall population dynamics of the three cell types. Of special interest is parameter a_{31}, since tumor-induced immunosuppression in cancer has strong implications in growth, expansion and differentiation of cancer stem cells [61]. For the sake of clarity, we briefly explain the biological meaning of such parameters, which are given by $a_{13} = \tilde{a}_{13}k_3/r_1$ (i.e., inactivation of tumor

Variables and parameters		Meaning
Dependent variables	x_1	fraction of tumor cells
	x_2	fraction of healthy host cells
	x_3	fraction of effector immune cells
Parameters	a_{12}	tumor cells inactivation rate by the healthy cells: $a_{12} = 1.0$
	a_{21}	healthy cells inactivation rate by the tumor cells: $a_{21} = 1.5$
	a_{13}	tumor cells inactivation rate by the effector cells: $0.05 \leq a_{13} \leq 10$
	a_{31}	effector cells inactivation rate by the tumor cells: $0.9 \leq a_{31} \leq 1.5$
	r_2	intrinsic growth rate of the healthy tissue cells: $r_2 = 0.6$
	r_3	proliferation rate of the effector cells: $r_3 = 4.5$
	d_3	density-dependent death rate of the effector cells: $d_3 = 0.5$
	k_3	maximum carrying capacity of effector cells: $k_3 = 1.0$

Table 2.1: List of variables and parameters.

cells by effector cells) and $a_{31} = \tilde{a}_{31}k_1/r_1$ (inactivation of effector cells by tumor cells). Here $\tilde{a}_{13}$ and $\tilde{a}_{31}$ are the values of the parameters before the non-dimensionalization of the original model presented in [59]. The parameter k_1 denotes the maximum carrying capacity of tumor cells that grow logistically. Parameter r_1 corresponds to the proliferation rate of tumor cells while r_3 denotes the proliferation rate of the immune system effector cells, which depends on the density-dependent interaction between effector and tumor cells and the constant k_3, included in the first saturating term of Eq.(2.3) (see [59] for a detailed description of the model and the parameters). We will hereafter use as initial conditions:

$$x_1(0) = 0.22459..., x_2(0) = 0.48945... \text{ and } x_3(0) = 0.13534....$$

2.2 Chaos in tumor growth: Topological and dynamical properties

In this section we study numerically the dynamical behavior of the Itik-Banks model, paying special attention to the regime of chaos. Using numerical integration and after discarding the initial transient, we show the strange attractor governing the dynamics of

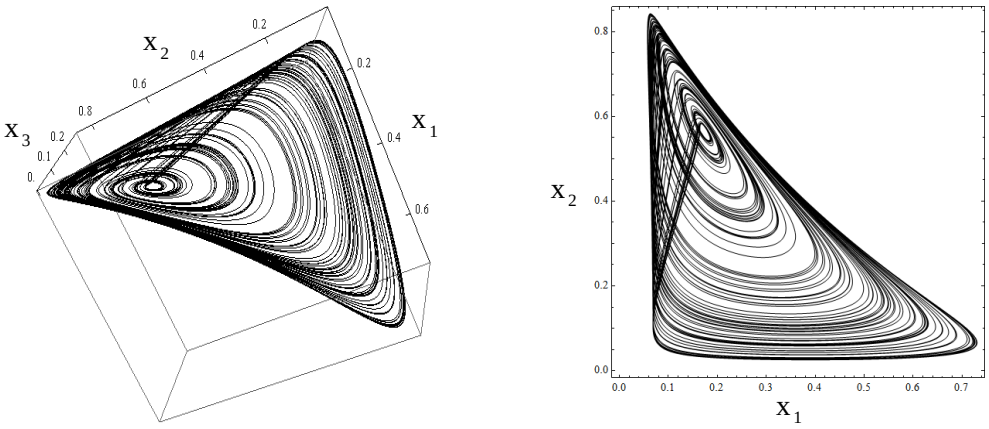

Figure 2.1: Strange attractor obtained from Eqs. (2.1)-(2.3) visualized in three-dimensional (left) and two-dimensional (right) phase space (with $a_{13} = 5.0$ and $a_{31} = 0.9435$).

the system Eqs. (2.1)-(2.3) in the $(x_1(t), x_2(t), x_3(t))$ phase space (Fig. 2.1 left) as well as a projection in the (x_1, x_2) phase space (Fig. 2.1 right). To start with, we present a family of one-dimensional iterated maps we identified studying the intrinsic properties of the dynamics. These maps are used to compute the topological entropy and to characterize special orbits in the parameter space in terms of symbolic dynamics theory. Furthermore, taking advantage of the computation of the whole spectrum of Lyapunov exponents, we measure the fractal dimension of the chaotic sets also determining how predictability changes under the influence of inactivation rates between tumor and effector cells. It is worth mentioning that Itik and Banks already studied the Lyapunov exponents and the Lyapunov dimension [59], but their analyses were restricted to a single parameter combination and thus the possible array of dynamics and the changes in the properties of the attractors were not investigated in detail.

2.2.1 Symbolic dynamics and topological entropy

We here introduce a family of one-dimensional maps identified in the Itik-Banks model for the chaotic regime, which are studied in terms of symbolic dynamics theory. For numerical investigation we will take the values of the parameters a_{13}, $(0.05 \leq a_{13} \leq 10)$: the tumor cell inactivation rate (i.e., killing rate) by the effector cells; and parameter a_{31}, $(0.9 \leq a_{31} \leq 1.5)$: inactivation of effector cells by the tumor cells. We can study the dynamics of the strange attractor constructing one-dimensional maps that reproduce the behavior of the temporal dynamics of the tumor cells corresponding to their successive local maxima (as an example of a time series corresponding to x_1, see Fig. 2.2(a)).

These iterated maps consist of pairs $(x_1^{(n)}, x_1^{(n+1)})$, where $x_1^{(n)}$ denotes the n^{th} relative maximum. As shown in Fig. 2.2(b), the obtained discrete map takes the form of a logistic map. The obtained iterated maps dynamically behave like a continuous map with a single critical point, c, which maps an interval $I = [a, b]$ into itself.

The following example illustrates the computation of the topological entropy, in the context of symbolic dynamics theory, using the procedure established in Chapter 1, Section 1.1.

Example 4 *Let us consider the map of Fig. 2.2(b). The symbolic orbit of the turning point, c, determines the period-5 kneading sequence* $(RLLLC)^{\infty}$. *After ordering the orbital points, we obtain*

$$x_2 < x_3 < x_4 < x_0 < x_1 \ .$$

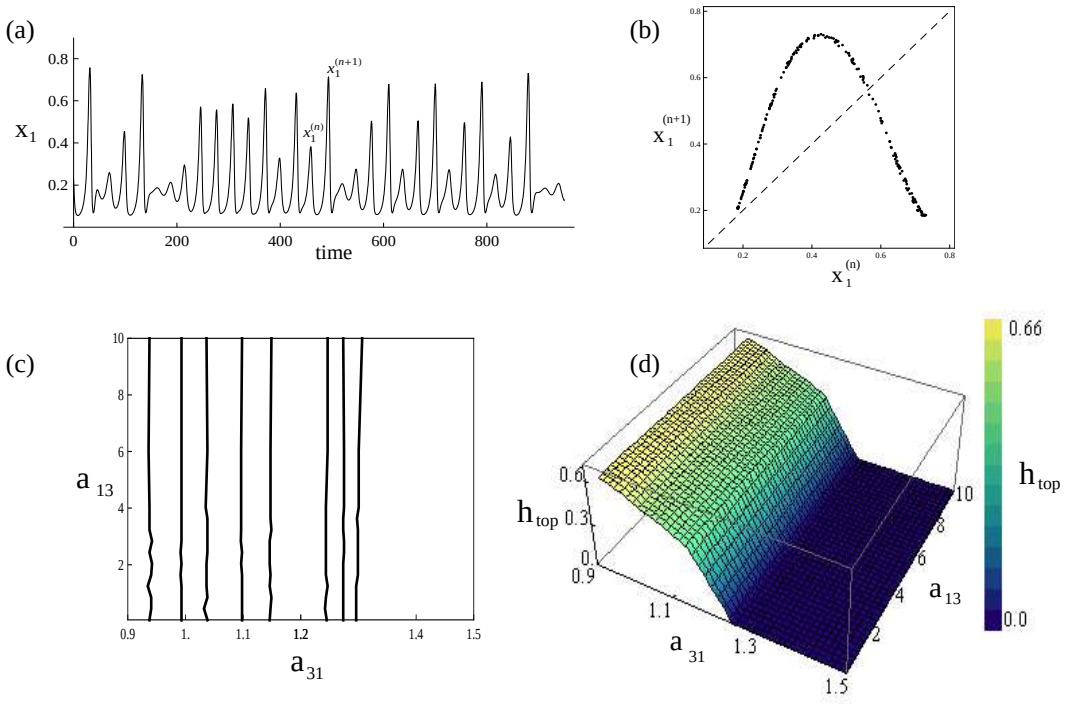

Figure 2.2: (a) Chaotic time series of the tumor cells population, $x_1(t)$, using $a_{13} = 5.0$ and $a_{31} = 0.9435$. (b) Iterated unimodal map obtained from plotting successive local maxima of the time dynamics of tumor cells, x_1, on the strange attractor, also using the previous parameter values. (c) Codimension-two bifurcation diagram showing the period orbits $(n \leq 5)$ of the turning point C in the parameter regions $a_{13} \in$[0.05,10] and $a_{31} \in$[0.9,1.5]. From left to right, the corresponding kneading sequences are: $(RLLLC)^\infty$, $(RLLC)^\infty$, $(RLLRC)^\infty$, $(RLC)^\infty$, $(RLRRC)^\infty$, $(RLRC)^\infty$, $(RC)^\infty$and C^∞. (d) Variation of the topological entropy, h_{top}, in the same parameter regions.

The associated transition matrix is

$$M(f) = \begin{bmatrix} 0 & 1 & 0 & 0 \\ 0 & 0 & 1 & 0 \\ 0 & 0 & 0 & 1 \\ 1 & 1 & 1 & 1 \end{bmatrix}$$

which has the characteristic polynomial

$$p(\lambda) = \det(M(f) - \lambda I) = -1 - \lambda - \lambda^2 - \lambda^3 + \lambda^4.$$

The growth number $s(f)$ (the spectral radius of matrix $M(f)$) is 1.92756.... *Therefore, the*

value of the topological entropy is given by

$$h_{top}(f) = \log s(f) = 0.65625... \ .$$

Figure 2.2(d) shows the variation of the topological entropy in the parameter region. As we can observe, the dynamics of the Itik-Banks system is associated with positive topological entropy, highlighting a large region of the parameter space where chaos occurs. As we will characterize in the following lines, the dynamics is very sensitive to the inactivation rate of effector cells by tumor cells. Our analyses reveal that when tumor cells do not exert a strong inactivation of effector cells, the topological entropy takes values $0.609378... \lesssim h_{top} \lesssim 0.656255....$ However, the complexity of chaos decreases as this inactivation rate becomes more important, and the topological entropy decreases finally becoming non-positive at $a_{31} \gtrsim 1.24$, where chaos is not found.

The study of the kneading sequences allows us to identify pairs of values (a_{13}, a_{31}) corresponding to symbolic periodic orbits. In Fig. 2.2(c) we show the locations of these points in the parameter space associated to the kneading sequences, with periods $n \leq 5$, from left to right: 5-period - $(RLLLC)^\infty$, 4-period - $(RLLC)^\infty$, 5-period - $(RLLRC)^\infty$, 3-period - $(RLC)^\infty$, 5-period - $(RLRRC)^\infty$, 4-period - $(RLRC)^\infty$, 2-period - $(RC)^\infty$ and 1-period - C^∞. The identified kneading sequences correspond to logistic-type maps with different levels of complexity reflected in different values of the topological entropy. Therefore, we are able to find different pairs of values a_{13} (tumor cell killing rate by the effector cells) and of values a_{31} (effector cells inactivation rate by the tumor cells) localized in the same isentropic curve. The next table gives us information about the nuclear kneading sequences studied in terms of its characteristic polynomial and its topological entropy.

Kneading sequences	**Characteristic polynomial**	**Topological entropy**
RC	$1-t$	0
$RLRC$	$-1+t+t^2-t^3$	0
$RLRRC$	$-1+t-t^2-t^3+t^4$	0.414013...
RLC	$-1-t+t^2$	0.481212...
$RLLRC$	$1-t-t^2-t^3+t^4$	0.543535...
$RLLC$	$1+t+t^2-t^3$	0.609378...
$RLLLC$	$-1-t-t^2-t^3+t^4$	0.656255...

Figure 2.2(d) shows the variation of the topological entropy computed for the system in the parameter ranges $0.05 \leq a_{13} \leq 10$ and $0.9 \leq a_{31} \leq 1.5$. Our results show that the inactivation rate of effector cells by the tumor cells, a_{31}, has a profound and marked effect on the dynamics. Higher values of this control parameter tend to stabilize the dynamics from chaos to order. The chaotic behavior occurs when the ratio of the effector cells inactivated by the tumor cells is lower (which means that for lower values of a_{31} the tumor cells are not particularly aggressive towards the activated immune system cells (effector cells)). As far as the control parameter a_{13} is concerned, our analysis reveals that this parameter seems to have a modest effect on the dynamical behavior in the Itik-Banks cancer model. The variation of the tumor cells inactivation rate by the effector cells doesn't provoke a sharp reaction of the dynamics. The positive topological entropy, which decreases for growing a_{31}, allows us to identify the parameter region corresponding to $0.05 \leq a_{13} \leq 10$ and $0.9 \leq a_{31} \leq 1.24$ where the regimes of chaos occur. As a consequence, the feature of the original model that we are studying - *the temporal dynamical behavior of the successive local maxima of the tumor cells,* x_1 - is associated with regimes of chaotic behavior. We point out that a more regular and organized temporal behavior of x_1 occurs when the tumor cells are more aggressive, in the sense that effector cells inactivation rate by the tumor cells is higher, and the dynamics under this parametric regime is completely predictable (see next section).

2.2.2 Lyapunov exponents, Kaplan-Yorke dimension and predictability

As stated in Chapter 1, Section 1.2, Lyapunov exponents, dimensions and entropies are different ways of characterizing properties for chaotic attractors. In this section, we measure the Lyapunov exponents, the Kaplan-Yorke dimension and the predictability of the Itik-Banks model of cancer growth.

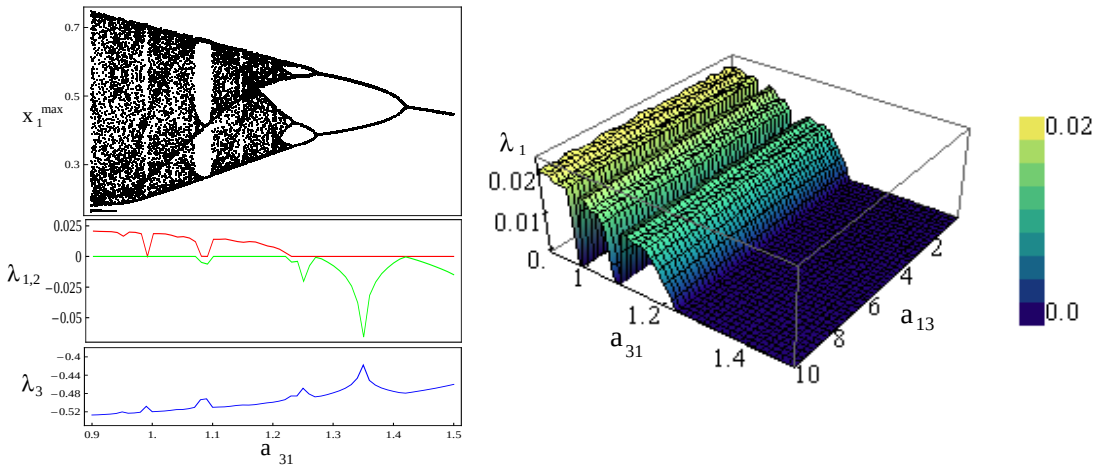

Figure 2.3: (Left) Bifurcation diagram obtained from $x_1^{\max}$ showing the period-halving (i.e., inverse Feigenbaum) scenario occuring as the inactivation of effector cells by tumor cells increases (here with $a_{13} = 5.0$ and $0.9 \leq a_{31} \leq 1.5$). Below we show the three Lyapunov exponents computed within the same parameter range. (Right) Variation of the first (i. e., maximum) Lyapunov exponent computed in the same parameter space used in the previous figure.

A positive *maximal Lyapunov exponent* (MLE) is commonly taken as an indicator of chaotic behavior. In the left hand-side of Fig. 2.3 we present a bifurcation diagram and the variation of the three Lyapunov exponents with a_{31} as a control parameter for $a_{13} = 5.0$. This figure shows clearly the three possible signs of the values for the Lyapunov exponents in the chaotic regime, $(+, 0, -)$, and in the non-chaotic regime. In agreement with the represented bifurcation diagram, the maximal Lyapunov exponent is positive

in the chaotic regime and $\lambda_1 = 0$ in the periodic windows. The $3D-$plot of the same figure shows the variation of the maximal Lyapunov exponent λ_1 in all the parameter region $0.05 \leq a_{13} \leq 10$ and $0.9 \leq a_{31} \leq 1.5$. The positiveness of this Lyapunov exponent indicates the region where the system is chaotic. We notice the existence of pairs (a_{13}, a_{31}) corresponding to $\lambda_1 = 0$ (signature of periodic behavior). The increase of the effector cells inactivation rate by the tumor cells, a_{31}, involves an inverse Feigenbaum bifurcation scenario, which results in the stabilization of the dynamics at higher values.

Our results, in agreement with classical numerical results displayed in the literature [14], show that for certain periodic windows there is a discrepancy between the topological entropy and the first (i. e., maximum) Lyapunov exponent. Within these periodic regimes, the topological entropy diverges from the maximum Lyapunov exponent, which decreases rapidly to zero, although initial conditions may wander chaotically in portions of the system. The surface representing the topological entropy (Fig. 2.2 (d)) upper bounds the surface that represents the variation of the maximum Lyapunov exponent (Fig. 2.3 (right)). The positive values of the topological entropy shape the variation tendency of λ_1. The variation of the Kaplan-Yorke dimension in the parameter space is depicted in Fig. 2.4. With the previous procedures, we have confirmed the chaotic dynamics by estimating the Lyapunov exponents and the Lyapunov dimension which is obtained to be fractal.

As mentioned in Chapter 1, Section 1.2, the ability to predict the future state of a dynamical system, given the present one, turns out to be particularly relevant with major implications in applied biology. Dynamically, the inverse of the Kolmogorov-Sinai entropy, $1/h_{KS}$, characterizes the predictability of the system. Naturally, as pointed out in

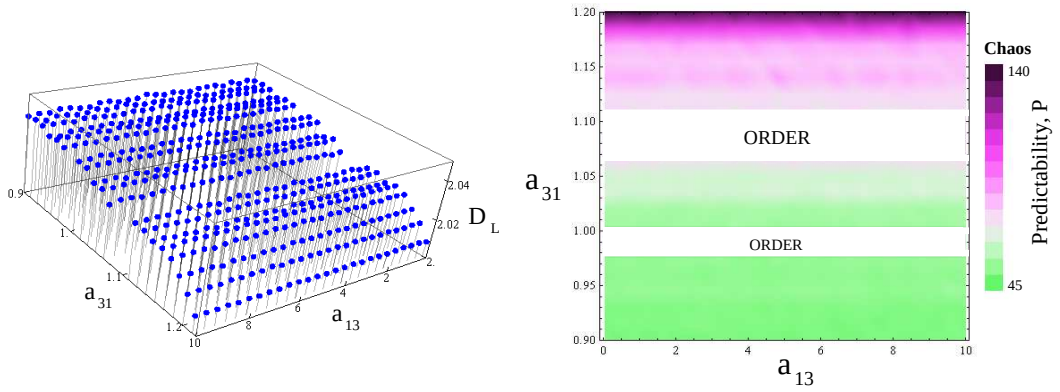

Figure 2.4: Variation of the Kaplan-Yorke (or Lyapunov) dimension, D_L (left); and the predictability, P (right), in the parameter space (a_{31}, a_{13}). The color gradient of the right panel shows the regions of chaotic dynamics and their corresponding predictability measures: increased inactivation of effector cells by tumor cells (i.e., increased a_{31}) gives place to a more predictability dynamics.

Chapter 1, Subsection 1.2.3, higher values of h_{KS} imply lower values of the predictability $1/h_{KS}$, that is, the more chaotic, the less predictable. This fact is made clear in the gradient diagram of Fig. 2.4, where higher values of the predictability correspond to higher values of the effector cells inactivation rate by the tumor cells, a_{31}.

2.3 Conclusions

Competitive interactions among cells, which are the basis of many biological processes, have been used to design several mathematical models developed in cancer research. A particularly important domain of research is the mathematical modeling of tumor growth which uses the ecosystem framework to study tumors as dynamic evolving systems, considering, not only the time change of cancer cells, but also the host components. In this context, cancer is regarded as a complex network of interactions and not merely as a disorganized growth of a certain population of cells ([62], [63]). In this chapter, we have quantitatively studied topological and dynamical properties of chaotic attractors arising

in the Itik-Banks cancer model [59]. This model aims to explain prominent features of the growth cancer dynamics for non-solid tumors, in particular the competition and the interactions among three cell populations: tumor cells, host tissue healthy cells and effector immune cells. The extremely rich and complex behavior of this model shows how the nonlinear interactions between the involved cells are able to generate a number of different kind of dynamical responses.

We analyzed the model using symbolic dynamics also computing local stability measures with the Lyapunov exponents. Specifically, we developed a rigorous study of iterated one-dimensional maps related to the fraction of tumor cells x_1, that incorporate the salient dynamical properties of the system. We found a Feigenbaum bifurcation scenario, and we quantified the decrease of the complexity of the dynamics by the variation of the topological entropy with the two control parameters a_{13} and a_{31}, describing the inactivation rates of tumor and effector cells, respectively. The representation of isentropic curves in the (a_{13}, a_{31})-parameter space allowed us to introduce the parameter space ordering of the dynamics. The previous results concerning chaotic scenarios have been confirmed with the computation of the Lyapunov exponents, used to estimate the Lyapunov dimension and the predictability of the cancer model. The variation of the maximal Lyapunov exponent and the fractal dimension further confirmed the chaoticity of the system.

Interestingly, we found that the dynamics is particularly sensitive to the variation of the effector cells inactivation rate by the tumor cells, given by parameter a_{31}, having a very important effect on the overall dynamics of the system. In this sense, our theoretical results match the established idea that tumor-induced immunosuppression in cancer has strong implications in growth, expansion and differentiation of cancer stem cells [61]. Increasing

values of this parameter tend to stabilize the dynamics, inducing less complexity to the model, also increasing predictability and weakening chaos (i.e., the positive Lyapunov exponent diminishes at increasing a_{31} values). As far as the control parameter a_{13} is concerned, our analyses reveal that this parameter has a minimal effect on the dynamical behavior of the model. The chaotic behavior, which is characterized by positive topological entropy, occurs for low values of a_{31}, which means that in the chaotic state the tumor cells are not particularly aggressive towards the effector cells. This particular result suggests that the possible manipulation of this parameter from a medical point of view could have an important role in the fate of the tumor cell populations. In a hypothetical case that chaos was real in tumor cells dynamics *in vivo*, and that, the strength of the inactivation of effector cells by tumor cells could qualitatively change the dynamics from strong chaos to weak chaos via the period-doubling scenario, one could take advantage of this property and artificially decrease the inactivation of effector cells by the tumoral ones with drugs. As our model shows, if tumor cells perform a strong inactivation on the effector cells, some important phenomena take place. For instance, the local minima of the tumor cells populations within the attractor increase their values, and strong chaos changes to weak chaos and to quasi periodic or periodic motions. In this sense, drugs diminishing the inactivation rates of effector cells by tumor cells could involve (beyond the increased availability of activated effector cells) tumor cells visiting lower population values because of strong fluctuations being much more sensitive to the effect of other sources of variation such as demographic noise. Such a noise could force tumor cell populations to achieve zero population values. This extinction effect has been previously discussed using discrete theoretical models in the context of single-species survival in ecosystems [64]. Such a

phenomenon would be especially important at the initial stages of tumorigenesis, when few tumor cells are found within the body and thus finite population sizes introduce strong demographic noise. Our hypothesis should be tested using a stochastic version of the model studied in this chapter.

Further research should also investigate our conclusions for solid tumors (such as throat or stomach cancer), using spatially-extended versions of the Itik-Banks model (e.g., reaction-diffusion equations or cellular automata models). Such model approaches would be useful to check if our results keep general for different tumor classes. Despite spatial interactions are known to introduce novel phenomena in nonlinear systems [65], if the spatial versions of the Itik-Banks model further confirmed our results concerning parameter a_{31}, blocking mechanisms of effector cells inactivation by tumor cells should be considered as a key target for the development of drugs against tumor cells progression.

Chapter 3

Activation of effector immune cells promotes tumor stochastic extinction: A homotopy analysis approach[2]

The nature of the interactions in biological systems gives place to nonlinear dynamics that can generate, for some parameter values, very complicated dynamics e.g. chaos. Hence, advances to better characterize the dynamics for nonlinear systems turn out to be extremely useful to analyze and understand such systems.

In the present chapter we apply the Homotopy Analysis Method (HAM) to obtain solutions of the cancer growth model proposed by Itik and Banks [59]. Such a model, based on Volterra-Lotka predator-prey dynamics, describes the interactions between tumor, healthy, and effector immune cells (CD8 T cells i.e., cytotoxic lymphocytes, CTLS). Predator-prey or competition Volterra-Lotka systems are known to display deterministic chaos for systems with three or more dimensions [67, 68, 69, 70]. Together with the model by Itik and Banks, several other theoretical models have addressed the dynamics of cancer

[2]This study has been published in [66].

and tumor cells [54, 56, 71]. Interestingly, the model by Itik and Banks can be considered as being qualitatively validated with experimental data, because its parameter values were chosen to match with some biological evidences. This model could be thus considered as being qualitatively validated with experimental data [51, 71]. Motivated by the characterization of chaos provided by Itik and Banks, a collection of questions pertaining to chaotic tumor behavior in terms of symbolic dynamics and predictability as well as to the control of healthy cells behavior corresponding to physiological relevant parameter regions, have been recently addressed in Refs. [72] and [73], respectively. In fact, chaos in tumor dynamics and its property of sensitivity to initial conditions have been suggested to have numerous analogies to clinical evidences [74, 75].

As stated in Chapter 1, Section 1.3, numerical algorithms have been extremely important to investigate complex dynamical systems such as cancer. However, they allow us to analyze the dynamics at discrete points only, thereby making impossible to obtain continuous solutions. By means of the HAM, accurate approximations allow a good semi-analytical description of the time variables, making also possible to use the homotopy solutions to explore the model dynamics, as well as to investigate possible scenarios of tumor clearance, either deterministic or stochastic. This is the aim that we pursue in this contribution. Specifically, we will calculate the homotopy solutions of the cancer model by means of the Step Homotopy Analysis Method (SHAM) (see [45]). Then, the homotopy solutions will be used to explore the effect of a key parameter in the population dynamics: the activation of the immune system cells due to tumor antigen recognition, given by parameter r_3 (see next Section). As we will show, the system is very sensitive to this parameter, and its change can involve the shift from order to chaos. This key parameter

is especially interesting because modulates the response of the immune system against tumor cells and, as we will show, the dynamics is especially sensitive to r_3. Despite its importance, the dependence of the dynamics of the model under investigation on r_3 remains poorly explored (see [73] for the analysis of a narrow range of r_3 values within the framework of chaotic crises and chaos control). Moreover, the impact of this parameter on possible extinction scenarios of tumor cells due to demographic fluctuations has, as far as we know, not being investigated. Interestingly, several therapeutic methods, that will be discussed in this chapter are currently available to clinically manipulate this parameter, thus being a realistic candidate to fight against tumor progression.

Finally, we will use the homotopy solutions to investigate the role of demographic stochasticity in the dynamics of the model, paying special attention to the role of noise in potential scenarios of tumor clearance and persistence of healthy cells due to changes in the activation levels of effector immune cells.

3.1 Cancer mathematical model

In this chapter we analyze a cancer mathematical model initially studied by Itik and Banks [59]. The model describes the dynamics of three interacting cell populations: tumor cells, healthy cells and effector immune cells i.e., CD8 cytotoxic T-cells, CTLs. Effector cells are the relative short-lived activated cells of the immune system that defend the body in an immune response. Similarly to previous cancer models [54, 55, 56, 71, 76, 77, 78], this model describes the competition dynamics of these three interacting cell types in a well-mixed system (e.g., liquid cancers such as leukemias or multiple lymphomas). Among several biologically-meaningful assumptions (see [59]), the model assumes that the antitu-

mor effect of the immune system response is carried out by cytotoxic T-cells i.e., mediated by the T-cell based adaptive arm. Alpha-beta T-cells are activated upon recognition of their cognate tumor specific antigens by the cell surface T-Cell Receptor (TCR) in the form of small peptides presented in the context of the major histocompatibility complex (MHC) molecules. CD8 T-cells are responsible for direct cell mediated cytotoxicity following activation by antigen presenting cells (APCs) and are thought to be central players in the anti-tumor immune response. To achieve full activation, the signal emanating from the TCR has to be enhanced by messages sent by costimulatory molecules such as CD28 also present in the surface of the T-cell. Failure of the engagement of costimulatory proteins, activation of coinhibitory receptors such as CTLA-4 or PD-1 or the presence of CD4 regulatory (T_{reg}) T cells may lead to the failure of the activation of the T-cell or to the downregulation of the immune response. Disarming these inhibitory mechanisms off may lead to the reactivation of the antitumor immune response and to supraphysiological levels of T-cell activation useful in the clinical setting (see Section 3.4).

For a self-contained presentation, we restate in the next lines the eye-catching and noteworthy features of the Itik and Banks cancer model. As mentioned in the previous chapter, in order to simplify the mathematical analysis, the initial model was non-dimensionalized [59]. The scaled resulting system of differential equations is given by

$$\frac{dx_1}{dt} = x_1\left(1 - x_1\right) - a_{12}x_1x_2 - a_{13}x_1x_3, \tag{3.1}$$

$$\frac{dx_2}{dt} = r_2x_2\left(1 - x_2\right) - a_{21}x_1x_2, \tag{3.2}$$

$$\frac{dx_3}{dt} = \frac{r_3x_1x_3}{x_1 + k_3} - a_{31}x_1x_3 - d_3x_3. \tag{3.3}$$

The variables x_1, x_2 and x_3 denote, respectively, the population numbers of tumor cells,

healthy cells and effector immune cells against their specific maxima carrying capacities k_1, k_2 and k_3 (see Section 4 in [59]). Parameter a_{12} is the tumor cells inactivation rate by the healthy cells; a_{13} is the tumor cells inactivation rate by the effector cells; r_2 is the intrinsic growth rate of the healthy tissue cells; a_{21} is the healthy cells inactivation rate by the tumor cells; r_3 corresponds to the activation rate of effector cells due to tumor cells' antigen recognition; a_{31} is the effector cells inactivation rate by the tumor cells. Finally, d_3 is the density-dependent death rate of the effector cells (see [59] for a detailed description of the model parameters).

We want to notice that the inactivation rate (or the elimination rate) of tumor cells by the action of the effector immune cells (modeled with the last term in Eq.(3.1) is assumed to be proportional to the number of effector immune cells, and no saturation is considered. A mechanism of elimination of tumor cells is given by the release of cytotoxic granules by the effector cells that impair or destroy tumor cells. Effector cells can clonally expand after antigen recognition, so the model assumes that they can be present in excess if needed. Hence, no saturation is considered for this term. The activation of effector immune cells due to antigen recognition used in the first term of Eq.(3.3) can be viewed as a Holling-II functional response, typically used to model predator feeding saturation in ecological dynamical systems. For our system, it is assumed a decelerating activation rate at increasing number of tumor cells since the activation of effector immune cells is limited by their requirement to recognize the tumor antigens in the context of the Antigen Presenting Cells (APCs). In this case, a process of cell-cell interaction and receptor recognition is required between APCs and tumor cells prior to activation, and thus an increasing number of tumor cells does not necessarily involve an increasing activation of

effector cells.

The dynamics of this model is very rich, and both ordered (e.g., stable points or periodic orbits) and disordered (i.e., chaos) dynamics can be found for different parameter values [59, 72].

The model parameters will be fixed, if not otherwise specified, following [59], i.e., $a_{12} = 1$; $a_{21} = 1.5$; $d_3 = 0.5$; $k_3 = 1$; $r_2 = 0.6$; $a_{13} = 2.5$; $a_{31} = 0.2$. This set of parameter values can involve chaos for a wide range of r_3 values (see below).

3.2 Homotopy analysis method

At this moment, following the procedure presented in Chapter 1, Section 1.3, we are able to apply the homotopy analysis approach for solving analytically the Itik-Banks cancer growth model.

Let us consider the Eqs. (3.1)-(3.3) subject to the initial conditions

$$x_1(0) = IC_1, \quad x_2(0) = IC_2, \quad x_3(0) = IC_3.$$

Following the HAM, it is straightforward to choose

$$x_{1,0}(t) = IC_1, \quad x_{2,0}(t) = IC_2, \quad x_{3,0}(t) = IC_3,$$

as our initial approximations of $x_1(t)$, $x_2(t)$ and $x_3(t)$, respectively. In this work we will use $IC_1 = 0.13858...$, $IC_2 = 0.69568...$, $IC_3 = 0.01380....$ We choose the auxiliary linear operators

$$L\left[\phi_i(t;q)\right] = \frac{\partial \phi_i(t;q)}{\partial t} + \phi_i(t;q),$$

with the property $L\left[C_i e^{-t}\right] = 0$, where C_i are integral constants (hereafter $i = 1, 2, 3$).

The Eqs. (3.1)-(3.3) suggest the definition of the nonlinear operators $\mathcal{N}_1$, $\mathcal{N}_2$ and $\mathcal{N}_3$ as

$$\begin{aligned}\mathcal{N}_1\left[\phi_1(t;q),\phi_2(t;q),\phi_3(t;q)\right] &= \frac{\partial\phi_1(t;q)}{\partial t}-\phi_1(t;q)+\phi_1^2(t;q)+a_{12}\phi_1(t;q)\,\phi_2(t;q)+\\ &\quad +a_{13}\phi_1(t;q)\,\phi_3(t;q),\end{aligned}$$

$$\mathcal{N}_2\left[\phi_1(t;q),\phi_2(t;q),\phi_3(t;q)\right] = \frac{\partial\phi_2(t;q)}{\partial t}-r_2\phi_2(t;q)+r_2\phi_2^2(t;q)+a_{21}\phi_1(t;q)\,\phi_2(t;q),$$

$$\begin{aligned}\mathcal{N}_3\left[\phi_1(t;q),\phi_2(t;q),\phi_3(t;q)\right] &= \phi_1(t;q)\frac{\partial\phi_3(t;q)}{\partial t}+k_3\frac{\partial\phi_3(t;q)}{\partial t}-r_3\phi_1(t;q)\,\phi_3(t;q)+\\ &\quad +a_{31}\phi_1^2(t;q)\,\phi_3(t;q)+a_{31}k_3\phi_1(t;q)\,\phi_3(t;q)+\\ &\quad +d_3\phi_1(t;q)\,\phi_3(t;q)+d_3k_3\phi_3(t;q).\end{aligned}$$

If $q\in[0,1]$ and h_0 the non-zero auxiliary parameter, the $zero^{th}$-order deformation equations are of the following form

$$(1-q)\,L\left[\phi_i(t;q)-x_{i,0}(t)\right]=qh_0\mathcal{N}_i\left[\phi_1(t;q),\phi_2(t;q),\phi_3(t;q)\right], \tag{3.4}$$

subject to the initial conditions

$$\phi_1(0;q)=0.13858...,\phi_2(0;q)=0.69568...,\ \phi_3(0;q)=0.01380....$$

For $q=0$ and $q=1$, the above $zero^{th}$-order equations (3.4) have the solutions

$$\phi_1(t;0)=x_{1,0}(t),\ \phi_2(t;0)=x_{2,0}(t),\ \phi_3(t;0)=x_{3,0}(t) \tag{3.5}$$

and

$$\phi_1(t;1)=x_1(t),\ \phi_2(t;1)=x_2(t),\ \phi_3(t;1)=x_3(t). \tag{3.6}$$

When q increases from 0 to 1, the functions $\phi_1(t;q)$, $\phi_2(t;q)$ and $\phi_3(t;q)$ vary from $x_{1,0}(t)$, $x_{2,0}(t)$ and $x_{3,0}(t)$ to $x_1(t)$, $x_2(t)$ and $x_3(t)$, respectively. Expanding $\phi_1(t;q)$, $\phi_2(t;q)$ and $\phi_3(t;q)$ in Taylor series with respect to q, we have the homotopy-Maclaurin series

$$\phi_i(t;q) = x_{i,0}(t) + \sum_{m=1}^{+\infty} x_{i,m}(t) q^m, \tag{3.7}$$

in which

$$x_{i,m}(t) = \frac{1}{m!} \frac{\partial^m \phi_i(t;q)}{\partial q^m}\bigg|_{q=0}, \tag{3.8}$$

where h_0 is chosen in such a way that these series are convergent at $q = 1$. Thus, through Eqs (3.5)-(3.8), we have the homotopy series solutions

$$x_i(t) = x_{i,0}(t) + \sum_{m=1}^{+\infty} x_{i,m}(t), \tag{3.9}$$

Taking the m^{th}-order homotopy derivative of $zero^{th}$-order Eq.(3.4), and using the properties

$$\begin{aligned}
D_m(\phi_i) &= x_{i,m}, \\
D_m\left(q^k \phi_i\right) &= D_{m-k}(\phi_i) = \begin{cases} x_{i,m-k} & , 0 \le k \le m \\ 0 & , \text{ otherwise} \end{cases}, \\
D_m\left(\phi_i^2\right) &= \sum_{k=0}^{m} x_{i,m-k}\ x_{i,k},
\end{aligned}$$

and

$$D_m(\phi_i \psi_i) = \sum_{k=0}^{m} D_k(\phi_i)\ D_{m-k}(\psi_i) = \sum_{k=0}^{m} x_{i,k}\ y_{i,m-k},$$

where D_m means the m^{th}-order derivative in order to q, we obtain the m^{th}-order deformation equations

$$L\left[x_{i,m}(t) - \chi_m x_{i,m-1}(t)\right] = h_0 \mathcal{R}_{i,m}\left[x_{1,m-1}(t), x_{2,m-1}(t), x_{3,m-1}(t)\right], \tag{3.10}$$

with

$$\chi_m = \begin{cases} 0, & m \leq 1 \\ \\ 1, & m > 1 \end{cases}$$

and the following initial conditions

$$x_{1,m}(0) = 0,\ x_{2,m}(0) = 0,\ x_{3,m}(0) = 0. \tag{3.11}$$

Defining the vector $\overrightarrow{x}_{m-1} = (x_{1,m-1}(t), x_{2,m-1}(t), x_{3,m-1}(t))$,

$$\begin{aligned} \mathcal{R}_{1,m}\left[\overrightarrow{x}_{m-1}\right] &= \dot{x}_{1,m-1}(t) - x_{1,m-1}(t) + \sum_{k=0}^{m-1} x_{1,m-1-k}(t)\ x_{1,k}(t) + \\ &+a_{12} \sum_{k=0}^{m-1} x_{1,k}(t)\ x_{2,m-1-k}(t) + a_{13} \sum_{k=0}^{m-1} x_{1,k}(t)\ x_{3,m-1-k}(t), \end{aligned} \tag{3.12}$$

$$\begin{aligned} \mathcal{R}_{2,m}\left[\overrightarrow{x}_{m-1}\right] &= \dot{x}_{2,m-1}(t) - r_2 x_{2,m-1}(t) + r_2 \sum_{k=0}^{m-1} x_{2,m-1-k}(t)\ x_{2,k}(t) + \\ &+a_{21} \sum_{k=0}^{m-1} x_{1,k}(t)\ x_{2,m-1-k}(t), \end{aligned} \tag{3.13}$$

and

$$\begin{aligned} \mathcal{R}_{3,m}\left[\overrightarrow{x}_{m-1}\right] &= \sum_{k=0}^{m-1} \left(x_{1,k}(t)\dot{x}_{3,m-1-k}(t)\right) + k_3 \dot{x}_{3,m-1}(t) - \\ &-r_3 \sum_{k=0}^{m-1} \left(x_{1,k}(t)\ x_{3,m-1-k}(t)\right) + \\ &+a_{31} \sum_{k=0}^{m-1} \left[\left(\sum_{j=0}^{k} x_{1,k-j}(t)\ x_{1,j}(t) \right) x_{3,m-1-k} \right] + \\ &+a_{31} k_3 \sum_{k=0}^{m-1} \left(x_{1,k}(t)\ x_{3,m-1-k}(t)\right) + d_3 \sum_{k=0}^{m-1} \left(x_{1,k}(t)\ x_{3,m-1-k}(t)\right) + \\ &+d_3 k_3 x_{3,m-1}(t). \end{aligned} \tag{3.14}$$

Proceeding in this way, it is easy to solve the linear non-homogeneous Eqs.(3.10) at initial

conditions (3.11) for all $m \geq 1$, obtaining

$$x_{i,m}(t) = \chi_m \; x_{i,m-1}(t) + h_0 \; e^{-t} \int_0^t e^{\tau} \mathcal{R}_{i,m} \left[\overrightarrow{x}_{m-1} \right] d\tau, \tag{3.15}$$

As an example, for $m = 1$, we have:

$$\begin{aligned} x_{1,1}(t) &= 0.13858 - 0.119376h_0 + 0.0964073a_{12}h_0 + 0.0019124a_{13}h_0 + 0.119376e^{-t}h_0 - \\ &\quad -0.0964073a_{12}e^{-t}h_0 - 0.0019124a_{13}e^{-t}h_0, \end{aligned}$$

$$x_{2,1}(t) = 0.69568 + 0.0964073a_{21}h_0 - 0.0964073a_{21}e^{-t}h_0 - 0.211709h_0r_2 + 0.211709e^{-t}h_0r_2,$$

$$\begin{aligned} x_{3,1}(t) &= 0.0138 + 0.000265021a_{31}h_0 + 0.0019124d_3h_0 - 0.000265021a_{31}e^{-t}h_0 - \\ &\quad -0.0019124d_3e^{-t}h_0 + 0.0019124a_{31}h_0k_3 + 0.0138d_3h_0k_3 - \\ &\quad -0.0019124a_{31}e^{-t}h_0k_3 - 0.0138d_3e^{-t}h_0k_3 - 0.0019124h_0r_3 + \\ &\quad +0.0019124e^{-t}h_0r_3. \end{aligned}$$

It is straightforward to obtain terms for other values of m. In order to have an effective analytical approach of Eqs. (3.1)-(3.3) for higher values of t, we use the Step Homotopy Analysis Method (SHAM), in a sequence of subintervals of time step Δt and the 12^{th}-order HAM approximate solutions of the form

$$x_i(t) = x_{i,0}(t) + \sum_{m=1}^{11} x_{i,m}(t), \text{ with } i = 1, 2, 3, \tag{3.16}$$

at each subinterval. With the purpose of determining the value of h_0 for each subinterval, we plot the h_0-curves for Eqs. (3.1)-(3.3) (see an example for $t = 0$ in Fig. 3.1).

Accordingly to SHAM, the initial values $x_{1,0}$, $x_{2,0}$ and $x_{3,0}$ will be changed at each subinterval, i.e., $x_1(t^*) = IC_1^* = x_{1,0}$, $x_2(t^*) = IC_2^* = x_{2,0}$ and $x_3(t^*) = IC_3^* = x_{3,0}$ and

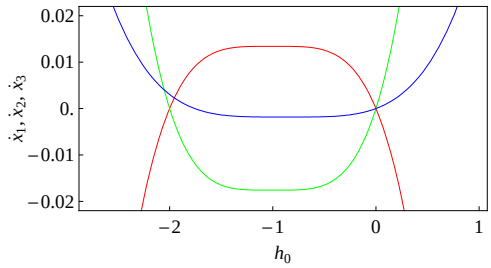

Figure 3.1: Samples of h_0-curves for the Itik-Banks system under 12^{th}-order approximation for $t = 0$, $a_{13} = 5.0$, $a_{31} = 1.3$ and $r_3 = 4.5$ (red - $\dot{x}_1\,(h_0)$, green - $\dot{x}_2\,(h_0)$ and blue - $\dot{x}_3\,(h_0)$).

we should satisfy the initial conditions $x_{1,m}(t^*) = 0$, $x_{2,m}(t^*) = 0$ and $x_{3,m}(t^*) = 0$ for all $m \geq 1$. So, the terms $x_{1,1}$, $x_{2,1}$ and $x_{3,1}$, presented before as an example for $m = 1$, take the form

$$\begin{aligned} x_{1,1}(t) &= 0.13858 - 0.119376h_0 + 0.0964073a_{12}h_0 + 0.0019124a_{13}h_0 + 0.119376e^{-(t-t^*)}h_0 - \\ &\quad -0.0964073a_{12}e^{-(t-t^*)}h_0 - 0.0019124a_{13}e^{-(t-t^*)}h_0, \end{aligned}$$

$$\begin{aligned} x_{2,1}(t) &= 0.69568 + 0.0964073a_{21}h_0 - 0.0964073a_{21}e^{-(t-t^*)}h_0 - 0.211709h_0r_2 + \\ &\quad +0.211709e^{-(t-t^*)}h_0r_2, \end{aligned}$$

$$\begin{aligned} x_{3,1}(t) &= 0.0138 + 0.000265021a_{31}h_0 + 0.0019124d_3h_0 - 0.000265021a_{31}e^{-(t-t^*)}h_0 - \\ &\quad -0.0019124d_3e^{-(t-t^*)}h_0 + 0.0019124a_{31}h_0k_3 + 0.0138d_3h_0k_3 - \\ &\quad -0.0019124a_{31}e^{-(t-t^*)}h_0k_3 - 0.0138d_3e^{-(t-t^*)}h_0k_3 - 0.0019124h_0r_3 + \\ &\quad +0.0019124e^{-(t-t^*)}h_0r_3. \end{aligned}$$

Identical changes occur naturally for the other terms. As a consequence, the analytical

solutions are

$$x_i(t) = x_i(t^*) + \sum_{m=1}^{11} x_{i,m}(t - t^*), \quad \text{with} \quad i = 1, 2, 3. \tag{3.17}$$

In general, we only have information about the values of $x_1(t^*)$, $x_2(t^*)$ and $x_3(t^*)$ at $t^* = 0$, but we can obtain these values by assuming that the new initial conditions is given by the solutions in the previous interval. Our previous calculations are in perfect agreement with numerical simulations (computed with an adaptive Runge-Kutta-Fehlberg method of order $7 - 8$). In Fig. 3.2 we show the comparison of the SHAM analytical solutions and the numerical solutions of the system under study, considering two dynamical regimes: period-2 dynamics (Fig. 3.2(a) and (b)) and chaos (Fig. 3.2(c) and (d)).

3.3 Impact of effector immune cells activation in the dynamics

The calculations developed in the previous section allow us to provide analytical approximations to the solutions of the cancer model given by Eqs. (3.1)-(3.3). In this section we will use the homotopy solutions to explore the role of a key parameter of the model: the stimulation and activation of the immune system cells (cytotoxic lymphocytes, CTLs) via the recognition of tumor cells antigens. This recognition process is parametrized in the model by means of r_3 and k_3. We will here focus on parameter r_3, which can be interpreted as the density-dependent activation rate of effector cells due to the recognition of the antigens present in the surface of tumor cells. The constant k_3 is a saturation parameter, and will be fixed following [59]. By using the time trajectories obtained from Eq.(3.16), we will first investigate the effect of increasing the activation rate of effector cells in the deterministic dynamics. Then, we will add stochasticity to the homotopy so-

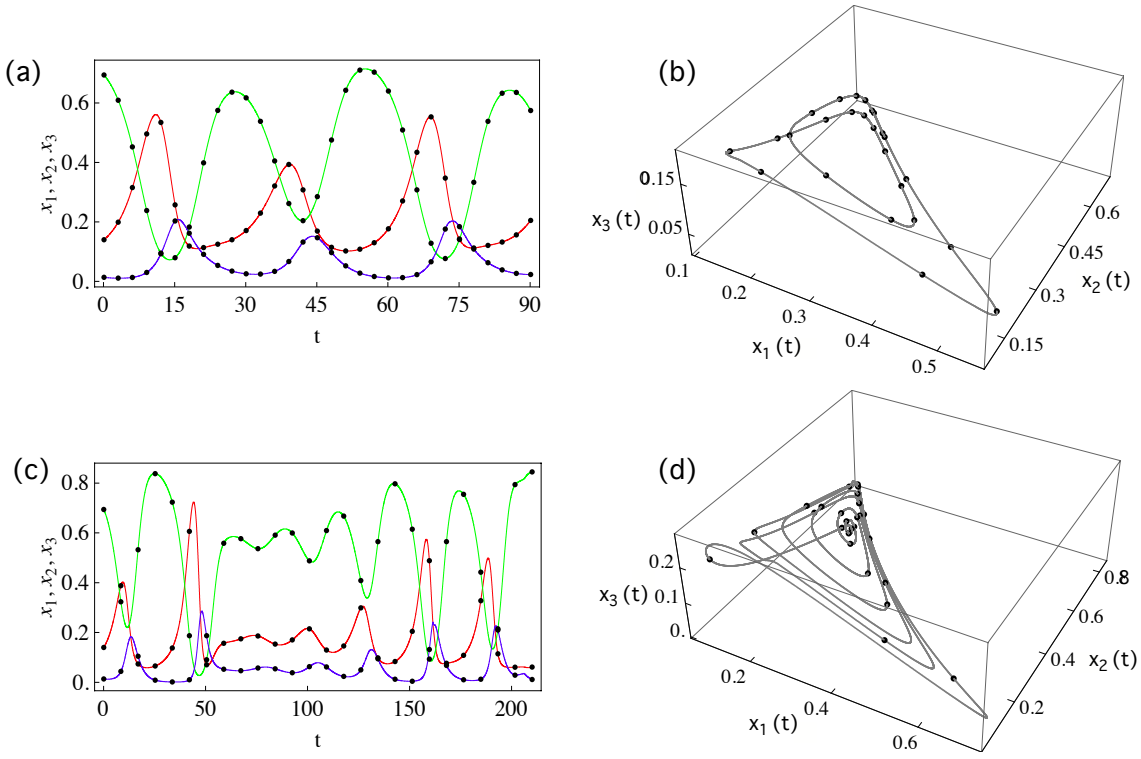

Figure 3.2: Comparison between the homotopy solutions (solid lines) obtained with the *Step Homotopy Analysis Method* (SHAM) developed in Section 3.2, and the numerical simulations (black dots) for Eqs. (3.1)-(3.3). Time series of the dynamical variables [x_1 (red), x_2 (green) and x_3 (blue)], and the corresponding attractors, represented in the phase space (x_1, x_2, x_3). In (a) and (b) we display the period 2 dynamics, using $a_{13} = 5$, $a_{31} = 1.3$, and $r_3 = 4$. In (c) and (d) we show the chaotic attractor obtained setting $(a_{13}, a_{31}, r_3) = (5, 0.9435, 4.5)$.

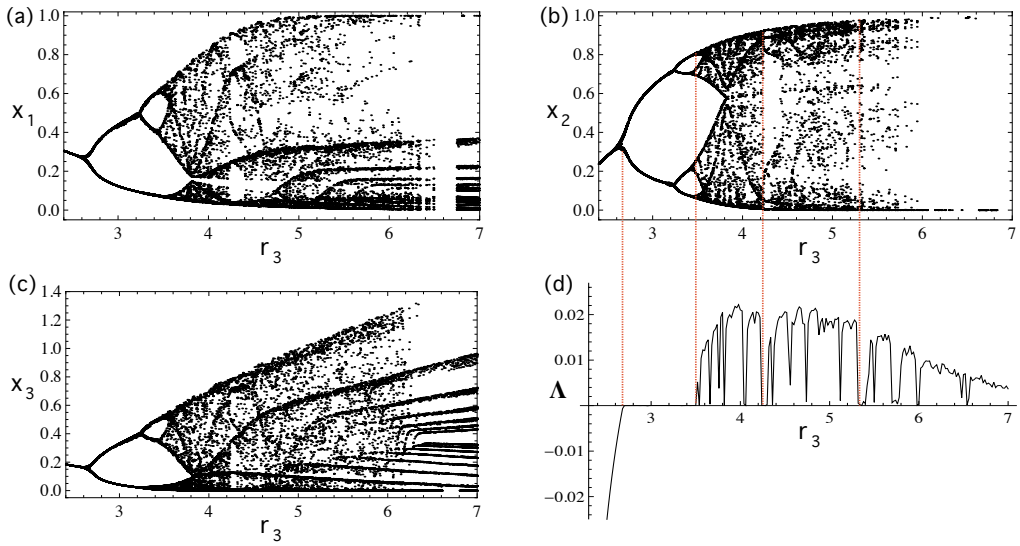

Figure 3.3: Bifurcation diagrams obtained from the deterministic homotopy solutions, using the activation rate of efector immune cells (within the range $2.4 \leq r_3 \leq 7$) as the control parameter. We plot the local maxima and minima of the homotopy solutions for the three model variables: (a) tumor cells: x_1, (b) healthy cells: x_2, and (c) effector immune cells: x_3. Panel (d) shows the maximum Lyapunov exponent, Λ, for the same range $2.4 \leq r_3 \leq 7$. The first red dashed line indicates a Hopf bifurcation, while the second one indicates the lowest value of r_3 where $\Lambda > 0$ i.e., chaos. Further increase of parameter r_3 involves other bifurcations e.g., $r_3 \sim 4.21$ or $r_3 \sim 5.35$.

lutions in order to explore the impact of demographic fluctuations in the overall dynamics of the system under investigation.

The deterministic dynamics tuning r_3 are displayed in Fig. 3.3 by means of bifurcation diagrams built with the homotopy solutions. To build the bifurcation diagrams we computed a time series using the homotopy solutions for each value of r_3, and we recorded the local maxima and minima after discarding some transient. By using this approach it is shown that the increase of r_3 involves a period-doubling bifurcation scenario i.e., Feigenbaum cascade, that causes the entry of the cell populations into chaotic dynamics. For $r_3 \gtrsim 2.6$ the dynamics suffers the first bifurcation which switches the dynamics from

a stable equilibrium towards a periodic orbit (dashed red line at the left in Fig. 3.3(d)). Further increase of r_3 involves period-doubling bifurcations, and, for $r_3 \gtrsim 3.5$ the dynamics undergo irregular fluctuations, which are confirmed to be chaotic with the computation of the maximal Lyapunov exponent, Λ (Fig. 3.3(d)). Λ has been computed within the range $2.4 \leq r_3 \leq 7$ from the model Eqs.(3.1)-(3.3) using a standard method [12]. The bifurcation diagrams reveal that the population of cells undergoes larger fluctuations at increasing r_3, and populations can, at a given time point, be close to zero population values (extinction), as discussed for single-species chaotic dynamics [64]. That is, one might expect extinctions at increasing values of r_3.

In order to analyze extinction scenarios for the populations of cells in our model, we will use the homotopy solutions developed in Section 3.2, including a noise term simulating demographic stochasticity. Demographic stochasticity may play an important role at the initial stages of tumor progression, where the number of tumor cells is low compared to the population of healthy cells. Hence, we will assume that noise in tumor cells populations and in effector cells populations is larger than in healthy cells populations. Hence, we will include an additive stochastic term, $\xi_i(t)$, to the homotopy solutions, now given by:

$$x_i(t) = x_i(t^*) + \sum_{m=1}^{11} x_{i,m}(t - t^*) + \xi_i(t) \cdot (t - t^*),\ i = 1, 2, 3. \tag{3.18}$$

Here $\xi_i(t)$ is a time-dependent random variable with uniform distribution i.e., $\xi_{i=1,2,3}(t) \in U(-\sigma_i, \sigma_i)$ that simulates demographic fluctuations, where parameter σ_i corresponds to the amplitude of the fluctuations. Previous works followed this approach to simulate decorrelating demographic noise in metapopulations [79] and host-parasitoid [80] dynamics. Notice that the noise term is scaled by the time-step used to compute the homotopy solutions. As mentioned, in our model approach we will assume that the popu-

lation of healthy cells is much larger than the populations of tumor and effector immune cells, setting $\sigma_2 = 0$. Hence, noise terms will be introduced to tumor and effector cells populations by means of $\sigma_{1,3} > \sigma_2 = 0$. We notice that we can analyze the deterministic dynamics setting $\sigma_{1,2,3} = 0$. Furthermore, the initial population numbers (initial conditions) for healthy cells populations are fixed to their carrying capacity $x_2(0) = k_2 = 1$, using $x_{1,3}(0) < x_2(0)$.

Using the homotopy solutions, we compute the extinction probabilities, $P^{ext}_{i=1,2,3}$, for each of the cell populations at increasing values of activation rates of effector immune cells, r_3. The extinction probabilities are computed as follows: for each value of r_3 analyzed, we built 200 different time series with the homotopy solutions using $t = 10^4$. Over these 200 time series, we calculated the number of time series for each variable fulfilling the extinction condition of variable i, assumed to occur when $x_i(t) \leq 10^{-30}$, normalizing the number of extinction events over 200. Then, we repeated the same process 10 times (replicas), and we computed the mean ($\pm SD$) of the normalized extinction events over these 10 replicas. Following the previous procedure, we consider random initial conditions for tumor and effector cells, setting $x_2(0) = 1$ and $x_{1,3}(0) < x_2(0)$, instead of using a single initial condition for each variable for all time series. Specifically, we will consider random initial populations of tumor and effector cells following a uniform distribution within the range $]0, 0.2]$. The results are displayed in Fig. 3.4 using parameter values from [59], except for the tuned parameter r_3. The deterministic simulations (solid triangles in Fig. 3.4(a)) reveal that extinction probabilities for tumor cells is zero within the range analyzed i.e., $2.4 \leq r_3 \leq 15.5$. For low values of r_3, the extinction probabilities for healthy and effector cells remain close and low ($P^{ext}_{2,3} \sim 0.05$).

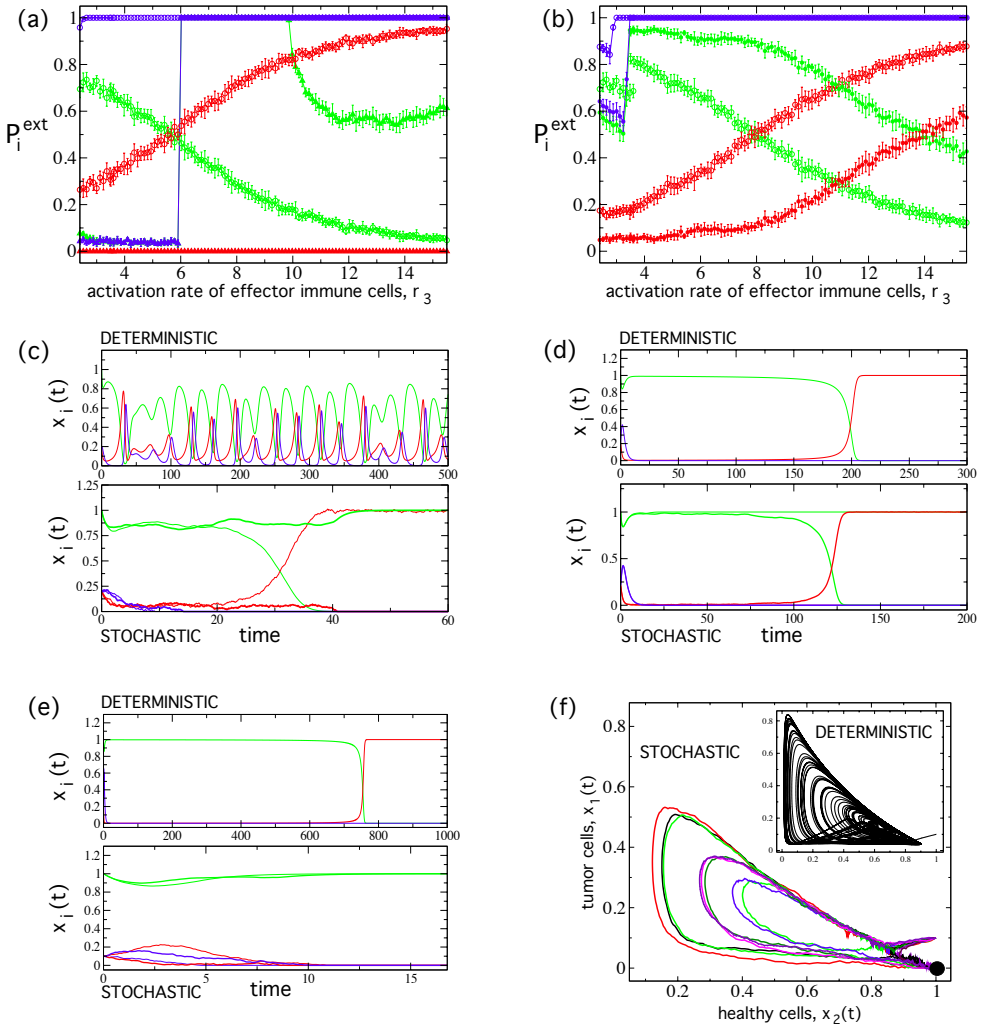

Figure 3.4: Extinction probabilities, P_i^{ext}, of tumor ($i = 1$, red), healthy ($i = 2$, green), and effector immune ($i = 3$, blue) cells at increasing activation rates of the immune cells (parameter r_3), fixing all other model parameters following [59]. (a) Extinction probabilities for the deterministic dynamics (solid triangles), and for the stochastic dynamics using $\sigma_{1,3} = 0.1 > \sigma_2 = 0$ (open circles). (b) Extinction probabilities using $\sigma_{1,3} = 0.05$ (open circles) and $\sigma_{1,3} = 0.01$ (solid circles), both also with $\sigma_2 = 0$. Each data point is the mean ($\pm SD$) computed over 10 replicas. Each of these replicas was obtained computing the extinction probability for each variable over 200 time series of length $t = 10^4$, starting from random low initial conditions for effector and tumor cells, $x_{1,3}(0) < x_2(0) = 1$ (see Section 3.3). In the lower panels we display the deterministic and stochastic dynamics for different values of r_3, with: $r_3 = 3.7$ (c); $r_3 = 9$ (d); and $r_3 = 12.5$. For the stochastic dynamics we display two different runs represented with thin and thick trajectories for each variable, with: (c) $\sigma_{1,3} = 0.1$; (d) $\sigma_{1,3} = 0.01$; and (e) $\sigma_{1,3} = 0.05$, all with $\sigma_2 = 0$. (f) Dynamics projected in the phase space (x_2, x_1) using $r_3 = 4$. We display 10 stochastic trajectories using $\sigma_{1,3} = 0.05$. The inset in (f) displays the chaotic attractor for the same initial conditions and parameter values with $\sigma_{1...3} = 0$ (i.e., deterministic dynamics).

Beyond $r_3 \gtrsim 6$, $P_{2,3}^{ext}$ drastically increases and extinctions take place with probability 1. Such extinction value is maintained for effector cells at increasing r_3. The extinction probability of healthy cells diminishes beyond $r_3 \gtrsim 9.8$ to $P_2^{ext} \sim 0.6$. In a counterintuitive way, these results indicate that increasing activation of effector immune cells (using the parameter values from [59]) does not involve tumor cells extinction or low extinction probabilities for healthy cells, due to the complexity of the dynamics in the chaotic or fluctuating regimes.

Now, we focus on the effect of demographic stochasticity in the overall dynamics of the system. Figure 3.4(a) displays the same analyses performed with the deterministic approach, but now using $\sigma_{1,3} = 0.1$ (recall $\sigma_2 = 0$). The observed extinctions patterns drastically change. For instance, the extinction probability of tumor cells, P_1^{ext}, ranges from $P_1^{ext} \sim 0.3$ to $P_1^{ext} \sim 0.97$ within the range $2.4 \leq r_3 \leq 15.5$. Moreover, the extinction probability of healthy cells significantly decreases at increasing r_3, having values of $P_2^{ext} \sim 0.05$ for $r_3 \gtrsim 12.2$. These results clearly indicate that when demographic noise is high (e.g., at initial tumor progression stages) stochastic fluctuations can involve increasing extinction probabilities of tumor cells and increasing survival probabilities of healthy cells when r_3 grows. In the stochastic simulations, effector immune cells always reached extinction, except for the cases with small r_3 and low noise amplitudes (Fig. 3.3(b)). Similar results were obtained by using $\sigma_{1,3} = 0.05$ (open circles in Fig. 3.4(b)) and $\sigma_{1,3} = 0.01$ (solid circles in Fig. 3.4(b)). As expected, the decrease of the noise levels involves lower extinction probabilities for both tumor and healthy cells, although the same tendencies are preserved i.e., increasing r_3 enlarges tumor cells extinctions and decreases host cells extinctions. Figure 3.4(c)-(d) displays several time series for different values of r_3 and

noise intensities, also representing the deterministic dynamics. For instance, in Fig. 3.4(c) (setting $r_3 = 3.7$) the deterministic dynamics is chaotic and no extinctions are found. However, the stochastic dynamics (here using $\sigma_{1,3} = 0.1$) can cause extinction or survival of tumor and healthy cells also with $r_3 = 3.7$. In Fig. 3.4(d) we use $r_3 = 9$. The deterministic dynamics for this case involves outcompetition of healthy and effector cells by tumor cells. However, the stochastic dynamics ($\sigma_{1,3} = 0.01$) can involve either the extinction or survival of tumor cells. Finally, Fig. 3.4(e) displays the dynamics using $r_3 = 12.5$. For this case, the deterministic dynamics also involves dominance of tumor cells, but the stochastic dynamics (with $\sigma_{1,3} = 0.05$) involves an extinction probability of tumor cells of $P_1^{ext} \sim 0.8$. In Fig. 3.4(f) we display the trajectories projected in the phase space $(x_2(t), x_1(t))$ using $r_3 = 4$ and $\sigma_{1,3} = 0.05$. The main plot shows ten stochastic trajectories that reach the $(0, 1, 0)$ attractor (solid black circle) that involves the survival of healthy cells and the extinction of both effector and tumor cells. The inset displays the deterministic dynamics also for $r_3 = 4$, which is governed by the chaotic attractor.

Finally, we want to note that the same qualitative extinction patterns were obtained using parameter values explored in [72], setting: $a_{31} = 0.9435$ and $a_{13} = 5$. Moreover, all the previous simulations (using parameter values from Refs. [59] and [72]) were repeated using different extinction thresholds i.e., $x_i(t) \leq 10^{-10}$ and $x_i(t) \leq 10^{-20}$, and the extinction probabilities remained qualitatively equal for both deterministic and stochastic dynamics (results not shown).

3.4 Conclusions

In this chapter, a semi-analytic method to find approximate solutions for nonlinear differential equations - the step homotopy analysis method (SHAM) - is applied to solve a cancer nonlinear model initially proposed by Itik and Banks [59]. With this algorithm, based on a modification of the homotopy analysis method (HAM) proposed by Liao [28, 29, 30], three coupled nonlinear differential equations are replaced by an infinite number of linear subproblems. This modified method has the advantage of giving continuous solutions within each time interval, which is not possible by purely numerical techniques. Associated to the explicit series solutions there is an auxiliary parameter, called convergence-control parameter, that represents a convenient way of controlling the convergence of approximation series, which is a critical qualitative difference in the analysis between HAM/SHAM and other methods.

The model by Itik and Banks [59] considers the dynamics of three interacting cell types: healthy cells, tumor cells, and effector immune cells (i.e., CD8 T cells, also named cytotoxic lymphocytes, CTLs). Our analytical results are found to be in excellent agreement with the numerical simulations. To the best of our knowledge, such kind of explicit series solutions, corresponding to each of the dynamical variables, have never been reported for the Itik-Banks cancer model. The results presented in this chapter suggest that SHAM is readily applicable to more complex chaotic systems such as Volterra-Lotka type models applied to cancer dynamics. In this work we used the homotopy solutions to investigate the impact of a key parameter in the dynamics of tumor growth: the activation of effector immune cells due to recognition of tumor antigens (parameter r_3). Previous research has focused on other key parameters of the model by Itik and Banks. For instance, the active

suppression of the immune response by the tumor cells has been recently explored in [72]. Interestingly, the dynamics were shown to be very sensitive to the suppression of the immune cells, involving an inverse period-doubling bifurcation scenario at increasing the suppression rate of immune cells [72]. For this case, strong chaos and low predictability was found at small suppression rates, and the chaotic dynamics became more predictable at increasing suppression values. The selective shutdown of the antitumor immune response can also be achieved by the escape of the recognition of the cancer cells by the immune system by selection of non-immunogenic tumor cell variants and in influencing immune cells with a negative regulatory function, such as regulatory T cells and myeloid-derived suppressor cells Thus, the cell-killing activity of the cytotoxic CD8 T cells can be inhibited by the presence within the tumor tissue of immunosuppressive CD4+ regulatory T cells (T_{reg} cells). The function of T_{reg} cells is essential for inducing tolerance to "self" antigens, preventing autoimmune reactions and for the downregulation of the immune response after the elimination of the antigenic source (such as pathogens, allogenic cells or cancer cells). However, their capacity to inhibit the innate and adaptive anti-tumor immune response also constitute a major obstacle to cancer immunotherapy.

We have used the homotopy solutions to characterize changes in the dynamics at increasing activation rates of the immune cells. Such a parameter is especially important since several clinical therapies are currently available to boost immune responses (see next paragraph). The increase of the immune cells activation rate is shown to cause a period-doubling bifurcation scenario that makes the system to enter into chaotic dynamics. Interestingly, the populations of tumor cells, although undergoing large fluctuations, are able to survive for all the range of r_3 analyzed. In order to simulate demographic

stochasticity that might be found at early stages of tumorigenesis, we added noise terms to the homotopy solutions for tumor and effector immune cells populations. As a difference from the deterministic dynamics, we found that an increase of r_3 increases the extinction probabilities for tumor cells, also diminishing the extinction probabilities of healthy cells. These results suggest that possible therapies enhancing the activation of effector immune cells (see next paragraph) at early stages of tumor progression could result in higher probabilities of stochastic tumor clearance. lt is worth to note that the model proposed by Itik and Banks does not explicitly model the clonal expansion of immune cells after tumor antigen recognition that could make the noise in CTLs populations to be even smaller or negligible. It is known that after being activated, the population of CTLs is expanded in order to exert strong cytotoxic effects. Then, the CD8 response is downregulated by programmed cell death mechanisms to avoid over-activation of the immune system [81]. Due to the complexity of the dynamics found at increasing r_3, it is not clear if clonal expansion would favor the extinction of tumor cells, as we would expect. In this sense, the effect of immune system activation together with production of large populations of effector immune cells due to clonal expansion (burst in the population of effector immune cells) should be modeled to determine if our observed results remain the same or change the probabilities of tumor cells extinction in response to increases in r_3.

Our results could be clinically relevant since several therapies to stimulate and activate immune cells are currently available. A foundational property of the immune system is its capacity to distinguish between the "self" and "non-self" antigens. In the context of an evolving tumor, it is likely that the tumoral cells will present to the immune cells a number of new antigens product of the genetic aberrations present in their genome. This

mechanism is probably involved in the control of early tumors. However, it is known that cancer cells escape innate and adaptive immune responses by selection of non-immunogenic tumor cell variants (immunoediting) or by active suppression of the immune response (immunosubversion) (see [81] for a review). Tumor antigens often elicit poor adaptive immune responses because they are recognized as "self-antigens" that induce tolerance, the natural mechanism of the body to prevent autoimmunity. The enhancement of the antitumor T cell responses by triggering TCR costimulatory molecules to break tolerance has been envisaged as a way to potentiate the antitumor immune functions. Agonists of the costimulatory tumor necrosis factor receptor (TNFR) family members, which include proteins involved in B and T cell development, survival, and immune activation, have been proven to enhance the antitumor immune responses. Preclinical and early clinical data of the use of agonists of 4-1BB (CD137) or OX40 (CD134) support further studies of these costimulatory molecules as potentiators of the antitumor response [82]. An increasingly successful anticancer strategy that aims to boost immune responses against tumor cells consists in enhancing the cell-killing activity of the cytotoxic CD8 T cells by the use of antibodies that block negative regulators of T-cell activation ("checkpoint inhibitors"). Fully humanized monoclonal antibodies blocking the inhibitory molecules Cytotoxic T-Lymphocyte antigen 4 (CTLL4, Ipilimumab, Tremelimumab) or Programmed Death Receptor-1 (PD-1, Nivolumab, MK-3475) have been proven to be useful in solid tumors such as melanoma, renal cell carcinoma, non small cell lung cancer or colorectal cancer (reviewed in [83]). More recently, the p110δ isoform of phosphoinositide-3-OH kinase (PI(3)K) activity has been shown to be required for the proliferation and differentiation of suppressive T_{reg} cells induced by tumor cells. PI(3)K δ inhibitors have been proven to be able to preferen-

tially inhibit CD4 T_{reg} cells over effector CTLs, opening new ways to unleash the power of dormant anti-tumor immune cells [84]. More recent and novel approaches suggest the possibility to increase CTLs activation by means of artificial APCs (see [85] for further details).

Summarizing, our results suggest that potential therapies increasing activation rates of effector immune cells might be much more effective at early stages of tumor progression, when demographic noise becomes important in tumor cells populations. Our results also suggest that the stimulation of immune cells may not facilitate tumor clearance in cancers with large population numbers of tumor cells, as the deterministic approach is considering. Further research should also analyze the robustness and generality of our results to changes in the other model parameters. As discussed in [72], it would be also interesting to explore the effect of increasing the activation of effector immune cells in solid tumors by means of a spatial version of the cancer model analyzed in this chapter.

Chapter 4

How complex, probable, and predictable is genetically driven Red Queen chaos?[3]

Coevolution pervades evolutionary change on multiple scales. The complexity of coevolution has been addressed by means of experimental research [87, 88, 89, 90] and a multitude of theoretical models have been also developed to characterize the dynamics of coevolving systems [91, 92] (see also [93] and references therein). Antagonistic coevolution describes the reciprocal evolutionary dynamics between exploiter-victim systems (e.g., predator or parasite interactions with prey or hosts). Coevolution involves changes in the genetic make-up of one population in response to a genetic change in the antagonistic population [94]. Antagonistic interactions can give rise to different dynamical outcomes, among them, a fluctuating selection labeled as Red Queen dynamics, which involves continuous reciprocal changes in the coevolving traits [95, 96, 97, 98, 99, 100].

The Red Queen theory has deep implications in the evolutionary biology of species. It has been suggested that coevolving pathogens may facilitate the persistence of outcrossing despite its costs. Coevolutionary interactions between hosts and pathogens might generate

[3]This study has been published in [86].

ever-changing conditions and thus favor the long-term maintenance of outcrossing relative to self-fertilization [101] or asexual reproduction [102, 103] (see also [104] for a review). Moreover, the Red Queen may be also behind the huge diversity of genes related to immune functions, virulence and resistance [105], as well as behind spatial diversity and local adaptation of coevolving species [106].

It is important to differentiate between two main types of Red Queen dynamics [107, 108, 109], both of them having a genetic basis. This distinction is important because these two types of coevolution differ on their mechanisms, on their underlying genetic architecture, and on the time scales on which they develop [108]. On one hand, ecologically driven dynamics characterized by negative frequency-dependent selection. On the other hand, genetically driven dynamics due to beneficial mutations. In the first type, variants of the exploiter genotype that benefit the most from the numerically dominant victim genotypes are favoured. Similarly, victim genotypes that better resist the numerical dominant exploiter genotpyes are favoured [110]. This pattern results in selection against common exploiter and victim genotypes in a time-lagged negative frequency dependent fashion (so-called ecological instability). Such a fluctuating selection ensures genetic polymorphisms for long periods (balanced selection) and alleles frequencies can oscillate over short periods of time [110]. Genetically driven Red Queen involves the repeated incidence, spread and fixation of new beneficial mutations that are stabilized in ecological populations by directional selection. Hence, genetic polymorphism is transitory only, and the evolutionary dynamics are slow because: (i) new mutations causing variation in the adaptive traits involved are rare events; (ii) new mutant starts with a very low frequency (i.e., $1/N$, where N is the number of wild-type alleles in the population), thus empirically

it can take hundreds of generations until the mutant becomes recognizable (e.g., 1%) at the population level [111]. The previous phenomenon involves that genetically driven Red Queen dynamics develop on an asymmetric time scale, which can be several orders of magnitude slower than the ecological time scale. This is of special importance in those coevolving organisms with low reproduction times, such as metazoan, or, in a more general sense, for those organisms with ecological K-strategies (i.e., K-selected species typically invest more heavily in fewer offspring, each of which has a relatively high probability of surviving to adulthood). Although for viruses, bacteria or protozoa there might also exist such an asymmetry in time scales, their fast reproduction cycles would make possible to fix beneficial mutations faster. Despite this observation, it is known that RNA viruses such as *Tobacco etch virus* does not produce beneficial mutations in a short time scale [112], and, for example, *Vesicular stomatitis virus* has a spontaneous fraction of new beneficial mutations of about 4.2% [113].

The slow time scale involved makes difficult to address genetically driven Red Queen dynamics experimentally. In this sense, mathematical models offer a unique tool to explore the conditions that could favour the Red Queen over escalation or specialization. The majority of the available models have focused on two coevolving species, ignoring the multispecies ecological context in which coevolution takes place. In this setting, genetically driven Red Queen dynamics develop as regular, predictable cycles in the adaptive traits space. More recently, Dercole and colleagues proposed a mathematical model describing genetically driven coevolution in a food chain formed by a prey, a predator and a superpredator [110]. They found that conditions leading to genetically driven periodic cycles in the two traits of coevolving predator and prey promoted chaos in the coevolution

between the three-species forming the food chain, similarly to previous works showing that the addition of a third species in a two-species system usually involves the possibility of chaos [67, 114].

In this chapter we investigate the model proposed by Dercole *et al.* [110], focusing on the analysis of the complexity and predictability of genetically driven Red Queen chaos. The predictability horizons in evolution are a matter of debate [115, 116]. Indeed, some authors pointed out the existence of an inherent limit on the predictability of evolution by establishing connections between evolutionary theory, computability, and logics [117]. Several works have recently addressed this subject exploring evolutionary trajectories in fitness landscapes [118]. Moreover, evolution experiments with microbes have begun to address predictability of adaptation on a microevolutionary scale [119, 120, 121, 122, 123]. In particular, strong signatures of parallel evolution have been observed in the context of the evolution of antibiotic resistance in pathogens, a finding that is of direct relevance to strategies of drug design and deployment [124, 125, 126, 127]. In the context of coevolution, as far as we know, predictability in genetically driven Red Queen dynamics still remains completely unexplored. In this chapter we aimed to cover this gap, providing a detailed analysis of the dynamical complexity and the predictability of this coevolutionary complex dynamics.

The chapter is organized as follows. In Section 4.1 we briefly introduce the mathematical model for genetically driven Red Queen dynamics. Section 4.2, which is divided in five subsections, contains all our results. In Subsection 4.2.1 we analytically show that the chaotic attractor is positively invariant. In Subsection 4.2.2, we compute the coupling complexity by means of observability indices, which allow us to rank the dynamical

variables from more to less observable. Then, in Subsection 4.2.3 we analyze a family of one-dimensional iterated maps identified in the chaotic dynamics for the state variable with the highest observability index. Different symbolic orbits associated with these maps are used to compute the topological entropy using mutation rates as control parameters. Subsection 4.2.4 contains the computation of the spectrum of Lyapunov exponents and of the predictability of coevolutionary chaos also focusing on the impact of mutation rates. In Subsection 4.2.5 we will perform a systematic sampling of a given region of the parameter space to estimate how probable is chaotic dynamics. Finally, Section 4.3 is devoted to some conclusions.

4.1 Three-species coevolutionary model

The mathematical model investigated in this chapter was recently introduced by Dercole and colleagues [110] as an extension of a simple two-species predator-prey system [91], including another species forming a food chain. The function of each species in the food chain is determined by a continuous character subject to rare and small genetic mutations. The model focuses on a single adaptive trait for each species, which determines the competitive ability of the prey and foraging success in the predator and superpredator. On the evolutionary time scale, *de novo* trait variation is caused by rare genetic mutation. The current phenotypes determine the ecological equilibrium of the food chain, and hence the selective pressures acting on variants of the traits. Each species is characterized by one genetic trait for the prey (x_1), the predator (x_2) and the superpredator (x_3), respectively. The long-term coevolution of traits x_1, x_2, and x_3 on the evolutionary time scales obeys the canonical equation of adaptive dynamics [92], given by the next set of nonlinear

differential equations:

$$\frac{dx_1}{dt} = \frac{1}{2}\mu_1\sigma_1^2\overline{n}_1(\vec{x})\cdot\{-\overline{n}_1(\vec{x})\cdot[2e_2(x_1-e_1)]- \tag{4.1}$$

$$-\overline{n}_2(\vec{x})\left[-\frac{2}{a_{21}}\left(\frac{x_1-a_{24}}{a_{21}}\right)+\left(\frac{2a_{23}}{a_{21}}\cdot\frac{x_2-a_{25}}{a_{22}}\right)\right]a_2(x_1,x_2)\Bigg\},$$

$$\frac{dx_2}{dt} = \frac{1}{2}\mu_2\sigma_2^2\overline{n}_2(\vec{x})\left\{e_2\overline{n}_1(\vec{x})\left[\frac{2a_{23}}{a_{22}}\left(\frac{x_1-a_{24}}{a_{21}}\right)-\frac{2}{a_{22}}\left(\frac{x_2-a_{25}}{a_{22}}\right)\right]a_2(x_1,x_2)\right. \tag{4.2}$$

$$\left.-\overline{n}_3(\vec{x})\left[-\frac{2}{a_{31}}\left(\frac{x_2-a_{34}}{a_{31}}\right)+\frac{2a_{33}}{a_{31}}\left(\frac{x_3-a_{35}}{a_{32}}\right)\right]a_3(x_1,x_2)\right\},$$

$$\frac{dx_3}{dt} = \frac{1}{2}\mu_3\sigma_3^2\overline{n}_3(\vec{x})e_3\overline{n}_2(\vec{x})\left[\frac{2a_{33}}{a_{32}}\left(\frac{x_2-a_{34}}{a_{31}}\right)-\frac{2}{a_{32}}\left(\frac{x_3-a_{35}}{a_{32}}\right)\right]a_3(x_2,x_3) \tag{4.3}$$

Here $\vec{x}=(x_1,x_2,x_3)$,

$$\overline{n}_1(\vec{x}) = \frac{r}{c}-\frac{a_2d_3}{ce_3a_3},\quad \overline{n}_2(\vec{x})=\frac{d_3}{e_3a_3},\quad \overline{n}_3(\vec{x})=\frac{e_2a_2}{a_3}\left(\frac{r}{c}-\frac{a_2d_3}{ce_3a_3}\right)-\frac{d_2}{a_3},$$

$$c = c_0+c_2(x_1-c_1)^2$$

and

$$a_2(x_1,x_2) = \exp\left(-\left(\frac{x_1-a_{24}}{a_{31}}\right)^2+2a_{23}\frac{(x_1-a_{24})(x_2-a_{25})}{a_{21}a_{22}}-\left(\frac{x_2-a_{25}}{a_{22}}\right)^2\right)$$

$$a_3(x_1,x_2) = \exp\left(-\left(\frac{x_2-a_{34}}{a_{31}}\right)^2+2a_{33}\frac{(x_2-a_{34})(x_3-a_{35})}{a_{31}a_{32}}-\left(\frac{x_3-a_{35}}{a_{32}}\right)^2\right).$$

The model under investigation is here presented in its extended version. We refer the reader to Section *Model construction* in Ref. [110] (see also Refs. [91, 92]) for a detailed

description of all the steps followed to built the mathematical model.

Parameter r is the prey intrinsic *per capita* growth rate; c is the sensitivity to intraspecific competition; $a_{i=2,3}$ are the attack rates in the predator ($i = 2$) and the superpredator ($i = 3$). Parameter $e_{i=2,3}$ are the efficiencies in the predator and the superpredator; while $d_{i=2,3}$ are the intrinsic death rates of both predators and superpredators. Parameters $\mu_{i=1,2,3}$ are mutation rates of preys ($i = 1$), predators ($i = 2$) and superpredators ($i = 3$). Parameters σ_i^2 and $\bar{n}_i$ are, respectively, mutational step variances and equilibrium densities for species $i = 1, 2, 3$ (i.e., prey, predator and superpredator). Attack rates a_2 and a_3 are bidimensional Gaussian functions with elliptic contour lines centered at (a_{24}, a_{25}) and (a_{34}, a_{35}), respectively, and controlled in amplitude and orientation by parameters $a_{21} - a_{23}$ and $a_{31} - a_{33}$ (see [110] for further details on the other terms and parameters of the model above). In our work we will first consider as control parameters the mutation rates μ_i, to analyze the impact of the rates of evolution on the dynamics of the model. For these analyses we will fix the values of the remaining parameters following [110]:

$$
\begin{aligned}
\sigma_1^2 &= 0.3,\ \sigma_2^2 = 2 \text{ and } \sigma_3^2 = 2,\\
r &= 0.5,\\
d_2 &= 0.05 \text{ and } d_3 = 0.02,\\
e_2 &= 0.14 \text{ and } e_3 = 0.14,\\
a_{21} &= 0.22,\ a_{22} = 0.25,\ a_{23} = 0.6 \text{ and } a_{25} = 0.04,\\
a_{31} &= 0.22,\ a_{32} = 0.25,\ a_{33} = 0.6,\ a_{34} = 0 \text{ and } a_{35} = -0.04,\\
c_0 &= 0.5,\ c_1 = 0 \text{ and } c_2 = 3.
\end{aligned}
$$

Then, in Subsection 4.2.5 we will use some of the previous parameters also as control

parameters. In all our analysis we will use as initial conditions (if not otherwise specified):

$$x_1(0) = -0.11,\ x_2(0) = 0.11 \text{ and } x_3(0) = 0.012.$$

For numerical integrations of the differential equations we used the *StiffnessSwitching NDSolve* method from Mathematica 9.0.

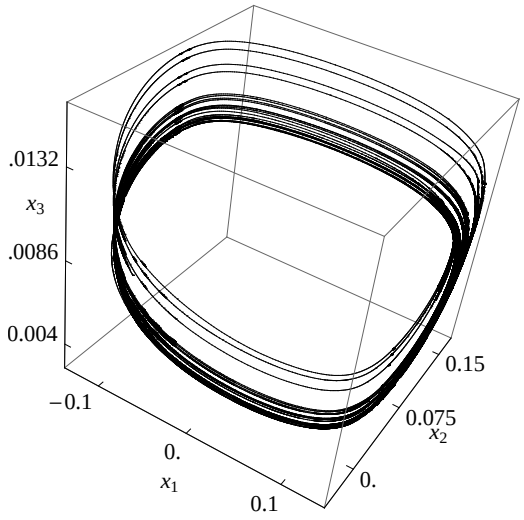

Figure 4.1: The chaotic attractor, with maximum Lyapunov exponent (MLE) $\lambda_1 = 0.016868$, arising in the model of Dercole and colleagues [110], given by Eqs. (4.1)-(4.3). The trajectories are displayed in the traits phase space (x_1, x_2, x_3), using $\mu_1 = 4.325$ and $\mu_2 = \mu_3 = 1$.

4.2 Results

4.2.1 Positively invariant sets

In the following Sections we will examine the long-term behavior of the three-dimensional chaotic attractors arising in the coevolutionary system modeled by Eqs. (4.1)-(4.3). The chaotic attractor, which is displayed in Fig. 4.1, can govern the dynamics of the genetic traits of the three species of the food chain, given by x_1 (prey), x_2 (predator) and x_3 (super

predator). As mentioned in Chapter 1, Section 1.4, a significant preliminary question to answer before doing any further analysis is to find conditions for which trajectories will not "escape to infinity", so that they will remain confined to a compact set. In biological terms, this boundedness means that no trait grows without limit and thus the model captures correctly the coevolutionary dynamics. Let us consider a new function $\Psi = x_1 + x_2 + x_3$, i.e., the sum of the traits involved in the 3D system. The temporal derivative of Ψ is

$$\frac{d\Psi}{dt} = \frac{dx_1}{dt} + \frac{dx_2}{dt} + \frac{dx_3}{dt}.$$

Adding $\varepsilon\Psi$ to $\frac{d\Psi}{dt}$, gives $\frac{d\Psi}{dt} + \varepsilon\Psi = \chi(\vec{x})$, for $\varepsilon > 0$. An upper bound of $\chi(\vec{x})$ is given by

$$\chi(\vec{x}) \leq |\chi^*(\vec{x})| = \left| -c_2\mu_1\left(\frac{r}{c_0}\right)^2 x_1^2 - c_1c_2\mu_1\sigma_1^2\left(\frac{r}{c_0}\right)^2 - \frac{1}{2}\mu_1\sigma_1^2\frac{r^2}{c_0}A^2 - \frac{1}{2}\mu_2\sigma_2^2\frac{e_2r^2}{c_0}B^2 \right.$$

$$\left. -\frac{1}{2}\mu_2\sigma_2^2\frac{e_2r^2}{c_0}C^2 - \frac{1}{2}\mu_3\sigma_3^2\frac{e_2e_3r^2}{c_0}D^2 - \varepsilon x_1 - \varepsilon x_2 - \varepsilon x_3 \right|,$$

with

$$A = -\frac{2}{a_{21}}\left(\frac{x_1 - a_{24}}{a_{21}}\right) + \frac{2a_{23}}{a_{21}}\left(\frac{x_2 - a_{25}}{a_{22}}\right),$$

$$B = \frac{2a_{23}}{a_{22}}\left(\frac{x_1 - a_{24}}{a_{21}}\right) - \frac{2}{a_{22}}\left(\frac{x_2 - a_{25}}{a_{22}}\right),$$

$$C = -\frac{2}{a_{31}}\left(\frac{x_2 - a_{34}}{a_{31}}\right) + \frac{2a_{33}}{a_{31}}\left(\frac{x_3 - a_{35}}{a_{32}}\right),$$

$$D = \frac{2a_{33}}{a_{32}}\left(\frac{x_2 - a_{34}}{a_{31}}\right) - \frac{2}{a_{32}}\left(\frac{x_3 - a_{35}}{a_{32}}\right).$$

We obtain $\chi(\vec{x}) \leq |\chi^*(x_1^*, x_2^*, x_3^*)| = L$, being $\chi^*(x_1^*, x_2^*, x_3^*)$ the maximum of χ^* and taking $0 < \varepsilon \leq 0.8$. It follows that $d\Psi/dt \leq -\varepsilon\Psi + L$. Using the differential form of the Gronwall's inequality [48], we find

$$\Psi(t) \leq \Psi(0)e^{-\varepsilon t} + \frac{L}{\varepsilon}\left(1 - e^{-\varepsilon t}\right) \leq \max\left(\frac{L}{\varepsilon}, \Psi(0)\right).$$

Therefore, we can conclude that the trajectories starting from any arbitrary initial condition will remain confined to a compact set.

4.2.2 Observability analysis

Our present application of the outlined formalism concerning the observability concept, where the observability matrix is interpreted as the Jacobian matrix of the coordinate transformation in study, $O_s = J(\Phi_s)$, leads to the computation of the observability indices of the traits x_1, x_2 and x_3. In particular, for $\mu_1 = 4.325$, $\mu_2 = 1$ and $\mu_3 = 1$, the observability indices averaged over a trajectory are $\delta_{x_1} = 0.005447...$, $\delta_{x_2} = 0.002449...$ and $\delta_{x_3} = 0.000037...$ From the previous values, the variables can be ranked in descending degree of observability according to

$$x_1 \rhd x_2 \rhd x_3,$$

where $\rhd$ means "provides better observability index of the underlying dynamics than". We notice that the previous ordering of the observability indices holds for all the mutation rates analyzed in this chapter (results not shown). The three induced phase portraits from the coevolutionary system using the derivative coordinates are displayed in Fig. 4.2. The computation of the observability indices indicates that variable x_1 is the best observable, while x_3 is the poorest. The important message of this analysis is that

the dynamics of the three-species coevolutionary model is observed with higher reliability from the genetic trait of the prey (variable x_1), rather than from the genetic traits of predator and superpredator (variables x_2 and x_3, respectively). Genetic trait x_2 provides an observability of the dynamics that is slightly less than the one provided by the genetic trait x_1, but genetic trait x_3 is associated with a clearly poor observability (δ_{x_3} is smaller than δ_{x_1} and δ_{x_2} by two orders of magnitude).

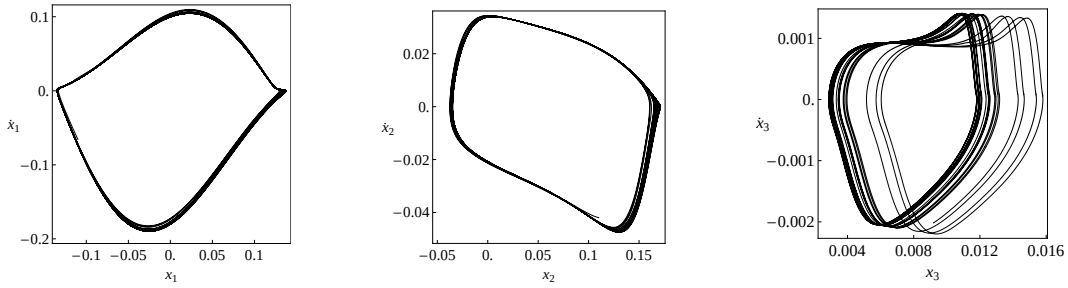

Figure 4.2: Projections of the dynamics on the $(x_1, \dot{x_1})$, $(x_2, \dot{x_2})$ and $(x_3, \dot{x_3})$ planes used to compute observability indices in Subsection 4.2.2. We here use $\mu_1 = 4.325$ and $\mu_2 = \mu_3 = 1$.

A 3D-reconstructed attractor would be the result of the representation of the points (X_1, X_2, X_3), with coordinates given by the transformation Φ_s. Only this 3D-representation can be directly compared with the original 3D attractor. The 2D-representations of (X_1, X_2) are different entities, they are just phase portraits, and not necessarily similar to the 3D attractor. In the observability theory, the dynamical states (X_1, X_2) are used to provide the first brief glances over the complexity of the orbits.

In the next paragraphs, we devote a special attention to the dynamical variable x_1. Actually, we could choose also x_2 because the observability index is of the same order of magnitude than x_1. However, for concreteness we will hereafter focus on x_1.

4.2.3 Topological entropy

Taking the state variable with the highest index, x_1, previously characterized, we present a family of one-dimensional iterated maps identified in the studied model [128]. In our analyses, we will take the following values of mutation rates

$$3.9 \leq \mu_1 \leq 4.325,\ 1 \leq \mu_2 \leq 1.08 \text{ and } 0.85 \leq \mu_3 \leq 1.0047.$$

The one-dimensional maps that we are analyzing have been obtained by recording the successive local maxima of a trajectory within the chaotic attractor for the genetic trait x_1 (see Fig. 4.3). Hence, these iterated maps consist of pairs $(x_1^{(n)}, x_1^{(n+1)})$, where $x_1^{(n)}$ denotes the n^{th} relative maximum. As shown in Fig. 4.3(Right), the obtained discrete map dynamically behaves like a continuous map with a single critical point, c, which maps an interval $I = [a, b]$ into itself.

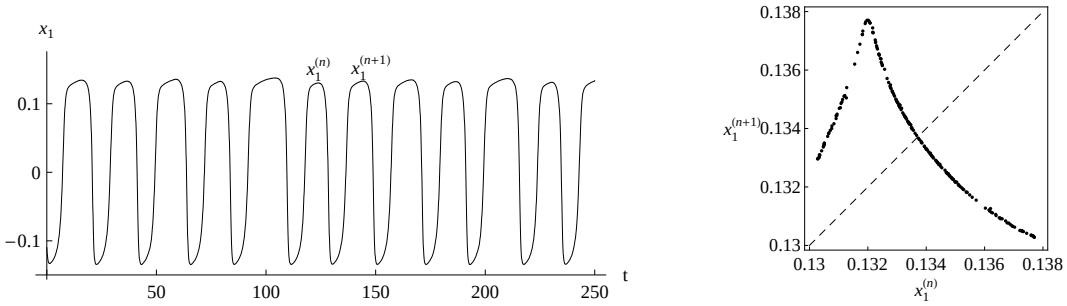

Figure 4.3: (Left) Chaotic time series of the genetic trait $x_1(t)$, using $\mu_1 = 4.325$, $\mu_2 = 1$ and $\mu_3 = 1$. (Right) Iterated unimodal map obtained from plotting successive local maxima of the temporal dynamics of x_1, also using the previous parameter values.

In order to illustrate the outlined formalism about the computation of the topological entropy, we discuss the following example. Let us consider the map of Fig. 4.3(Right). The symbolic orbit of the turning point, c, determines the period-12 kneading sequence

$(RLRRRRLRRRRC)^{\infty}$. After ordering the orbital points, we obtain:

$$x_2 < x_7 < x_0 < x_5 < x_{10} < x_3 < x_8 < x_9 < x_4 < x_{11} < x_6 < x_1.$$

The associated transition matrix is

$$M(f) = \begin{bmatrix} 0 & 0 & 0 & 0 & 0 & 1 & 0 & 0 & 0 & 0 & 0 \\ 0 & 0 & 0 & 0 & 0 & 0 & 1 & 1 & 1 & 1 & 1 \\ 0 & 0 & 0 & 0 & 0 & 0 & 0 & 0 & 0 & 0 & 1 \\ 0 & 0 & 0 & 0 & 0 & 0 & 0 & 0 & 0 & 1 & 0 \\ 0 & 0 & 0 & 0 & 0 & 0 & 0 & 0 & 1 & 0 & 0 \\ 0 & 0 & 0 & 0 & 0 & 0 & 0 & 1 & 0 & 0 & 0 \\ 0 & 0 & 0 & 0 & 1 & 1 & 1 & 0 & 0 & 0 & 0 \\ 0 & 0 & 0 & 1 & 0 & 0 & 0 & 0 & 0 & 0 & 0 \\ 0 & 0 & 1 & 0 & 0 & 0 & 0 & 0 & 0 & 0 & 0 \\ 0 & 1 & 0 & 0 & 0 & 0 & 0 & 0 & 0 & 0 & 0 \\ 1 & 0 & 0 & 0 & 0 & 0 & 0 & 0 & 0 & 0 & 0 \end{bmatrix}$$

which has the characteristic polynomial

$$p(\lambda) = \det(M(f) - \lambda I) = -1 - \lambda - \lambda^2 - \lambda^3 + \lambda^4 + \lambda^5 - \lambda^6 + \lambda^7 - \lambda^8 + \lambda^9 + \lambda^{10} - \lambda^{11}.$$

The growth number $s(f)$ (the spectral radius of matrix $M(f)$) is 1.50771.... Therefore, the value of the topological entropy is given by: $h_{top}(f) = \log s(f) = 0.410591...$. The study of the kneading sequences allows us to identify pairs of values (μ_1, μ_2), (μ_1, μ_3) and (μ_2, μ_3) corresponding to symbolic periodic orbits (Figure 4.4 (Upper panel)). We show the locations of these points in the parameter space associated with small periods: 2-period - $(RC)^{\infty}$, 4-period - $(RLLC)^{\infty}$, and 8-period - $(RLRRRLRC)^{\infty}$, which indicates the beginning of the chaotic region. The identified kneading sequences correspond to logistic-type maps with different levels of complexity. Figure 4.4 (Lower panel) shows the variation of the topological entropy computed for the system in the parameter ranges

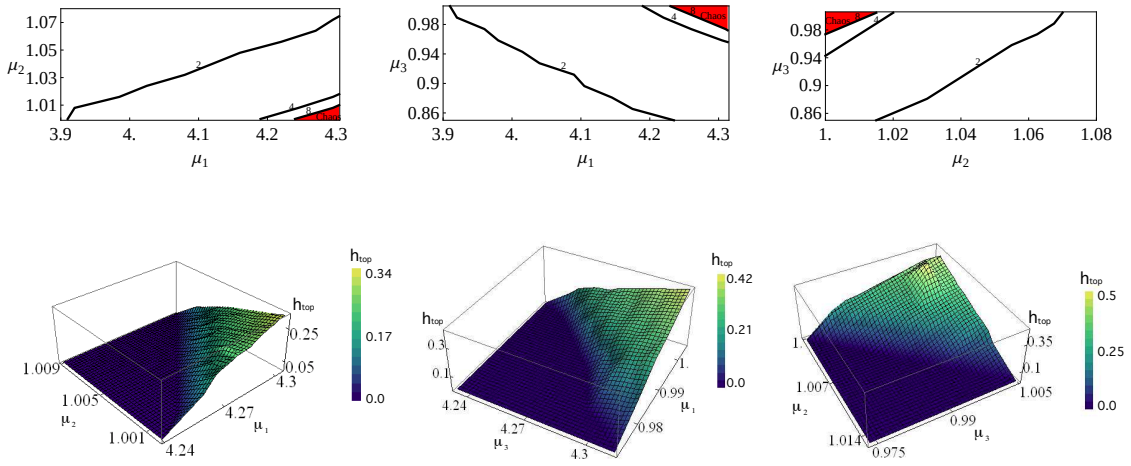

Figure 4.4: (Upper panel) Representation of the periods-2,4,8 and the chaotic region (displayed in red), which correspond to positive topological entropy for $3.9 \leq \mu_1 \leq 4.325$, $1 \leq \mu_2 \leq 1.08$ and $0.85 \leq \mu_3 \leq 1.0047$. (Lower panel) Variation of the topological entropy focusing on the chaotic regions.

corresponding to the chaotic scenarios. Bifurcation diagrams, obtained from $x_1^{\max}$, are exhibited in Fig. 4.5. The dynamics is sensitive to the mutation rates μ_i $(i = 1, 2, 3)$ and the chaotic scenarios occur for high values of μ_1 and μ_3 as well as for small values of μ_2. As a consequence of the positiveness of the topological entropy, the feature of the original model that we are studying - *the temporal dynamical behavior of the successive local maxima of the genetic trait,* x_1 - is associated with regimes of chaos. Notice that the regions of mutation rates where chaos is found are very narrow (see Subsection 4.2.5), while most of the mutation values correspond to periodic and quasiperiodic dynamics (white regions).

4.2.4 Lyapunov exponents and predictability

As mentioned previously, Lyapunov exponents and entropies are examples of ways of characterizing dynamical local properties for chaotic attractors.

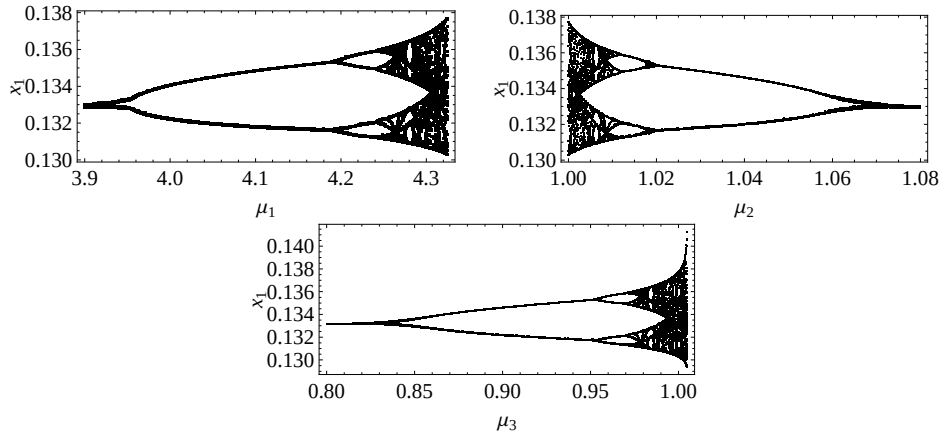

Figure 4.5: Bifurcation diagrams obtained from $x_1^{\max}$ for: $\mu_2 = \mu_3 = 1$ and $3.9 \leq \mu_1 \leq 4.325$; $\mu_1 = 4.325$, $\mu_3 = 1$ and $1 \leq \mu_2 \leq 1.08$; $\mu_1 = 4.325$, $\mu_2 = 1$ and $0.8 \leq \mu_3 \leq 1.0047$. For the three mutation rates analyzed the system undergoes the Feigenbaum scenario, i.e., period-doubling route to chaos.

A positive *maximal Lyapunov exponent* (MLE) is commonly taken as an indicator of chaos. In the left-hand side column of Fig. 4.6, we present $3D-$plots showing the variation of the maximal Lyapunov exponent λ_1 in the parameter regions where chaos occurs. We notice the existence of pairs (μ_j, μ_{j+1}), $j = 1, 2$ corresponding to $\lambda_1 = 0$ (signature of periodic behavior). Our results, in agreement with classical numerical results displayed in the literature**,** show that for certain periodic windows there is a discrepancy between the topological entropy and the MLE. Within these periodic regimes, the topological entropy diverges from the maximum Lyapunov exponent, which decreases rapidly to zero, although initial conditions may wander chaotically in portions of the system. The surfaces representing the topological entropy (Fig. 4.4 (Lower panel)) upper bounds the surfaces that represents the variation of the maximum Lyapunov exponent (Fig. 4.6 (Left hand-side column)). The positive values of the topological entropy shape the variation tendency of λ_1.

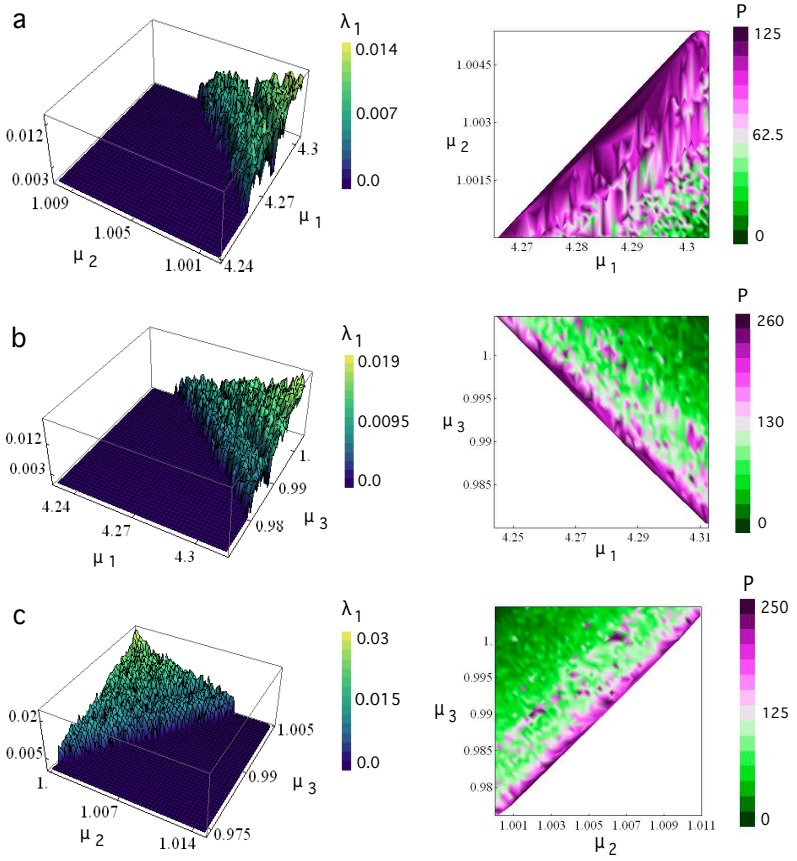

Figure 4.6: (Left hand-side column) Variation of the maximal Lyapunov exponent λ_1 in the mutational parameter spaces. (Right hand-side column) Predictability, P, computed from Eq. (1.11) for the chaotic dynamics shown at the three-dimensional plots on the left. In (a), (b) and (c) we used, respectively $\mu_3 = 1$, $\mu_2 = 1$, and $\mu_1 = 4.325$.

The ability to predict the future state of a dynamical system, given the present one, turns out to be particularly relevant with major implications in applied biology. As established previously, two tightly linked indicators for measuring the rate of the error growth and information produced by a dynamical system are: the Lyapunov exponents and the Kolmogorov-Sinai (or metric) entropy. In this context, the special connection between these two indicators allows us to characterize fine-grained properties of the system. The maximal Lyapunov exponent, λ_1, gives us a first quantitative information on how fast we lose the ability of predicting the system evolution. The sum of all positive Lyapunov characteristic exponents gives us an estimate of the Kolmogorov-Sinai (or metric) entropy. Dynamically, the inverse of the Kolmogorov-Sinai entropy characterizes the predictability of the system. Higher values of the predictability correspond to lower complexity of the dynamics. This fact is made clear in the gradient diagram of Fig. 4.6 (right hand-side column). More specifically, we found that most of the predictability values obtained within the explored regions of the mutation rates are close to zero, especially in the analysis projected onto the parameter spaces (μ_1, μ_3) and (μ_2, μ_3).

4.2.5 Chaos in parameter space

In this Section, we perform a simple numerical experiment to estimate how likely is the occurrence of chaos in a given region of the parameter space of the model. Since the model contains a lot of parameters, we will focus on the role of mutation rates in the overall dynamics, together with the prey's growth rates (r), the efficiencies of the predators in catching the preys (e_i) as well as in the sensitivity of intraspecific competition for the preys (c_i). Specifically, we will explore 8 different parameters within the following ranges: $4.23 \leq \mu_1 \leq 4.325$; $1 \leq \mu_2 \leq 1.01$; $0.972 \leq \mu_3 \leq 1.0047$; $0.49999 \leq r \leq 0.50004$;

$0.1398 \leq e_2 \leq 0.141$; $0.14 \leq e_3 \leq 0.14001$; $0.49995 \leq c_0 \leq 0.500015$ and $3 \leq c_2 \leq 3.0004$ (recall $c_1 = 0$).

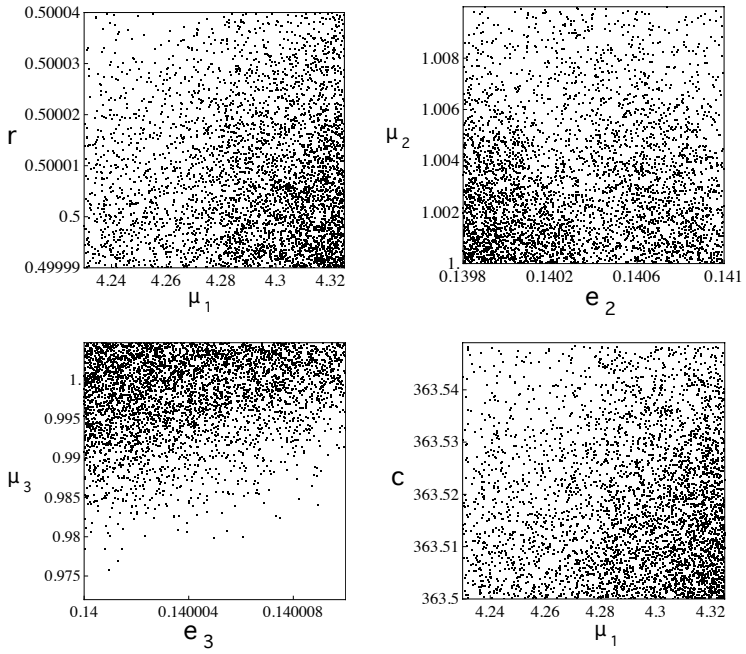

Figure 4.7: Two-dimensional projections of parameter spaces where the MLE is positive. The black dots indicate the pairs of parameters generating chaotic dynamics in the parameter subspaces (μ_1, r), (e_2, μ_2), (e_3, μ_3), and (μ_1, c). Constant r is the prey intrinsic *per capita* growth rate. Parameters μ_i are the mutation rates for the prey ($i = 1$), the predator ($i = 2$), and the superpredator ($i = 3$); e_2 and e_3 are, respectively, the efficiencies of the predator and the superpredator. Finally, c is a competition function.

Notice that instead of using parameters $c_{0,1,2}$, we will represent them together using the formula $c = c_0 + c_2(x_1 - c_1)^2$, which corresponds to the sensitivity of preys to intraspecific competition [110]. The remaining parameters are fixed following the values presented at the end of Section 4.1. All the previous ranges contain the dynamics ranging from period-1 to chaos. To systematically explore this region of the parameter space, we use a MonteCarlo (MC) algorithm, which works as follows: at each algorithm generation, m, we generate random values with uniform distribution for the ranges of all the parameters

previously listed (specifically, we used $m = 150,775$ iterations). For each set of parameters, we numerically compute the full spectrum of Lyapunov exponents following the method described in Section 1.2. Then, by considering the MLE for each set of parameters we can separate the dynamics into two types: ordered (non-positive MLE) or chaotic (positive MLE). This process was repeated at each iteration m. Figure 4.7 displays two-dimensional projections of the parameter space where the chaotic dynamics are found. Specifically, those pairs of parameters giving place to chaotic dynamics are indicated with a black dot. The MC algorithm also allowed us to compute three other interesting measures.

We first computed the probability of finding chaos, π_c, in the sampled parameter space, using $\pi_c = m_c/m$, where m_c is the number of parameters sets generated with the MC algorithm producing a positive MLE. We specifically obtained $\pi_c \sim 0.0306$. We also computed the mean value ($\pm$ SEM) of the MLE in the chaotic regions, given by $\hat{\lambda}_1 = 0.00222177 \pm 0.0000316$; and the mean predictability ($\pm$ SEM), given by $\hat{P} = 148.685 \pm 0.6847$. These computations revealed that the probability of finding chaos in the explored parameter region of the model was extremely small, suggesting that genetically driven coevolution may be driven by ordered dynamics (e.g., periodic or quasiperiodic attractors). However, the analyses presented in Fig. 4.6 indicate that the system can be highly unpredictable in the parameter regions in the chaotic regime.

4.3 Conclusions

Although the inherent complexity tied to evolutionary and coevolutionary processes makes difficult their prediction, several works have attempted to explore predictability in evolutionary processes [118, 119, 120, 121, 122, 123]. However, the degree of predictability in biological coevolution remains poorly explored. Predictability measures for genetically driven Red Queen chaotic dynamics are still lacking in the literature. The difficulty to obtain experimental data for genetically driven Red Queen dynamics make mathematical models a unique tool to understand and quantify the dynamics of such systems as well as their degree of predictability. Recently, Dercole and colleagues [110] presented a model for genetically driven Red Queen dynamics, providing mathematical evidences for the existence of chaos. Here we develop several analyses providing measures quantifying the complexity of genetically driven Red Queen chaos. We specifically computed the topological entropy of this system, also computing the full spectrum of Lyapunov exponents used to characterize the predictability using the rates of evolution as control parameters. These analyses, together with the exploration of some other model parameters, reveal that the parameter ranges leading to chaotic behavior in this deterministic model are very narrow. For the identified chaotic regions predictability was found to be very low, indicating that genetically driven Red Queen chaos may be highly unpredictable.

The model under investigation undergoes the period-doubling route to chaos (i.e., Feigenbaum scenario), which is a typical route to chaos in three-species predator-prey dynamical systems [110]. Hence, the investigated system is also governed by periodic and quasiperiodic attractors. Moreover, we found wide regions of the parameter space with zero MLE, meaning that oscillatory behavior is a very likely outcome of the investigated

system. In this sense, we notice that the presence of genetic noise, such as random drift or stochastic gene flow, as well as demographic noise could increase the regions of the parameter space displaying chaos due to the phenomenon of noise-induced chaos [129, 130, 131]. Future research should quantify the predictability for genetically driven Red Queen chaos considering such sources of noise.

Chapter 5

An optimal homotopy analysis of a HIV-1 model incorporating AIDS-related cancer cells[4]

Nowadays, over 60 million people worldwide have been infected with HIV, more than 80% of whom live in developing countries. For HIV-infected individuals, cancer remains a significant burden. In particular, the *Kaposi's sarcoma* (KS) is the most common neoplasm that occurs in patients with AIDS (AIDS-KS).

Gaining insight into the epidemiology and mechanisms that underlie AIDS-related cancers can provide us with a better understanding of cancer immunity and viral oncogenesis. How can the combination of immunosuppression and activation of inflammation promote cancer development? Our purpose is to try to give a glancing analysis using a simple dynamical model.

The use of mathematical models as an aid in understanding features of HIV-1 and virus infection dynamics has been substantial in the past 20 years. It has been shown in the studies [133], [134] and [135] that there are two ways for HIV-1 to disseminate in vivo: (i) circulating free viral particles to T cells directly, or (ii) through HIV-infected T cells to

[4]This study has been submitted for publication in [132].

healthy T cells (please, see also [136], [137] and [138]). Most of these models focus on cell-free virus spread in the bloodstream ([139] and [140]). A model concerning the cell-to-cell spread of HIV-1 is relevant, since understanding the dynamics of the HIV infection within lymphatic tissues is vital to uncovering information regarding cellular infection and viral production.

The model studied here appeared in [141] as a cell-to-cell spread of HIV-1 together with cancer cells in tissue cultures (in vitro). This model is aimed at explaining some quantitative features concerning cancer occurring during HIV-1 infection that are unusual and, in the absence of a model, perplexing. The basic starting point of this model has three parts. First, the cancer cells are caused by the changes of the normal cells in the individual due to some physical, chemical or biological factor (for instance, a virus such as human papilloma virus (HPV)) - under normal conditions, the healthy cells in our body can mutate into cancer cells with probability of 10^{-6}. Second, the cancer cells have some special genes and so they proliferate in a special way which is different from normal cells. Third, the immune system can recognize the difference between cancer cells and normal cells, so it can survey them and then carry out its killing function.

As pointed out in [141], the studied HIV-1 model has a number of steady states whose existence and stability properties are quite consistent with their biological meanings. Periodic solutions and chaos appear alternately along with the changing of the bifurcation parameters. With this HIV-1 model it is possible to investigate the cancer situation in an individual who is invaded by HIV-1.

The chapter is organized as follows. We give in Section 5.1 a brief description of the HIV-1 model presented in [141]. In Section 5.2, we analytically show that the chaotic

attractor is positively invariant. In Section 5.3, we compute the coupling complexity by means of observability indices, which allow us to rank the dynamical variables from more to less observable. An analytical study, using the homotopy analysis methodology, is carried out in Section 5.4. This section contains the explicit series solution (Subsection 5.4.1) and an optimal homotopy analysis approach of solutions to improve the computational efficiency of HAM (Subsection 5.4.2). In particular, we obtain for each dynamical variable an optimal value of the HAM convergence-control h using an appropriate ratio and using the exact squared residual error. Finally, Section 5.5 is devoted to significative conclusions.

5.1 The HIV-1 cancer model

Due to the immune response caused by HIV-1 in tissue culture in vivo, the HIV-1 cancer model presented in [141] is given by the following ordinary differential equations

$$\frac{dC}{dt} = C\left[r_1\left(1-\frac{C+T+I}{m}\right)-k_1\,T\right], \tag{5.1}$$

$$\frac{dT}{dt} = T\left[r_2\left(1-\frac{C+T+I}{m}\right)-pk_1C-k_2I\right], \tag{5.2}$$

$$\frac{dI}{dt} = I\,\left(k_2T-\mu_I\right). \tag{5.3}$$

Table 5.1 summarizes the meanings of variables and parameters. We will consider throughout our study $r_2 = 0.3$, $k_2 = 0.0005$, $m = 1500$, $p = 0.1$, $\mu_I = 0.3$ and take the uncontrolled proliferation rate of the cancer cell r_1 and the immune system's killing rate of cancer cells k_1 as control parameters ($0.1775 \leq r_1 \leq 0.18425$ and $0.0001 \leq k_1 \leq 0.000107$).

According to the literature ([135], [142] and [143]), the probability that a healthy cell will become a cancer cell is very small, even if there some factors that urge the

Variables and parameters		Meaning
Dependent variables	C	Concentration of cancer cells
	T	Concentration of healthy cells
	I	Concentration of infected cells
Parameters	r_1	Uncontrolled proliferation rate of the cancer cell
	r_2	Intrinsic growth rate of healthy cells
	k_1	Immune system's killing rate of cancer cells
	k_2	Infection rate coefficient
	m	Effective carrying capacity of the system
	p	Losing rate of the immune cells
	μ_I	Immune system's killing effect on the infected cells

Table 5.1: List of variables and parameters.

transformation. We assume that the cancer is caused by just one cell because of gene mutation.

5.2 Positively invariant sets

In the following sections we will examine the long-term behavior of the three-dimensional chaotic attractors arising in the HIV-1 system modeled by Eqs. (5.1)-(5.3). The chaotic attractor, displayed in Fig. 5.1, governs the concentration dynamics of the cancer cells, healthy CD_4+ T lymphocytes and infected CD_4+ T lymphocytes, given by C, T and I, respectively.

In biological terms, the boundedness of the attractors means that no concentration grows without limit and thus the model captures correctly the dynamics.

According to the theory established in Chapter 1, Section 1.4, let us consider a new function

$$\Psi = C + T + I,$$

i.e., the sum of the concentrations involved in the 3D system. The temporal derivative of

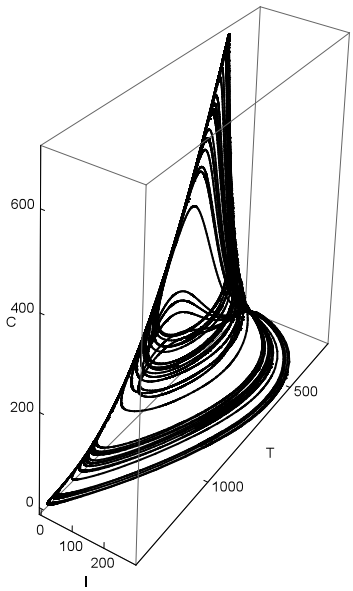

Figure 5.1: Chaotic attractor corresponding to the HIV-1 system of Eqs. (5.1)-(5.3), for $r_1 = 0.1842$ and $k_1 = 0.0001$.

Ψ is

$$\frac{d\Psi}{dt} = \frac{dC}{dt} + \frac{dT}{dt} + \frac{dI}{dt}.$$

Adding $\varepsilon\Psi$ to $\frac{d\Psi}{dt}$, we consider $\frac{d\Psi}{dt} + \varepsilon\Psi = \chi(C,T,I)$, for $\varepsilon > 0$. An upper bound of $\chi(C,T,I)$ is given by

$$\begin{aligned}\chi(C,T,I) &\leq \frac{1}{m}\left|(r_1 m + \varepsilon m - r_1 C)C + (r_2 m + \varepsilon m - r_2 T)T + (-m\mu_I + \varepsilon m - r_1 I)I\right| \\ &\leq H_1 + H_2 + H_3.\end{aligned}$$

with

$$H_1 = \frac{(r_1 m + \varepsilon m)^2}{4r_1}, \quad H_2 = \frac{(r_2 m + \varepsilon m)^2}{4r_2} \text{ and } H_3 = \frac{(-m\mu_I + \varepsilon m)^2}{4r_1}.$$

We obtain $\chi(C,T,I) \leq H_1 + H_2 + H_3 = H$. It follows that $\frac{d\Psi}{dt} \leq -\varepsilon\Psi + H$. Using the

differential form of the Gronwall's inequality [48], we find

$$\Psi(t) \leq \Psi(0)e^{-\varepsilon t} + \frac{H}{\varepsilon}\left(1 - e^{-\varepsilon t}\right) \leq \max\left(\frac{H}{\varepsilon}, \Psi(0)\right).$$

As a consequence, the trajectories starting from any arbitrary initial condition will remain confined to a compact set.

5.3 Observability analysis

Our present application of the outlined formalism of Chapter 1, Section 1.5, where the observability matrix is interpreted as the Jacobian matrix of the coordinate transformation in study, $O_s = J(\Phi_s)$, leads to the computation of the observability indices of the concentrations $C = x_1$, $T = x_2$ and $I = x_3$. In particular, for $r_1 = 0.1842$ and $k_1 = 0.0001$, the observability indices averaged over a trajectory are $\delta_{x_1} = 0.000634602...$, $\delta_{x_2} = 0.0000124925...$ and $\delta_{x_3} = 0.000000107349...$

From the previous values, the original variables can be ranked in descending degree of observability according to

$$C \rhd T \rhd I,$$

where $\rhd$ means "*provides better observability index of the underlying dynamics than*". As illustrated in Fig. 5.2, the previous ordering of the observability indices holds for all the concentrations analyzed in this chapter. More details about the behavior of the highest observability index, δ_C, in the parameter space are given in Fig. 5.3.

The three induced phase portraits from the system using the derivative coordinates are displayed in Fig. 5.4. The computation of the observability indices indicates that variable C is the best observable, while I is the poorest. The important message of this analysis is that the dynamics of the three-variable HIV-1 model is observed with higher reliability

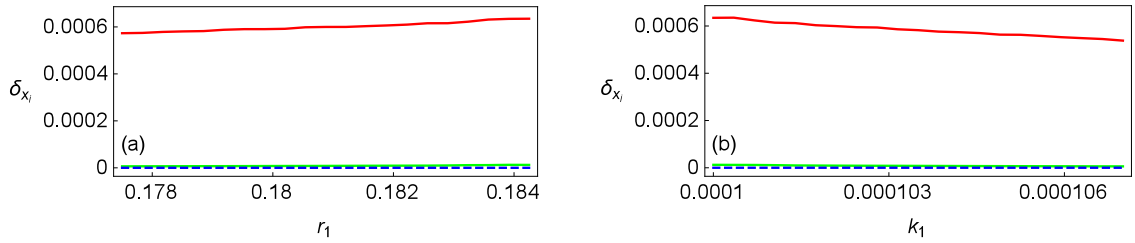

Figure 5.2: Variation of the three observability indices, δ_{x_i} $(i = 1, 2, 3)$, with $C = x_1$, $T = x_2$ and $I = x_3$, where $\delta_C > \delta_T > \delta_I$. (a) $k_1 = 0.0001$ and $0.1775 \leq r_1 \leq 0.18425$; (b) $r_1 = 0.1842$ and $0.0001 \leq k_1 \leq 0.000107$.

from the concentration of cancer cells (variable C), rather than from the concentrations of healthy and infected cells (variables T and I, respectively). Concentration of healthy cells T provides an observability of the dynamics that is less than the one provided by the concentration of cancer cells C, but concentrations of infected cells I is associated with a clearly poor observability (δ_I is smaller than δ_C by three orders of magnitude).

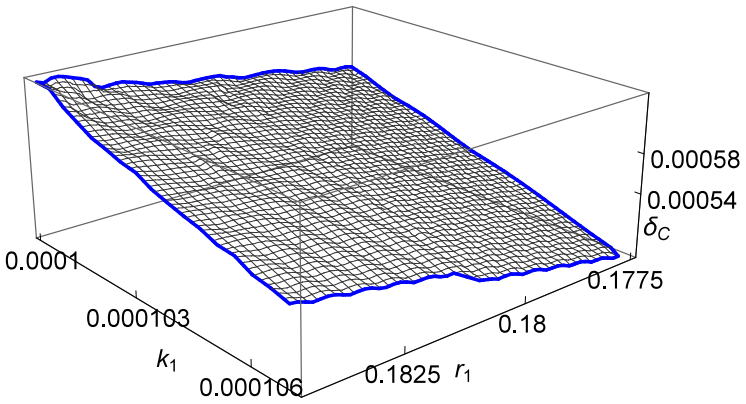

Figure 5.3: Variation of the highest observability index, δ_C considering $0.1775 \leq r_1 \leq 0.18425$ and $0.0001 \leq k_1 \leq 0.000107$.

A 3D-reconstructed attractor would be the result of the representation of the points (X_1, X_2, X_3), with coordinates given by the transformation Φ_s (result not shown). Only this 3D-representation can be directly compared with the original 3D attractor. The 2D-representations of (X_1, X_2) are different entities, they are just phase portraits, and not

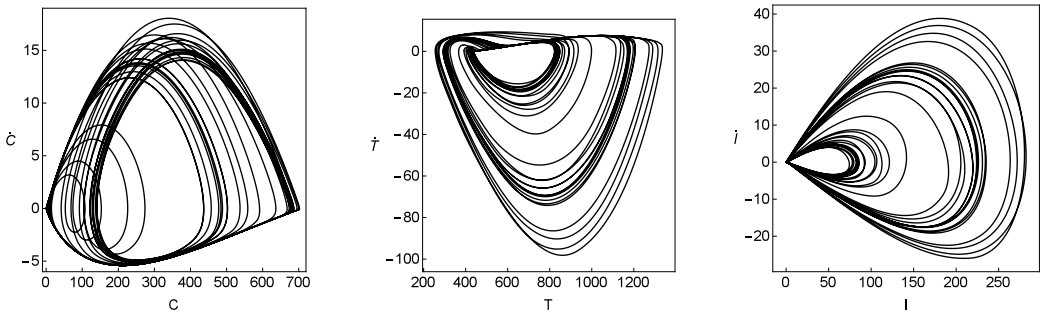

Figure 5.4: Projections of the dynamics on the $(C, \dot{C})$, $(T, \dot{T})$ and $(I, \dot{I})$ planes used to compute observability indices. Here, we use $r_1 = 0.1842$ and $k_1 = 0.0001$.

necessarily similar to the 3D attractor. In the observability theory, the dynamical states (X_1, X_2) are used to provide the first brief glances over the complexity of the orbits.

In the next paragraphs, we devote a special attention to the dynamical variable C. In order to gain insights about the long time behavior of variable C, we display in Fig. 5.5 bifurcation diagrams as a result of the variation of the control parameters r_1 and k_1.

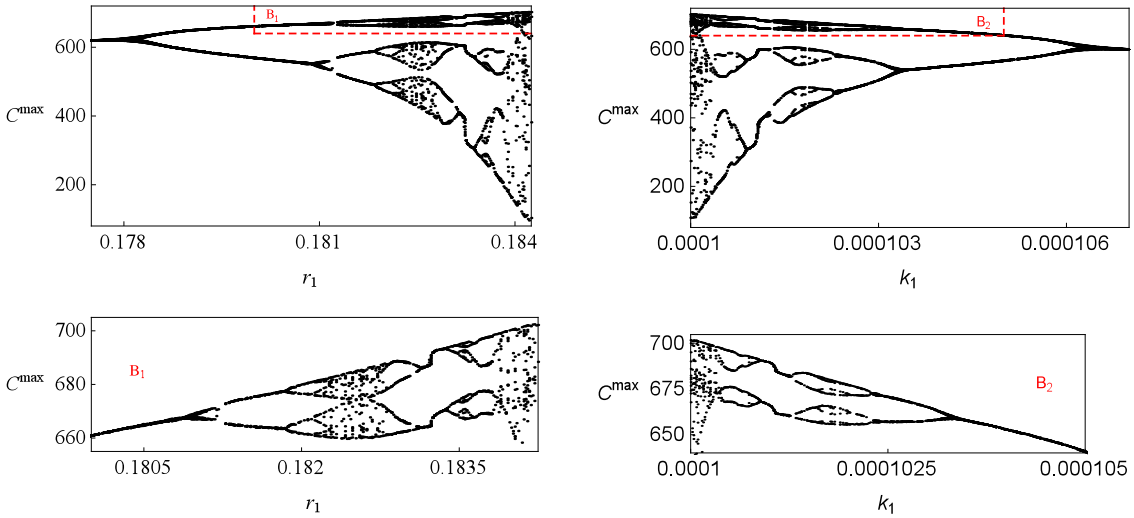

Figure 5.5: Bifurcation diagrams obtained from the successive $C^{\max}$. In the *Upper panel - left*, $k_1 = 0.0001$ and $0.1775 \leq r_1 \leq 0.18425$; in the *Upper panel - right*, $r_1 = 0.1842$ and $0.0001 \leq k_1 \leq 0.000107$. A amplification of the boxes B_1 and B_2 is exhibited in the *Lower panel*.

5.4 The homotopy analysis methodology and the analytic solutions

At this moment, we are able to carry out an analytical study, using the homotopy analysis methodology. This section contains the explicit series solution and an optimal homotopy analysis approach of solutions to improve the computational efficiency of HAM. More precisely, we obtain for each dynamical variable an optimal value of the HAM convergence-control h using an appropriate ratio and using the exact squared residual error.

5.4.1 Explicit series solution

Following the previous considerations presented in Chapter 1, Section 1.3, we are able now to perform an analytical approach of the HIV-1 model by using SHAM. Our goal is to obtain the explicit series solution for C, T, I and focus our analysis on the analytic solution of the dynamical variable C, which represents the concentration of cancer cells.

Let us consider the Eqs. (5.1)-(5.3) subject to the initial conditions

$$C(0) = IC_1, \quad T(0) = IC_2, \quad I(0) = IC_3,$$

which are taken in the form

$$C_0(t) = IC_1, \quad T_0(t) = IC_2, \quad I_0(t) = IC_3,$$

as our initial approximations of $C(t)$, $T(t)$ and $I(t)$, respectively. In our analysis, we will consider

$$IC_1 = 678, \quad IC_2 = 452, \quad IC_3 = 0.25$$

As auxiliary linear operators, we choose

$$L\left[\phi_i\left(t;q\right)\right]=\frac{\partial\phi_i\left(t;q\right)}{\partial t},\quad i=1,2,3,$$

with the property $L\left[C_i\right]=0$, where C_i $(i=1,2,3)$ are integral constants. The equations of the HIV-1 model lead to the following nonlinear operators $\mathcal{N}_1$, $\mathcal{N}_2$ and $\mathcal{N}_3$

$$\begin{aligned}\mathcal{N}_1\left[\phi_1\left(t;q\right),\phi_2\left(t;q\right),\phi_3\left(t;q\right)\right] &= \frac{\partial\phi_1\left(t;q\right)}{\partial t}-r_1\phi_1\left(t;q\right)+\\ &+\frac{r_1}{m}\left(\phi_1^2\left(t;q\right)+\phi_1\left(t;q\right)\phi_2\left(t;q\right)+\right.\\ &\left.+\,\phi_1\left(t;q\right)\phi_3\left(t;q\right)\right)+k_1\phi_1\left(t;q\right)\phi_2\left(t;q\right),\end{aligned}$$

$$\begin{aligned}\mathcal{N}_2\left[\phi_1\left(t;q\right),\phi_2\left(t;q\right),\phi_3\left(t;q\right)\right] &= \frac{\partial\phi_2\left(t;q\right)}{\partial t}-r_2\phi_2\left(t;q\right)+\\ &+\frac{r_2}{m}\left(\phi_1\left(t;q\right)\phi_2\left(t;q\right)+\phi_2^2\left(t;q\right)+\right.\\ &\left.+\,\phi_2\left(t;q\right)\phi_3\left(t;q\right)\right)+pk_1\phi_1\left(t;q\right)\phi_2\left(t;q\right)+\\ &+k_2\phi_2\left(t;q\right)\phi_3\left(t;q\right)\end{aligned}$$

$$\mathcal{N}_3\left[\phi_1\left(t;q\right),\phi_2\left(t;q\right),\phi_3\left(t;q\right)\right]=\frac{\partial\phi_3\left(t;q\right)}{\partial t}-k_2\phi_3\left(t;q\right)\phi_2\left(t;q\right)+\mu_I\phi_3\left(t;q\right).$$

Considering $q\in[0,1]$ and h the non-zero auxiliary parameter, the $zero^{th}$-order deformation equations are

$$\left(1-q\right)L\left[\phi_1\left(t;q\right)-C_0(t)\right]=qh\mathcal{N}_1\left[\phi_1\left(t;q\right),\phi_2\left(t;q\right),\phi_3\left(t;q\right)\right],\tag{5.4}$$

$$\left(1-q\right)L\left[\phi_2\left(t;q\right)-T_0(t)\right]=qh\mathcal{N}_2\left[\phi_1\left(t;q\right),\phi_2\left(t;q\right),\phi_3\left(t;q\right)\right],\tag{5.5}$$

$$\left(1-q\right)L\left[\phi_3\left(t;q\right)-I_0(t)\right]=qh\mathcal{N}_3\left[\phi_1\left(t;q\right),\phi_2\left(t;q\right),\phi_3\left(t;q\right)\right]\tag{5.6}$$

and subject to the initial conditions

$$\phi_1\left(0;q\right)=678,\quad \phi_2\left(0;q\right)=452,\quad \phi_3\left(0;q\right)=0.25.$$

Obviously, for $q = 0$ and $q = 1$, the above $zero^{th}$-order equations (5.4)-(5.6) have the solutions

$$\phi_1(t;0) = C_0(t),\ \phi_2(t;0) = T_0(t),\ \phi_3(t;0) = I_0(t) \tag{5.7}$$

and

$$\phi_1(t;1) = C(t),\ \phi_2(t;1) = T(t),\ \phi_3(t;1) = I(t), \text{ respectively.} \tag{5.8}$$

When q increases from 0 to 1, the functions $\phi_1(t;q)$, $\phi_2(t;q)$ and $\phi_3(t;q)$ vary from $C_0(t)$, $T_0(t)$ and $I_0(t)$ to $C(t)$, $T(t)$ and $I(t)$. As a result of expanding $\phi_1(t;q)$, $\phi_2(t;q)$ and $\phi_3(t;q)$ in MacLaurin series with respect to q, we obtain the homotopy series

$$\phi_1(t;q) = C_0(t) + \sum_{m=1}^{+\infty} C_m(t) q^m, \tag{5.9}$$

$$\phi_2(t;q) = T_0(t) + \sum_{m=1}^{+\infty} T_m(t) q^m, \tag{5.10}$$

$$\phi_3(t;q) = I_0(t) + \sum_{m=1}^{+\infty} I_m(t) q^m, \tag{5.11}$$

in which

$$\begin{aligned} C_m(t) &= \frac{1}{m!}\frac{\partial^m \phi_1(t;q)}{\partial q^m}\Big|_{q=0}, \\ T_m(t) &= \frac{1}{m!}\frac{\partial^m \phi_2(t;q)}{\partial q^m}\Big|_{q=0}, \\ I_m(t) &= \frac{1}{m!}\frac{\partial^m \phi_3(t;q)}{\partial q^m}\Big|_{q=0}, \end{aligned} \tag{5.12}$$

and where h is chosen in such a way that these series are convergent at $q = 1$. Therefore, considering Eqs. (5.7)-(5.12), we end up obtaining the homotopy series solutions

$$C(t) = C_0(t) + \sum_{m=1}^{+\infty} C_m(t), \tag{5.13}$$

$$T(t) = T_0(t) + \sum_{m=1}^{+\infty} T_m(t), \tag{5.14}$$

$$I(t) = I_0(t) + \sum_{m=1}^{+\infty} I_m(t). \tag{5.15}$$

Differentiating the $zero^{th}$-order Eqs. (5.4)-(5.6) m times and using the properties, where D_m is the m^{th}-order derivative in order to the homotopy parameter q,

$$\begin{aligned} D_m\left(\phi_i\right) &= x_{i,m}, \\ D_m\left(q^k\phi_i\right) &= D_{m-k}\left(\phi_i\right) = \begin{cases} x_{i,m-k} & , 0 \leq k \leq m \\ 0 & , \text{ otherwise} \end{cases}, \\ D_m\left(\phi_i^2\right) &= \sum_{k=0}^{m} x_{i,m-k}\ x_{i,k}, \end{aligned}$$

and

$$D_m\left(\phi_i\psi_i\right) = \sum_{k=0}^{m} D_k\left(\phi_i\right) D_{m-k}\left(\psi_i\right) = \sum_{k=0}^{m} x_{i,k}\ y_{i,m-k},$$

we obtain the m^{th}-order deformation equations

$$L\left[C_m(t) - \chi_m C_{m-1}(t)\right] = h\mathcal{R}_{1,m}\left[C_{m-1}(t), T_{m-1}(t), I_{m-1}(t)\right], \tag{5.16}$$

$$L\left[T_m(t) - \chi_m T_{m-1}(t)\right] = h\mathcal{R}_{2,m}\left[C_{m-1}(t), T_{m-1}(t), I_{m-1}(t))\right], \tag{5.17}$$

$$L\left[I_m(t) - \chi_m I_{m-1}(t)\right] = h\mathcal{R}_{3,m}\left[C_{m-1}(t), T_{m-1}(t), I_{m-1}(t)\right], \tag{5.18}$$

with the following initial conditions

$$C_m(0) = 0,\ T_m(0) = 0,\ I_m(0) = 0. \tag{5.19}$$

Defining the vector $\overrightarrow{u}_{m-1} = (C_{m-1}(t), T_{m-1}(t), I_{m-1}(t))$, we derive

$$\begin{aligned}\mathcal{R}_{1,m}[\overrightarrow{u}_{m-1}] &= \frac{dC_{m-1}(t)}{dt} - r_1 C_{m-1}(t) + \\ &+\frac{r_1}{m}\left(\sum_{k=0}^{m-1} C_{m-1-k}(t)C_k(t) + \sum_{k=0}^{m-1} C_k(t)T_{m-1-k}(t) + \right. \\ &\left. + \sum_{k=0}^{m-1} C_k(t)I_{m-1-k}(t)\right) + k_1 \sum_{k=0}^{m-1} C_k(t)T_{m-1-k}(t)\end{aligned}$$

$$\begin{aligned}\mathcal{R}_{2,m}[\overrightarrow{u}_{m-1}] &= \frac{dT_{m-1}(t)}{dt} - r_2 T_{m-1}(t) + \\ &+\frac{r_2}{m}\left(\sum_{k=0}^{m-1} C_{m-1-k}(t)T_k(t) + \sum_{k=0}^{m-1} T_k(t)T_{m-1-k}(t) + \right. \\ &\left. + \sum_{k=0}^{m-1} T_k(t)I_{m-1-k}(t)\right) + pk_1 \sum_{k=0}^{m-1} C_{m-1-k}(t)T_k(t) + \\ &+k_2 \sum_{k=0}^{m-1} T_k(t)I_{m-1-k}(t)\end{aligned}$$

and

$$\mathcal{R}_{3,m}[\overrightarrow{u}_{m-1}] = \frac{dI_{m-1}(t)}{dt} - k_2 \sum_{k=0}^{m-1} T_{m-1-k}(t)I_k(t) + \mu_I I_{m-1}(t).$$

According to the notations and definitions provided above, the solution of the linear m^{th}-order deformation equations (5.16)-(5.18) at initial conditions (5.19), for all $m \geq 1$,

becomes

$$C_m(t) = \chi_m \; C_{m-1}(t) + h \int_0^t \mathcal{R}_{1,m}\left[\overrightarrow{u}_{m-1}\right] d\tau, \tag{5.20}$$

$$T_m(t) = \chi_m \; T_{m-1}(t) + h \int_0^t \mathcal{R}_{2,m}\left[\overrightarrow{u}_{m-1}\right] d\tau, \tag{5.21}$$

and

$$I_m(t) = \chi_m \; I_{m-1}(t) + h \int_0^t \mathcal{R}_{3,m}\left[\overrightarrow{u}_{m-1}\right] d\tau. \tag{5.22}$$

As an example, we present some initial terms of the series solutions (corresponding to $m = 1$ and $m = 2$)

$$C_1(t) = 678 + h(306456(k_1 + r_1/1500) - 371.431r_1)t$$

$$T_1(t) = 452 + h(-9.41516 + 306456(0.00002 + 0.1k_1))t$$

$$I_1(t) = 0.25 + 0.0185ht$$

and

$$\begin{aligned} C_2(t) &= 678 + 2h(306456(k_1 + r_1/1500) - 371.431r_1)t + \\ &+h(306456hk_1t - 167.127hr_1t - 1113.97hk_1t^2 + \\ &+643.558hk_1r_1t^2 - 17.1723hr_1^2t^2) \end{aligned}$$

$$\begin{aligned} T_2(t) &= 452 + 2h(-9.41516 + 306456(0.00002 + 0.1k_1))t + \\ &+h(-3.28604ht + 30645.6hk_1t - 0.000734025ht^2 + \\ &+1300.91hk_1t^2 + 7.96479 \times 10^6 hk_1^2t^2 - \\ &-0.755414hr_1t^2 - 3777.07hk_1r_1t^2) \end{aligned}$$

$$I_2(t) = 0.25 + 0.037ht + h(0.000889877ht^2 - 1.91535hk_1t^2)$$

where h is the convergence control parameter, r_1 is the uncontrolled proliferation rate of the cancer cells and k_1 is the immune system's killing rate of cancer cells. At this moment, it is easy to obtain terms for other values of m. In particular, truncating the homotopy series (5.13)-(5.15) we get the M^{th}-order approximate analytic solution (which corresponds to a series solution with $M + 1$ terms)

$$C_M(t) = C_0(t) + \sum_{m=1}^{M} C_m(t), \tag{5.23}$$

$$T_M(t) = T_0(t) + \sum_{m=1}^{M} T_m(t), \tag{5.24}$$

$$I_M(t) = I_0(t) + \sum_{m=1}^{M} I_m(t). \tag{5.25}$$

The *exact solutions* are given by the limits

$$C(t) = \lim_{M\to+\infty} C_M(t), \quad T(t) = \lim_{M\to+\infty} T_M(t), \quad I(t) = \lim_{M\to+\infty} I_M(t).$$

Within the purpose of having an effective analytical approach of Eqs. (5.1)-(5.3) for higher values of t, we use the step homotopy analysis method, in a sequence of subintervals of time step Δt and the 9-term HAM series solutions (8^{th}-order approximations)

$$C(t) = C_0(t) + \sum_{m=1}^{8} C_m(t), \tag{5.26}$$

$$T(t) = T_0(t) + \sum_{m=1}^{8} T_m(t), \tag{5.27}$$

$$I(t) = I_0(t) + \sum_{m=1}^{8} I_m(t), \tag{5.28}$$

at each subinterval. Accordingly to SHAM, the initial values C_0, T_0 and I_0 change at each subinterval, i.e., $C(t^*) = IC_1^* = C_0$, $T(t^*) = IC_2^* = T_0$ and $I(t^*) = IC_3^* = I_0$ and the initial conditions $C_m(t^*) = T_m(t^*) = I_m(t^*) = 0$ should be satisfied for all $m \geq 1$. Therefore, the terms C_m, T_m and I_m, exhibited before as an example for $m = 1, 2$, take now the form

$$\begin{aligned} C_1(t) &= 678 + h(306456(k_1 + r_1/1500) - 371.431r_1)(t - t^*), \\ T_1(t) &= 452 + h(-9.41516 + 306456(0.00002 + 0.1k_1))(t - t^*), \\ I_1(t) &= 0.25 + 0.0185h(t - t^*) \end{aligned}$$

and

$$\begin{aligned} C_2(t) &= 678 + 2h(306456(k_1 + r_1/1500) - 371.431r_1)(t - t^*) + \\ &+h(306456hk_1(t - t^*) - 167.127hr_1(t - t^*) - 1113.97hk_1(t - t^*)^2 + \\ &+643.558hk_1r_1(t - t^*)^2 - 17.1723hr_1^2(t - t^*)^2), \end{aligned}$$

$$\begin{aligned} T_2(t) &= 452 + 2h(-9.41516 + 306456(0.00002 + 0.1k_1))(t - t^*) + \\ &+h(-3.28604h(t - t^*) + 30645.6hk_1(t - t^*) - 0.000734025h(t - t^*)^2 + \\ &+1300.91hk_1(t - t^*)^2 + 7.96479 \times 10^6 hk_1^2(t - t^*)^2 - \\ &-0.755414hr_1(t - t^*)^2 - 3777.07hk_1r_1(t - t^*)^2), \end{aligned}$$

$$I_2(t) = 0.25 + 0.037h(t - t^*) + h(0.000889877h(t - t^*)^2 - 1.91535hk_1(t - t^*)^2).$$

In a similar way, identical changes occur for the other terms. As a consequence, the analytical approximate solution for each dynamical variable is given by

$$C(t) = C(t^*) + \sum_{m=1}^{8} C_m(t - t^*), \tag{5.29}$$

$$T(t) = T(t^*) + \sum_{m=1}^{8} T_m(t - t^*), \tag{5.30}$$

$$I(t) = I(t^*) + \sum_{m=1}^{8} I_m(t - t^*). \tag{5.31}$$

In general, we only have information about the values of $C(t)$, $T(t)$ and $I(t)$ at $t = 0$, but we can obtain the values of $C(t)$, $T(t)$ and $I(t)$ at $t = t^*$ by assuming that the new initial

conditions are given by the solutions in the previous interval. Another illustration of the use of SHAM can be seen in [45].

The homotopy terms depend on both the physical variable t and the convergence control parameter h. The artificial parameter h can be freely chosen to adjust and control the interval of convergence, and even more, to increase the convergence at a reasonable rate, fortunately at the quickest rate. This concept plays a key role in the HAM and is generally used to gain sufficiently accurate approximations with the smallest number of homotopy terms in the homotopy series (5.23)-(5.25). In fact, the use of such an auxiliary parameter clearly distinguishes the HAM from other perturbation-like analytical techniques.

How to find a proper convergence control parameter h to get a convergent series solution or, even better, to get a faster convergent one? In the following subsection, an optimal homotopy analysis approach is described to improve the computational efficiency of the homotopy analysis method for nonlinear problems.

5.4.2 An optimal homotopy analysis approach of solutions

Using an optimal approach, the homotopy analysis method might be applied to solve complicated differential equations with strong nonlinearity. Firstly, with the purpose of determining an interval of convergence and the optimum value of h, corresponding to each dynamical variable, we state a recent convergence criterion addressed in [46]. Finally, an exact Squared Residual Error (SRE) is defined and efficiently used to find optimal convergence values for the convergence control parameter h.

It is found that all optimal homotopy analysis approaches greatly accelerate the convergence of series solution.

Interval of convergence and optimal value from an appropriate ratio

Following the procedure established in Chapter 1, Section 1.3, and as an illustration at the order of approximation $M = 8$, the curves of ratio β versus h, corresponding to $C(t)$, $T(t)$ and $I(t)$ (β_C vs h_C, β_T vs h_T and β_I vs h_I, respectively), are displayed in Fig. 5.6. In Table 5.2, we exhibit the intervals of convergence of h and the respective optimum values h^* corresponding to the dynamical regime presented in Fig. 5.6.

β-Curves	Intervals of convergence and optimal values of h
β_C	$-1.55274 < h_C < -1.09974$ $h_C^* = -1.18485$
β_T	$-1.66625 < h_T < 0$ $h_T^* = -1.28944$
β_I	$-0.190914 < h_I < 0$ $h_I^* = -0.122441$

Table 5.2: Intervals of convergence of h and the respective optimum values h^*, corresponding to the dynamical regimes presented in Fig. 5.6 (for $r_1 = 0.1842$ and $k_1 = 0.0001$).

Indeed, the use of such ratio, by solving the inequality mentioned above, allows us to obtain the exact interval of convergence for the artificial parameter h and, in addition, it yields an optimal value. This represents a central advantage in the study of the convergence of HAM.

In Fig. 5.7 we show the comparison of the SHAM analytical solutions for C, T and I with the numerical results using precisely the optimum values presented in Table 5.2.

Squared residual error and different orders of approximation

A procedure to check the convergence of a homotopy-series solution is to substitute this series into the original governing equations and initial conditions, and then to evaluate the corresponding squared residual errors - the more quickly the residual error decays to zero,

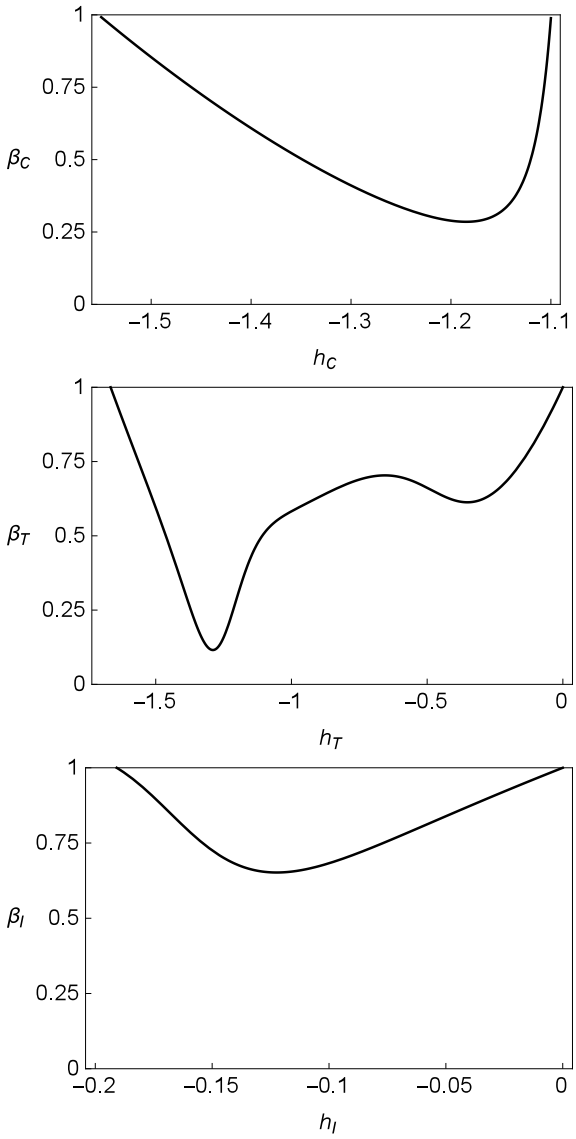

Figure 5.6: The curves of ratios β_C, β_T and β_I versus h_C, h_T and h_I, respectively, corresponding to a 8^{th}-order approximation of solutions $C(t)$, $T(t)$ and $I(t)$ for $r_1 = 0.1842$ and $k_1 = 0.0001$. The optimum value of h, h^*, gives rise to the minimum value of β.

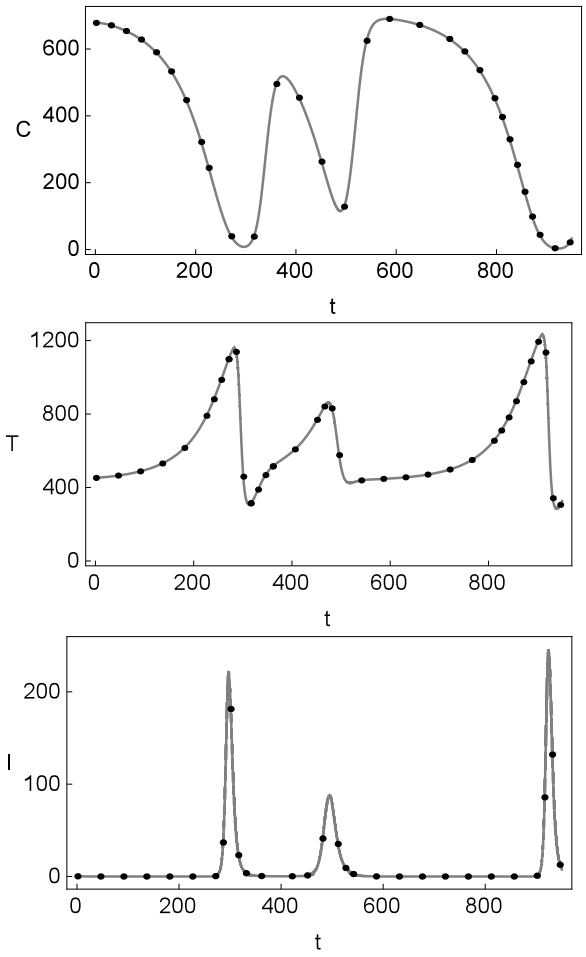

Figure 5.7: Comparison of the SHAM analytical solutions (5.29)-(5.31) of C, T and I (solid lines) with the respective numerical solutions (dotted lines) of the HIV-1 cancer model. The value of the control parameters are $r_1 = 0.1842$ and $k_1 = 0.0001$.

the faster the homotopy-series converges. In this context, an error analysis is performed in the following lines.

Taking the expressions (5.23)-(5.25), let us consider

$$\varphi_C(t,h_C) = C_M(t),\ \varphi_T(t,h_T) = T_M(t),\ \varphi_I(t,h_I) = I_M(t).$$

With the substitution of these solutions into Eqs. (5.1)-(5.3), we are able to construct *Residual Error* (RE) functions as follows:

$$\begin{aligned} RE_C(h_C,t) &= \frac{\partial\varphi_C(t,h_C)}{\partial t} - r_1\varphi_C(t,h_C) + \\ &+\frac{r_1}{m}\left(\varphi_C^2(t,h_C) + \varphi_C(t,h_C)\,\varphi_T(t,h_T) + \right. \\ &\left. + \varphi_C(t,h_C)\,\varphi_I(t,h_I)\right) + k_1\varphi_C(t,h_C)\,\varphi_T(t,h_T), \end{aligned} \tag{5.32}$$

$$\begin{aligned} RE_T(h_T,t) &= \frac{\partial\varphi_T(t,h_T)}{\partial t} - r_2\varphi_T(t,h_T) + \\ &+\frac{r_2}{m}\left(\varphi_C(t,h_C)\,\varphi_T(t,h_T) + \varphi_T^2(t,h_T) + \right. \\ &\left. + \varphi_T(t,h_T)\,\varphi_I(t,h_I)\right) + pk_1\varphi_C(t,h_C)\,\varphi_T(t,h_T) + \\ &+k_2\varphi_T(t,h_T)\,\varphi_I(t,h_I), \end{aligned} \tag{5.33}$$

$$RE_I(h_I,t) = \frac{\partial\varphi_I(t,h_I)}{\partial t} - k_2\varphi_I(t,h_I)\,\varphi_T(t,h_T) + \mu_I\varphi_I(t,h_I). \tag{5.34}$$

In 2007, Yabushita *et al.* [144] suggested an *optimization method* for convergence control parameters. Their work is based on the Squared Residual Error. Inspired by this approach, and following the studies carried out in [145] and in [146], we consider the exact *Squared Residual Error* (SRE) for the M^{th}-order approximations to be

$$SRE_C\left(h_C\right) = \int_0^1 \left[RE_C\left(h_C, t\right)\right]^2 dt, \tag{5.35}$$

$$SRE_T\left(h_T\right) = \int_0^1 \left[RE_T\left(h_T, t\right)\right]^2 dt, \tag{5.36}$$

$$SRE_I\left(h_I\right) = \int_0^1 \left[RE_I\left(h_I, t\right)\right]^2 dt. \tag{5.37}$$

Values of h_C, h_T and h_I for which $SRE_C\left(h_C\right)$, $SRE_T\left(h_T\right)$ and $SRE_I\left(h_I\right)$ are minimum can be obtained. For a given M^{th}-order of approximation, the optimal value of h_C, h_T and h_I are given by the nonlinear algebraic equations

$$\frac{d\left[SRE_C\left(h_C\right)\right]}{dh_C} = 0, \quad \frac{d\left[SRE_T\left(h_T\right)\right]}{dh_T} = 0 \quad \text{and} \quad \frac{d\left[SRE_I\left(h_I\right)\right]}{dh_I} = 0.$$

The optimal values for all of these considered cases are h_C^*, h_T^* and h_I^*. The curves of SRE_C, SRE_T and SRE_I regarding different orders of approximation, namely $M = 6$, $M = 8$ and $M = 10$, are show in Fig. 5.8. Central information regarding the orders of approximation, optimal values of h_C, h_T, h_I and minima of the respective squared residual error functions is summarized in Table 5.3.

This analysis provides an illustration of how our understanding of a model arising in the context of biology can be directly enhanced by the use of numerical and analytical techniques, for different combinations of control parameters and time.

5.5 Conclusions

In this chapter we have provided new insights into the study of a HIV-1 model, which mimics the concentrations of cancer cells, healthy CD_4+ T lymphocytes and infected

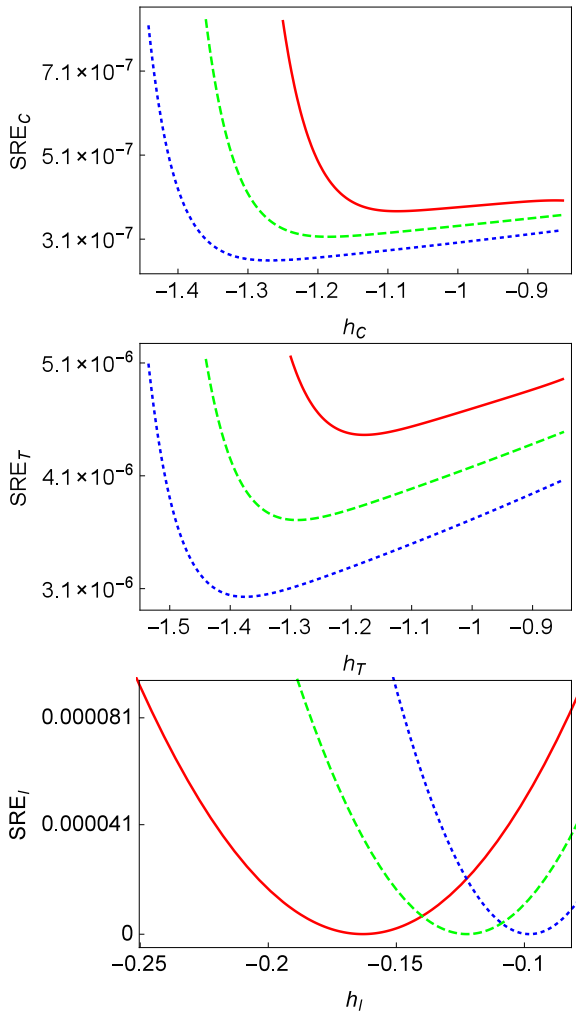

Figure 5.8: Exact Squared Residual Error functions, SRE_C, SRE_T and SRE_I, versus h_C, h_T and h_I, respectively. These functions correspond to different orders of approximation for the solutions $C(t)$, $T(t)$ and $I(t)$. Solid line: 6^{th}-order approximation; Dashed line: 8^{th}-order approximation; Dotted line: 10^{th}-order approximation ($r_1 = 0.1842$ and $k_1 = 0.0001$). Each optimum value h^* gives rise to the minimum value of the SRE.

M, order of approximation of $C(t)$	Optimal value h_C^*	Minimum value of SRE_C
6	-1.08697	3.76497×10^{-7}
8	-1.18485	3.15689×10^{-7}
10	-1.26551	2.5934×10^{-7}
M, order of approximation of $T(t)$	Optimal value h_T^*	Minimum value of SRE_T
6	-1.17838	4.46271×10^{-6}
8	-1.28944	3.70809×10^{-6}
10	-1.37576	3.02756×10^{-6}
M, order of approximation of $I(t)$	Optimal value h_I^*	Minimum value of SRE_I
6	-0.163095	5.14312×10^{-8}
8	-0.122441	4.78534×10^{-8}
10	-0.0979792	4.57679×10^{-8}

Table 5.3: Orders of approximation, optimal values of h_C, h_T, h_I and minima of the respective squared residual error functions, corresponding to the dynamical regime presented in Fig. 5.8 ($r_1 = 0.1842$ and $k_1 = 0.0001$).

CD_4+ T lymphocytes. The rich and complex behavior of this model allowed us to apply different theoretical approaches.

After analytically proving the boundedness of the trajectories in the system's attractor, we have studied the complexity of the coupling between the dynamical variables with the quantification of the observability indices. We have identified different dynamical behaviors of the system varying two biologically meaningful parameters: r_1, representing the uncontrolled proliferation rate of cancer cells and k_1, representing the immune system's killing rate of cancer cells.

Nonlinear equations are significantly more difficult to solve than linear ones, especially in terms of analytical methods. In general, there are two standards for a *satisfactory* approach of nonlinear equations: (i) it can always give approximation expressions *efficiently*; (ii) it can guarantee that approximation expressions are *accurate* enough in the studied

region of biophysical parameters. Using these two standards as a criterion, we have successfully applied the homotopy analysis method (HAM) to construct the explicit series solution of the HIV-1 model incorporating AIDS-related cancer cells. The HAM solution contains the auxiliary parameter h, which gives a simple way to adjust and control the convergence region of the resulting series solution. In order to increase the computational efficiency, an optimal homotopy analysis approach was developed to obtain optimal values for the convergence-control parameter h by means of an appropriate ratio and the definition of an exact Squared Residual Error. This analysis provided a fast convergence of the homotopy series solution and illustrated that the homotopy analysis method indeed satisfies the two standard aspects, (i) and (ii), mentioned previously. The results presented in this chapter are likely to inspire applications of the HAM analytical procedure for solving highly nonlinear problems in theoretical biology.

Final considerations

The complexity of biological sciences makes the interdisciplinary involvement essential. Indeed, there is a sustained effort to include mathematical precision in the new approaches of the physiological mechanisms, in the development and evaluation of new techniques to support the diagnosis and in the optimization of conventional methods. The mathematical tools can describe, explain, predict and decide in different situations. They allow us to reveal quantitatively as well as qualitatively the behavior of physiological systems. The use of an integrated approach, involving numerical evidences and theoretical reasoning, emerges as a methodological unifying factor within the theory of dynamical systems, gives a surprisingly structured character, revealing hidden dynamical features and properties of life sciences motivated models.

The research work presented throughout the previous chapters motivates new and enthusiastic developments. In fact, certain branches of mathematics are a result of interdisciplinary experiences that arouse curiosity, placing new questions, which contribute to the development of the theory.

Bibliography

[1] A. Sharkovsky, *Coexistence of cycles of a continuous map of a line into itself*, Ukr. Math. Z. 16, 61-71 (1964).

[2] D. Singer, *Stable orbits and bifurcations of maps of the interval*, SIAM J. Appl. Math. 35, 260-267 (1978).

[3] M. Morse and G. Hedlund, *Symbolic Dynamics*, American Journal of Mathematics, 60, 815-866 (1938).

[4] J. Milnor and W. Thurston, *On iterated maps of the interval I and II*, Lect. Notes in Math,.Springer-Verlag,.1342, 465-563 (1988).

[5] J. P. Lampreia and J. Sousa Ramos, *Symbolic dynamics of bimodal maps*, Portugal. Math. Vol. 54, 1, 1-18 (1997).

[6] H. Bai-Lin and Z. Wei-Mou, *Applied symbolic dynamics and chaos,* Directions in Chaos 7, World Scientific (1998).

[7] A. Katok and B. Hasselblatt, *Introduction to the modern theory of dynamical systems,* (Cambridge University Press) (1995).

[8] M. Misiurewicz and W. Szlenk, *Entropy of piecewise monotone mappings*, Studia Math. 67, 45-63 (1980).

[9] T. Matsumoto, L. O. Chua and M. Komuro, *The double scroll*, IEEE Trans. Circuits Syst. 32, 797-818 (1985).

[10] L. O. Chua, M. Komuro and T. Matsumoto, *The double scroll family: Rigorous proof of chaos*, IEEE Trans. Circuits Syst. 33, 1072-1097 (1986).

[11] K. Ramasubramanian and M. S. Sriram, *A comparative study of computation of Lyapunov spectra with different algorithms*, Physica D: Nonlin. Phenom. 139, 72-86 (2000).

[12] T. Parker and L. O. Chua, *Practical numerical algorithms for chaotic systems* (Springer-Verlag) (1989).

[13] L. Changpin and C. Guanrong, *Estimating the Lyapunov exponents of discrete systems*, Chaos 14, 343-346 (2004).

[14] J. P. Crutchfield and N. H. Packard, *Symbolic Dynamics of One-dimensional Maps:Entropies, Finite Precision, and Noise*, International Journal of Theoretical Physics 21, 433-466 (1982).

[15] J-P. Eckmann and D. Ruelle, *Ergodic theory of chaos and strange attractors*, Rev. Mod. Phys. 57, 617-656 (1985).

[16] K. Fraedrich, *Estimating weather and climate predictability on attractors*, Journal of the Atmospheric Sciences 44, 722-728 (1987).

[17] Y. B. Pesin, *Lyapunov characteristic exponent and ergodic properties of smooth dynamical systems with an invariant measure*, Sov. Math. Dokl. 17, 196-199 (1976).

[18] A. N. Kolmogorov, *New metric invariant of transitive dynamical systems and automorphism of Lebesgue spaces*, Dokl. Akad. Nauk SSSR 119, 861-864 (1958).

[19] V. Sinai, *On the concept of entropy for a dynamical system*, Dokl. Akad. Nauk SSSR 124, 768–771 (1959).

[20] P. Billingsley, *Ergodic Theory and Information* (Wiley, New York) (1965).

[21] A. M. Lyapunov, *General problem on stability of motion,* (English translation), Taylor & Francis, London (1992).

[22] A. V. Karmishin, A. T. Zhukov and V. G. Kolosov, *Methods of dynamics calculations and testing for thin-walled structures*, Moscow: Mashinostroyenie (1990).

[23] J. Awrejcewicz, I. V. Andrianoc and L. I. Manevitch, *Asymtotic approaches in nonlinear dynamics*, Springer-Verlag, Berlin (1998).

[24] G. Adomian, *Nonlinear stochastic differential equations*, J. Math. Anal. Appl. 55, 441-452 (1976).

[25] G. Adomian, *A review of the decomposition method and some recent results for nonlinear equations*, Comput. Math. Appl. 21, 101-127 (1991).

[26] R. Rach, *On the Adomian method and comparisons with Picard's method*, J. Math. Appl. 10, 139-159 (1984).

[27] G. Adomian and G. E. Adomian, *A global method for solution of complex systems*, Math. Model. 5, 521-568 (1984).

[28] S. J. Liao, *The proposed homotopy analysis techniques for the solution of nonlinear problems*, Ph.D. dissertation. Shanghai: Shanghai Jiao Tong University (1992).

[29] S. J. Liao, *Beyond perturbation: introduction to the homotopy analysis method*, CRC Press, Boca Raton, Chapman and Hall (2003).

[30] S. J. Liao and Y. Tan, *A general approach to obtain series solutions of nonlinear differential equations*, Stud. Appl. Math. 119, 297-355 (2007).

[31] G. Adomian, *Solving frontier problems of physics: the decomposition method*, Kluwer Academic Publishers, Boston (1994).

[32] S. J. Liao, *An explicit, totally analytic approximation of Blasius' viscous flow problems*, Int. J. Nonlinear Mech. 34, 759-778 (1999).

[33] S. J. Liao, *On the homotopy analysis method for nonlinear problems*, Appl. Math. Comput. 147, 499-513 (2004).

[34] S. Sen, *Topology and geometry for physicists*, Florida: Academic Press (1983).

[35] T. Hayat and M. Khan, *Homotopy solutions for a generalized second-grade fluid past a porous plate*, Nonlinear Dyn. 42, 395-405 (2005).

[36] H. Li and Y. Guo, *New exact solutions to the Fitzhugh-Nagumo equation*, Appl. Math. Comp. 180, 524-528 (2006).

[37] S. Abbasbandy, *Solution for the FitzHugh-Nagumo equation with the homotopy analysis method*, Applied Mathematical Modelling 32, 2706-2714 (2008).

[38] A. M. M. Arafa, S. Z. Rida and H. Mohamed, *Homotopy analysis method for solving biological population model*, Commun. Theor. Phys. 56, 797-800 (2011).

[39] V. S. Putcha, *Two Species and Three Species Ecological Modeling - Homotopy Analysis, Diversity of Ecosystems*, Prof. Mahamane Ali (Ed.), ISBN: 978-953-51-0572-5, InTech, DOI: 10.5772/37146 (2012).

[40] H. Khan, R. N. Mohapatra, K. Vajravelu and S. J. Liao, *The explicit series solution of SIR and SIS epidemic models*, Appl. Math. and Comp. 215, 653-669 (2009).

[41] S. Usha, V. Abinaya, S. Loghambal and L. Rajendran, *nonlinear mathematical model of the interaction between tumor and oncolytic viruses*, Appl. Math. 3, 1-8 (2012).

[42] A. S. Bataineh, M. S. M. Noorani and I. Hashim, *Solving systems of ODEs by homotopy analysis method*, Communications in Nonlinear Science and Numerical Simulation 13, 2060-2070 (2008).

[43] M. Mustafa, J. A. Khan, T. Hayat and A. Alsaedi, *Boundary layer flow of nanofluid over a nonlinearly stretching sheet with convective boundary condition*, IEEE-Transactions on Nanotechnology 14, 159-168 (2015).

[44] M. Mustafa, J. A. Khan, T. Hayat and A. Alsaedi, *Analytical and numerical solutions for axisymmetric flow of nanofluid due to nonlinearly stretching sheet, International Journal of nonlinear Mechanics*, doi:10.1016/j.ijnonlinmec.2015.01.005 (2015).

[45] A. K. Alomari, M. S. M. Noorani, R. Nazar and C. P. Li, *Homotopy analysis method for solving fractional Lorenz system*, Commun. Nonlinear Sci. Numer. Simulat. 15, 1864-1872 (2010).

[46] S. J. Liao, *Advances in the homotopy Analysis method*, World Scientific Publishing Co (2014).

[47] E. Venturino, *Simple Metaecoepidemic models*, Bull Math Biol 73, 917-950 (2011).

[48] J. Russell and R. Cohn, *Gronwall' s inequality*, Bookvika publishing (2013).

[49] C. Letellier and L. A. Aguire, *Investigating nonlinear dynamics from time series: the influence of symmetries and the choice of observables*, Chaos 12, 549-558 (2002).

[50] C. Letellier, L. A. Aguire and J. Maquet, *Relation between observability and differential embeddings for nonlinear dynamics*, Phys. Rev. E 71, 066213 (2005).

[51] C. Letellier, F. Denis and L. A. Aguirre, *What can be learned from a chaotic cancer model?,* J. Theor. Biol. 322, 7-16 (2013).

[52] J. Duarte, C. Januário, C. Rodrigues and J. Sardanyés, *Topological complexity and predictability in the dynamics of a tumor growth model with Shilnikov's chaos, Int. J Bifurcation Chaos* 23 (7), 1350124 (2013).

[53] J. S. Lowengrub, H. B. Frieboes, F. Jin, Y-L. Chuang, X. Li, P. Macklin, S. M. Wise and V. Cristini, *Nonlinear modeling of cancer: bridging the gap between cells and tumors*, Nonlinearity 23, R1-R9 (2010).

[54] V. A. Kuznetsov, I. A. Makalkin, M. A. Taylor and A. S. Perelson, *Nonlinear dynamics of immunogenic tumors: Parameter estimation and global bifurcation analysis*, Bull. Math. Biol. 56, 295-321 (1994).

[55] V. A. Kuznetsov and G. D. Knott, *Modeling tumor growth and immunotherapy*, Math. Comp. Model. 33, 1275-1287 (2001).

[56] D. Kirschner and J. C. Panetta, *Modeling immunotherapy of the tumor-immune interaction*, J. Math. Biol. 37, 235-252 (1998).

[57] J. A. Adam, *General aspects of modeling tumor growth and the immune response A Survey of Models on Tumor Immune Systems Dynamics*, (Boston, MA: Birkhauser) (1996).

[58] N. Bellomo, N. K. Li and P. K. Maini, *On the foundations of cancer modelling: selected topics, speculations, and perspectives*, Math. Models Methods Appl. Sci. 4, 593-646 (2008).

[59] M. Itik and S. P. Banks, *Chaos in a three-dimensional cancer model*, Internat J Bifur Chaos 20 (1), 71-79 (2010).

[60] H. Froehling, J. P. Crutchfield, D. Farmer, N. H. Packard, and R. Shaw, *On determining the dimension of chaotic flows*, Physica D 3, 605-617 (1981).

[61] A. Jewett and H-C Tseng, *Tumor induced inactivation of natural killer cell cytotoxic function; implications in growth, expansion and differentiation of cancer stem cells*, Journal of Cancer 2, 443-457 (2011).

[62] K. J. Pienta, N. McGregor, R. Axelrod and D. E. Exelrod, *Ecological therapy for cancer: defining tumors using an ecosystem paradigm suggests new opportunities for novel cancer treatments*, Translational Oncology 1 (4), 158-164 (2004).

[63] R. P. Jiménez and E. O. Hernandez, *Tumor-host dynamics under radiotherapy*, Chaos Solitons and Fractals 44, 685-692 (2011).

[64] A. A. Berryman and J. A. Millstein, *Are ecological systems chaotic: and if not, why not?*, Trends Ecol. Evol. 4, 26-28 (1989).

[65] M. Pascual, *Diffusion-induced chaos in a spatial predator-prey system*, Proc. Roy. Soc. London B 251, 1-7 (1993).

[66] J. Duarte, C. Rodrigues, C. Januário, G. Gil-Gómez, N. Martins and J. Sardanyés, *Activation of effector immune cells promotes stochastic tumor extinction: A homotopy analysis approach*, Applied Mathematics and Computation 252, 484-495 (2015).

[67] A. Hastings and T. Powell, *Chaos in a three-species food chain*, Ecology 72 (3), 896-903 (1991).

[68] J. A. Vano, J. C. Wildenberg, M. B. Anderson, J. K. Nodel and J. C. Sprott, *Chaos in low-dimensional Lotka-Volterra models of competition*, Nonlinearity **19**, 2391-2404 (2006).

[69] S. Gakkhar and R. K. Naji, *Existence of chaos in two-prey, one-predator system*, Chaos Solit. Fract. 17, 639-649 (2003).

[70] S. Tang and L. Chen, *Chaos in functional response host-parasitoid ecosystem models*, Chaos Solit. Fract. 13, 875-884 (2002).

[71] L. G. de Pillis and A. Radunskaya, *The dynamics of an optimally controlled tumor model: A case study*, Math. Comput. Model. 37, 1221-1244 (2003).

[72] J. Duarte, C. Januario, C. Rodrigues and J. Sardanyés, *Topological complexity and predictability in the dynamics of a tumour growth model with Shilnikov's Chaos*, Int. J. Bifurc. Chaos 23, 1350124 (2013).

[73] A. G. López, J. Sabuco, J. M. Seoane, J. Duarte, C. Januário and M-A. S. Sanjuán, *Avoiding healthy cells extinction in a cancer model*, J. Theor. Biol. 349, 74-81 (2014).

[74] F. Denis and C. Letellier, *Chaos theory: a fascinating concept for oncologists*, Cancer Radiotherapy 16, 230-235 (2012).

[75] F. Denis and C. Letellier, *Radiotherapy and chaos therapy: the tit and the butterfly*, Cancer Radiotherapy 16, 404-409 (2012).

[76] L. G. de Pillis, W. Gu and A. E. Radunskaya, *Mixed immunotherapy and chemotherapy of tumors: Modeling, applications and biological interpretations*, J. Theoret. Biol. 238, 841-862 (2006).

[77] M. Itik, M. U. Salamci and S. P. Banks, *Optimal control of drug therapy in cancer treatment*, Nonlin. Anal. Th. Meth. Appl. 71, e1473-e1486 (2009).

[78] Z. Bajzer, M. Marusic and S. Vuk-Pavlovic, *Conceptual frameworks for mathematical modeling of tumor growth dynamics*, Math. Comput. Model. 23, 31-46 (1996).

[79] J. C. Allen, W. M. Schaffer and D. Rosko, *Chaos reduces species extinction by amplifying local population noise*, Nature 364, 229-232 (1993).

[80] J. Sardanyés, *Low-dimensional homeochaos in coevolving host-parasitoid dimorphic populations: Extinction thresholds under local noise*, Comm. Nonlin. Sci. Numer. Simula 16, 3896-3903 (2011).

[81] R. R. Raval, A. B. Sharabi, A. J. Walker, C. G. Drake. and P. Sharma, *Tumor immunology and cancer immunotherapy: summary of the 2013 SITC primer*, J. Immunother Cancer 14 (2014).

[82] D. A. Schaer, D. Hirschhorn-Cymerman and J. D. Wolchok, *Targeting tumor-necrosis factor receptor pathways for tumor immunotherapy*, J Immunother Cancer 2:7 (2014).

[83] C. Kyi and M. A. Postow, *Checkpoint blocking antibodies in cancer immunotherapy*, FEBS Lett. 588, 368-376 (2014).

[84] K. Ali, D. R. Soond, R. Pieiro, T. Hagemann, W. Pearce, E. L. Lim, H. Bouabe, C. L. Scudamore, T. Hancox, H. Maecker, L. Friedman, M. Turner, K. Okkenhaug and B. Vanhaesebroeck, *Inactivation of PI(3)K p110? breaks regulatory T-cell-mediated immune tolerance to cancer*, Nature 509, 407-411 (2014).

[85] L. J. Eggermont, L. E. Paulis, J. Tel and C. G. Figdor, *Toward efficient cancer immunotherapy: advances in developing artificial antigen-presenting cells*, Trends in Biotechnology (2014).

[86] J. Duarte, C. Rodrigues, C. Januário, N. Martins and J. Sardanyés, *How complex, probable, and predictable is genetically driven Red Queen chaos?*, Acta Biotheoretica, DOI 10.1007/s10441-015-9254-z (2015).

[87] C. M. Lively, *Evidence from a New Zealand snail for the maintenance of sex by parasitism*, Nature 328, 519-521 (1987).

[88] E. Decaestecker, S. Gaba, J. A. M. Raeymaekers, R. Stoks, Van Kerckhoven, D. Ebert and L. D. Meester, *Host-parasite 'Red Queen' dynamics archived in pond sediment*, Nature 450, 870-873 (2007).

[89] K. C. King, L. F. Delph, J. Jokela and C. M. Lively, *The geographic mosaic of sex and the Red Queen*, Curr. Biol. 19, 1438-1441 (2009).

[90] L. T. Morran, O. G. Schmidt, I. A. Gelarden, R. C. Parrish II and C. M. Lively, *Running with the Red Queen: Host-parasite coevolution selects for biparental sex*, Science 333, 216-218 (2011).

[91] U. Dieckmann, P. Marrow and R. Law, *Evolutionary cycling in predator-prey interactions: Population dynamics and the Red Queen*, J. Theor. Biol. 176, 91-92 (1995).

[92] U. Dieckmann, and R. Law, *The dynamical theory of coevolution: a derivation from stochastic ecological processes*, J. Math. Biol. 34, 579-612 (1996).

[93] R. V. Solé and J. Sardanyés, *Red Queen coevolution on fitness landscapes, in Recent Advances in the theory and application of fitness landscapes,* (eds. Richter, H., and Engelbrecht, A. P.). Emergence, Complexity and Computation EEC series (Springer) (2013).

[94] J. N. Thompson, *The coevolutionary process*, Chicago, IL: Chicago University Press (1994),

[95] L. Van Valen, *new evolutionary law*, Evol. Theory 1, 1-30 (1973).

[96] L. Van Valen, *Energy and evolution*, Evol. Theory 1, 179-229 (1976).

[97] L. Van Valen, *Evolution as a zero-sum game for energy*, Evol. Theory 4, 129-142 (1980).

[98] N. C. Stenseth and J. Maynard Smith, *Coevolution in ecosystems: Red Queen evolution or stasis?,* Evolution 38, 870-880 (1984).

[99] A. Hoffman, *Testing the Red Queen hypothesis*, J. Evol. Biol. 4, 1-7 (1991).

[100] G. J. Vermeij, *The evolutionary interaction among species - selection, escalation, and coevolution*, Annu. Rev. Ecol. Syst. 25, 219-236 (1991).

[101] A. F. Agrawal and C. M. Lively, *Parasites and the evolution of self-fertilization*, Evolution 55, 869-879 (2001).

[102] J. Jaenike, *An hypothesis to account for the maintenance of sex in populations*, Evol. Theor. 3, 191-194 (1978).

[103] W. D. Hamilton, *Sex vs. non-sex vs. parasite*, Oikos 35, 282-290 (1980).

[104] W. D. Hamilton, A. Axelrod and R. Tanese, *Sexual reproduction as an adaptation to resist parasites (a review)*, Proc. Natl. Acad. Sci. U.S.A. 87, 3566-3573 (1990).

[105] M. Salathe, R. D. Kouyos and S. Bonhoeffer, *The state of affairs in the Kingdom of the Red Queen*, Trends Ecol. Evol. 23, 439-445 (2008).

[106] S. Gandon, *Local adaptation and the geometry of host-parasite coevolution*, Ecol. Lett. 5, 246-256 (2002).

[107] A. I. Khibnik and A. S. Kondrashov, *Three mechanisms of Red Queen dynamics*, Proc. Roy. Soc. Lond. B 264, 1049-1056 (1997).

[108] D. Ebert, *Host-parasite coevolution: insights from the Daphnia-parasite model system*, Curr. Opin. Microbiol. 11, 290-301 (2008).

[109] S. Gaba and D. Ebert, *Time-shift experiments as a tool to study antagonistic coevolution*, Trends Ecol. Evol. 24, 226-232 (2009).

[110] F. Dercole, R. Ferriere and S. Rinaldi, *Chaotic Red Queen coevolution in three-species food chains*, Proc. R. Soc. Lond. B 277, 2321-2330 (2013).

[111] S. F. Elena, V. S. Cooper and R. E. Lenski, *Punctuated evolution caused by selection of rare beneficial mutations*, Science 272, 1802-1804 (1996).

[112] P. Carrasco, F. de la Iglesia and S. F. Elena, *Distribution of fitness and virulence effects caused by single-nucleotide substitutions in Tobacco etch virus*, J. Virol. 81, 12979-12984 (2007).

[113] R. Sanjuán, A. Moya and S. F. Elena, *The distribution of fitness effects caused by single-nucleotide substitutions in an RNA virus*, Proc. Natl. Acad. Sci. U.S.A. 101, 8396-8401 (2004).

[114] Bo Deng, *Food chain chaos due to junction-fold point*, Chaos 11, 514-525 (1991).

[115] S. C. Morris, *The predictability of evolution: glimpses into a post-Darwinian world*, Naturwiss. 96, 1313-1337 (2009).

[116] S. C. Morris, *Evolution: like any other science it is predictable,* Phil. Trans. R. Soc. B 365, 133-145 (2010).

[117] T. Day, *Computability, Gödel's incompleteness theorem, and an inherent limit on the predictability of evolution*, J. R. Soc. Interface 9, 624-639 (2012).

[118] A. E. Lovkovksy, Y. I. Wolf, Y.I and E. V Koonin, *Predictability of evolutionary trajectories in fitness landscapes*, PLOS Comp. Biol. 7, e1002302 (2011).

[119] T. F. Cooper, D. E. Rozen and R.E. Lenski, *Parallel changes in gene expression after 20,000 generations of evolution in Escherichia coli*, Proc. Natl. Acad. Sci. U.S.A. 100, 1072Ã1077 (2003).

[120] Z. D. Blount, C. Z. Borland and R. E. Lenski, *Historical contingency and the evolution of a key innovation in an experimental population of Escherichia coli*, Proc Natl Acad Sci USA 105, 7899-7906 (2008).

[121] G. Saxer, M. Doebeli and M. Travisano, *The repeatability of adaptive radiation during long-term experimental evolution of Escherichia coli in a multiple nutrient environment*, PLoS One 5, e14184 (2010).

[122] H. A. Wichman and C. J. Brown, *Experimental evolution of viruses: Microviridae as a model system*, Philos. Trans. R. Soc. Lond. B. Biol. Sci. 365, 2495-2501 (2010).

[123] D. M. Weinreich, N. F. Delaney, M. A. Depristo and D. L. Hartl, *Darwinian evolution can follow only very few mutational paths to fitter proteins*, Science 312, 111-114 (2006).

[124] E. R. Lozovsky, T. Chookajorn, K. M. Brown, M. Imwong, P. J. Shaw, S. Kamchonwongpaisan, D. E. Neafsey, D. M. Weinreich and D. L. Hartl, *Stepwise acquisition*

of pyrimethamine resistance in the malaria parasite, Proc. Natl. Acad. Sci. U.S.A. 106, 12025-12030 (2009)

[125] M. L. M. Salverda et al., *Initial mutations direct alternative pathways of protein evolution*, PLoS Genet. 7, e1001321 (2011).

[126] E. Toprak et al. *Evolutionary paths to antibiotic resistance under dynamically sustained drug selection*, Nat. Genet. 44, 101-105 (2012).

[127] M. F. Schenk, I. G. Szendro, J. Krug and J. A. G. M. de Visser, *Quantifying the adaptive potential of an antibiotic resistance enzyme*, PLoS Genet. 8, e1002783 (2012).

[128] F. Dercole and S. Rinaldi, *Evolutionary dynamics can be chaotic: A first example*, Int. J. Bif. and Chaos 20, 3473 (2010).

[129] D. A. Rand and H. B. Wilson, *Chaotic stochasticity- a ubiquitous source of unpredictability in epidemics*, Proc. R. Soc. Lond. B 246, 179-184 (1981).

[130] Y. C. Lai, Z. Liu and L. Billings, *Noise-induced unstable dimension variability and transition to chaos in random dynamical systems*, Phys. Rev. E 67, 026210 (2003).

[131] S.P. Ellner and P. Turchin, *When can noise induce chaos and why does it matter: a critique.* Oikos 111, 620-631 (2005)

[132] J. Duarte, C. Januário, N. Martins, C. Correia Ramos, C. Rodrigues and J. Sardanyés, *Optimal homotopy analysis of a chaotic HIV-1 model incorporating AIDS-related cancer cells,* Numerical Algorithms, 1- 28 (2017).

[133] M. P. Cranage, *Macaques infected with live attenuated SIVmac are protected against superinfection via the rectal mucosa*, Virol. 229, 143-54 (1997).

[134] D. Klatzmann and F. Barr-Sinoussi, *Selective tropism of lymphadenopathy associated virus (LAV) for helper-inducer T lymphocytes*, Science 225, 59-63 (1984).

[135] D. Klatzmann, E. Champagne, S. Chamaret, J. Gruest, D. Guetard, T. Hercend, J. C Gluckman, L. Montagnier L, *T-lymphocyte T4 molecule behaves as the receptor for human retrovirus LAV*, Nature 312, 767-768 (1984).

[136] P. Gupta and R. Balachandran, *Cell-to-cell transmission of human immunodeficiency virus type 1 in the presence of azidothymidine and neutralizing antibody*, J. Virol 63, 2361–2365 (1989).

[137] M. L. Diegel and P. A. Moran, *Regulation of HIV production by blood mononuclear cells from HIV-infected donors: II. HIV-1 production depends on T cell-monocyte interaction*, AIDS Res. Hum. Retro. 9465-73 (1993).

[138] R. D. Schrier, J. A. McCutchan and C. A. Wiley, *Mechanisms of immune activation of human immunodeficiency virus in monocytes/macrophages*, J. Virol. 67, 5713-5720 (1993).

[139] D. S. Callaway and A. S. Perelson, *HIV-1 infection and low steady state viral loads*, Bull. Math. Biol. 64, 29-64 (2002).

[140] D. E. Kirschner, S. Lenhart and S. Serbin, *Optimal control of the chemotherapy of HIV*, J. Math. Biol. 35, 775-792 (1997).

[141] J. Lou, T. Ruggeri and C. Tebaldi, *Modeling cancer in HIV-1 infected individuals: Equilibria, cycles and chaotic behavior*, Math. Biosciences and Engineering 3, 313-324 (2006).

[142] R. Lefever and T. Erneux, *On the Growth of Cellular Tissues Under Constant and Fluctuating Environmental Conditions*, Nonlinear Electrodynamics in Biological Systems, 287-305 (1984).

[143] A. S. Qi and Y. Du, *The nonlinear medeles for immunity,* Shangai Scientific and Technology Education Publishing House (1998).

[144] K. Yabushita, M. Yamashita and K. Tsuboi, *An analytical solution of projectile motion with the quadratic resistance law using the homotopy analysis method*, J. Phys. A: Math. Theor. 40, 8403-8416 (2007).

[145] S. J. Liao, *An optimal homotopy analysis approach for strongly nonlinear differential equations*, Commun. Nonlinear Sci. Numer. Simulat. 15, 2003-2016 (2010).

[146] M. Ghoreishi, A. I. B. Md. Ismail and A. K. Alomari, *Application of the homotopy analysis method for solving a model for HIV infection of $CD4^+$ T-cells*, Mathematical and Computer Modelling 54, 3007-3015 (2011).